CARRIER MOBILITY, CHARGE TRAPPING EFFECTS ON THE EFFICIENCY OF HEAVILY DOPED ORGANIC LIGHT-EMITTING DIODES, AND EU(lll) BASED RED OLEDs

Ming-Te Lin, B.S., M.S.

Dissertation Prepared for the Degree of

DOCTOR OF PHILOSOPHY

UNIVERSITY OF NORTH TEXAS

August 2010

APPROVED:

Nigel Shepherd, Major Professor
Richard F. Reidy, Committee Member
Jincheng Du, Committee Member
Mohammed El Bouanani, Committee Member
Narendra Dahotre, Chair, Department of Materials Science and Engineering
Costas Tsatsoulis, Dean of the College of Engineering
James D. Meernik, Acting Dean of the Robert B. Toulouse School of Graduate Studies

Lin, Ming-Te. Carrier Mobility, Charge Trapping Effects on the Efficiency of Heavily Doped Organic Light-Emitting Diodes, and EU(lll) Based Red OLEDs. Doctor of Philosophy (Materials Science and Engineering), August 2010, 121 pp., 106 figures, 8 tables, 131 chapter references.

Transient electroluminescence (EL) was used to measure the onset of emission delay in OLEDs based on transition metal, phosphorescent bis[3,5-bis(2-pyridyl)-1,2,4-triazolato] platinum(II) and rare earth, phosphorescent $Eu(hfa)_3$ with 4'-(*p*-tolyl)-2,2":6',2" terpyridine (ttrpy) doped into 4,4'-bis(carbazol-9-yl) triphenylamine (CBP), from which the carrier mobility was determined. For the $Pt(ptp)_2$ doped CBP films in OLEDs with the structure: ITO/NPB (40nm)/mcp (10nm)/65% $Pt(ptp)_2$:CBP (25nm)/TPBI (30nm)/Mg:Ag (100nm), where NPB=N, N'-bis(1-naphthyl)-N-N'-biphenyl-1, 1'-biphenyl-4, MCP= N, N'-dicarbazolyl-3,5-benzene, TPBI=1,3,5-tris(phenyl-2-benzimidazolyl)-benzene, delayed recombination was observed and based on its dependence on frequency and duty cycle, ascribed to trapping and de-trapping processes at the interface of the emissive layer and electron blocker. The result suggests that the exciton recombination zone is at, or close to the interface between the emissive layer and electron blocker.

The lifetime of the thin films of phosphorescent emitter $Pt(ptp)_2$ were studied for comparison with rare earth emitter $Eu(hfa)_3$. The lifetime of 65% $Pt(ptp)_2$:CBP co-film was around 638 nanoseconds at the emission peak of 572nm, and the lifetime of neat $Eu(hfa)_3$ film was obtained around 1 millisecond at 616 nm, which supports the enhanced efficiency obtained from the $Pt(ptp)_2$ devices. The long lifetime and narrow emission of the rare earth dopant $Eu(hfa)_3$ is a fundamental factor limiting device performance.

Red organic light emitting diodes (OLEDs) based on the rare earth emitter $Eu(hfa)_3$ with 4'-(*p*-tolyl)-2,2":6',2" terpyridine (ttrpy) complex have been studied and improved with respect performance. The 4.5% $Eu(hfa)_3$ doped into CBP device produced the best power efficiency of 0.53 lm/W, and current efficiency of 1.09 cd/A. The data suggests that the long lifetime of the f-f transition of the Eu ion is a principal limiting factor irrespective of how efficient the energy transfer from the host to the dopant and the antenna effect are.

ACKNOWLEDGMENTS

First of all, I am heartily thankful to my main advisor Dr. Nigel Shepherd and co-advisor Dr. Mohammad Omary, whose supervision, guidance, support, and encouragement from the initial to the final step for accomplishing my dissertation. Also, I would like to thank my colleague Minghang for the great help in this project. This dissertation would not have been successful without your knowledge and assistance.

It's also thankful to have other three professors Dr. Rick Reidy, Dr. Mohammed El Bouanani and Dr. Jincheng Du as my committee members.

In addition, I would like to acknowledge Ravi and Joyce, who always offered me the great help. With their materials source support and suggestions, I completed this work in the expected.

I would also like to thank the friendship and help of Fangling Kuo, Mohammad Maneshian, Arun Devaraj, Antariksh Singh, Unnat Bhansali (UTD) and Huiping Jia(UTD).

Finally, I am indebted to my parents who always give me a lot of encouragement and love, and I couldn't complete this work and get this degree without their great support. Also, I would like to thank my lovely wife Shu-Fen for her support and encouragement.

TABLE OF CONTENTS

Page

LIST OF TABLES

LIST OF FIGURES

CHAPTER 1

INTRODUCTION

1.1 Motivation

Organic light-emitting diodes have attracted significant research attention for solid state lighting and electroluminescent displays due to their fast responsive time, thin structure, large viewing angle, color tenability, low power consumption, and potentially low production costs. However, the mobility and transport of carriers in the organic semiconductors is significantly lower than in inorganic semiconductors, and are often significant factors limiting device performance. A basic, deepened understanding of carrier mobility and transport is required in order to engineer materials and devices that yield optimal brightness and efficiency. However, organic semiconductors are essentially insulators and do not lend themselves to electrical characterization such as by Hall measurements. Optical methods such as those proposed in this dissertation are a versatile solution to the limitation of purely electrical methods. In addition, the lifetimes of thin films and organic light-emitting diodes (OLEDs) provide important information about the fundamental decay and emission processes, and can be studied with the transient electroluminescence (EL) method.

With the advance of science and technology, many display products have been developed into thin, light, cheap, and long lifetime products to satisfy commercial applications. Organic light-emitting diodes are considered one of the most promising candidates for self emitting, large viewing angle (over 170^0), low-cost, full-color, flat-panel displays with fast response time (~us), high efficiencies, low driving voltage (3-10V), and ultra thin screens (less than 2cm). Although OLEDs have now been investigated for a few decades, they have only been commercialized in

small sized display panels for use in car stereos, camera displays, etc. Color purity, efficiency and the lifetime of devices must be significantly improved for future, larger area products.

1.2 Contributions of the Dissertation

This present work provides the following:

a) An analysis of the charge trapping mechanism in heavily doped OLED structures using transient electroluminescence (EL).

b) Analysis of the excited state lifetimes for the phosphorescent, lanthanide based emitter, $Eu(hfa)_3$ for comparison with the phosphorescent, transition metal based $Pt(ptp)_2$ emitter.

c) Carrier mobility measurements using transient electroluminescence (EL).

d) Comparison of the energy transfer mechanisms in the host-guest systems based on b) above.

1.3 Organization of Dissertation

This dissertation has six chapters. Chapter 1 provides a brief introduction for the whole work. Chapter 2 presents a background of OLEDs as well as the principles of electroluminescent phenomena. Fluorescent and phosphorescent emitters are also discussed in this section. Chapter 3 describes the equipment and experimental procedures such as material synthesis, thin films growth and ITO plasma treatment. The methods used for electrooptical characterization of OLEDs are also discussed. In addition, Chapter 3 discusses the set-up for measuring thin film and device lifetimes. Chapter 4 includes the results of the films characterization using photoluminescence (PL) and photoluminescence excitation (PLE) and discusses the mechanisms of energy transfer. Chapter 4 also reports the lifetime comparison of the $Pt(ptp)_2$ based devices with and without MCP where MCP acts as an electron blocker layer in the device structure. Trapping at structural defects associated with the MCP/ emissive layer interface is proposed as

the mechanism responsible for the observed delayed recombination. The performance of OLEDs based on 4.5% $Eu(hfa)_3$ and $Eu(tta)_3$ doped into CBP and CDBP hosts are reported in Chapter 5. The dissertation shows the general effectiveness of pulsed DC methods for measuring the carrier mobility of inorganic semiconductors, and studying the effects of trapping in multilayer organic semiconductors structures. A comparison of the different emitters show that excellent color saturation is achieved with lanthanide emitters, but the long excited state lifetime, narrow emission profile and low doping concentration (necessary to prevent concentration quenching) result in low luminance and device efficiency even in device structures that confine injected electrons and holes to the emissive layer. In contrast, broad emitters do not provide the color saturation required for display applications, although high brightness and efficiency can be obtained even in devices with significant carrier trapping. Chapter 6 presents the conclusions and suggestions for future work.

CHAPTER 2

LITERATURE REVIEW

2.1 Transient Electroluminescence Measurements of OLEDs

2.1.1 Carrier Mobility

Organic light-emitting diodes (OLEDs) have generated significant research interest in the last decade because of their excellent properties which include high efficiency, low drive voltage, large viewing angle, fast response time, and potentially low production costs. However, this technology is still immature compared to other emissive sources. Most groups have been attempting to enhance the performance of OLEDs by lowering the driving voltage and increasing the operating lifetimes. Decreasing the driving voltage is not the only goal for the OLEDs systems. It is also important to increase the charge carrier mobility [1]. In particular, the charge balance issue and low carrier mobility in organic materials are often the main obstacles to improving the performance of OLED devices. We can also say that the most challenging factor in OLED system design is the charge balance issue, which is a key point in the research of amorphous organic molecular systems. It is already known that the performance of OLEDs is strongly determined by the carrier [2] transport properties. There are several different experimental methods to measure the charge carrier mobility. The most common are: (1) the field-effect transistor method (FET) [3, 4], (2) time of flight method (TOF) [5, 6, 7] and (3) space charge limit current (SCLC) method [8, 9]. Although these experimental methods have been around for a while, the experimental results can be very different for the same material. In contrast to the above method, the carrier mobility and kinetics can be also studied by transient electroluminescence. From this setup, the charge trapping mechanism active in the device and

the recombination zone in the emission layer can be estimated. In Tandon's group, they used this transient EL to investigate the performance of the OLEDs [13], and the result showed that the performance of the OLEDs corresponded with the mobility of the charge carriers. Besides, the architecture of OLEDs must be designed for charge balance because the mobility of holes and electrons are not the same. The concept of the whole design is to control the recombination zone by using the different mobility of holes and electrons. In order to achieve the charge balance, the holes and electrons must travel through the suitably thick hole transport layer (HTL) and electron transport layer (ETL), and recombine in the emission layer [14, 15, 16].

2.1.2 The Delay Time of Transient Electroluminescence

The delay time between the EL response and an applied voltage pulse contains important information about carrier transport in OLEDs. The EL delay time is related to the mobility of holes and electrons which are injected from the anode side and cathode side respectively, and then recombine in the emissive layer. "The delay time (t_d) consists of two components: (1) the charge injection time or charging time of the OLED (t_{inj}), (2) the charge transport delay time (t_{trans}) [13]." The sum of the charge injection time and charge transport delay time is the EL delay time which can be used to understand carrier mobility in OLEDs. Equations 1.1 to 1.3 describe these phenomena where RC is the device time constant. Figure 1 shows the basic experimental setup for transient EL measurements and Figure 2 schematically shows the delay time of the device as introduced by Tandon [13].

$$t_d = t_{inj} + t_{trans} \text{ ----------1.1}$$

$$t_{inj} = RCln(\frac{V_{max}}{V_{max}-V_{th}}) \text{----------1.2}$$

$$t_{trans} = \frac{d_e}{(u_e+u_h)E} \text{ ----------1.3}$$

Where d_e: the distance for electrons to meet the holes.

u_e: the electron mobility

u_h: the hole mobility

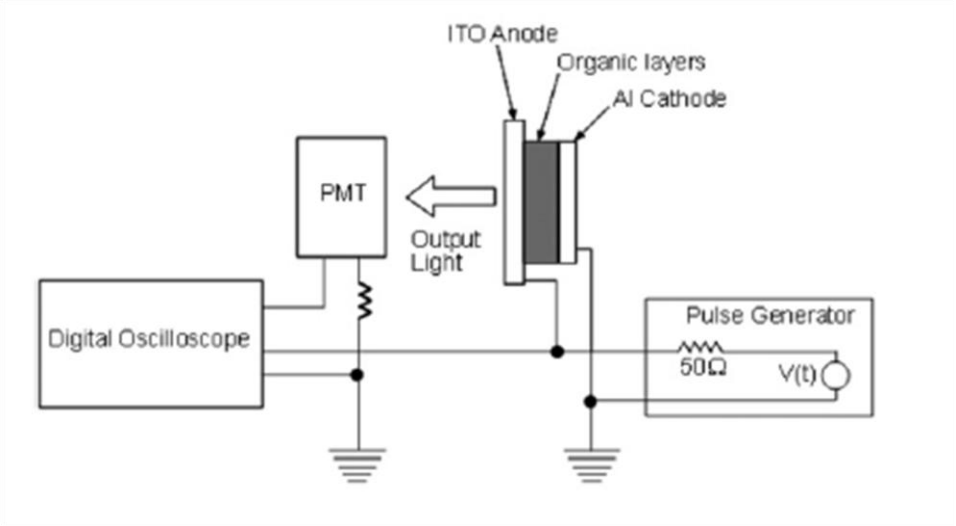

Figure 1: Experimental setup for transient EL measurements. Reproduced from reference [13].

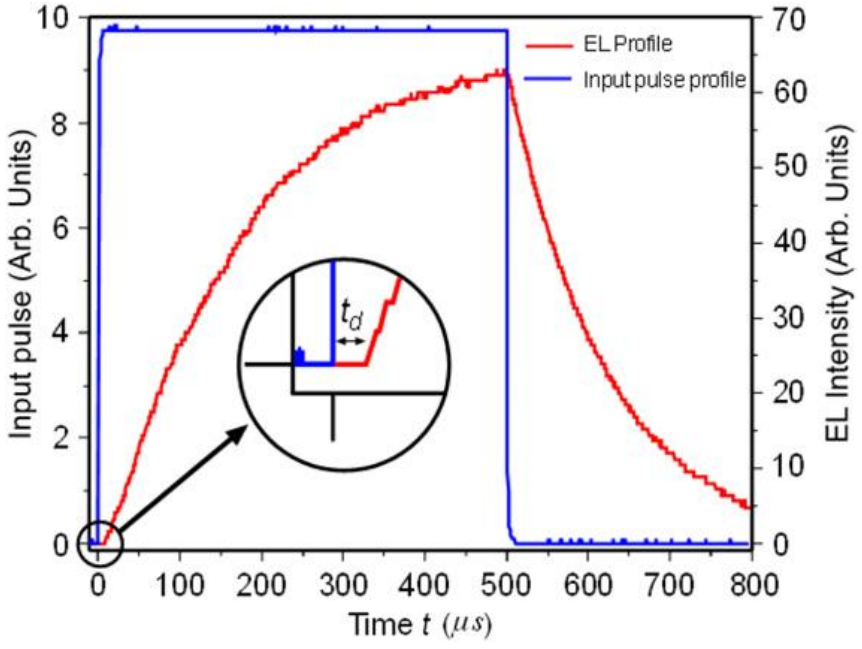

Figure 2: Delay time of the OLEDs. Reproduced from reference [13].

2.1.3 The Lifetime of OLEDs

When holes and electrons meet and recombine in the emissive layer, excitons are said to relax from the excited state to the ground state. There are two different kinds of excited states. The first one is the singlet excited state, and radiative decay is from the singlet state to ground state is defined as fluorescence. Another one is the triplet excited state with the spin-symmetry, and the phosphorescence is formed when the excitons decay from the triplet excited state to ground state. In quantum theory, the decay of the electrons from singlet excited states to the ground state are allowed, and it occurs in short time to emit fluorescent light. Therefore, the lifetime for electrons relaxing from singlet excited states to ground is around 1-10 ns [17]. In contrast to fluorescence, the life time of the phosphorescent light is around us~ms [18].

2.2 Introduction to Organic Light-Emitting Diodes

2.2.1 Fundamental Theory of OLEDs

The light emission principle of SMOLED/Polymer OLED [19,20,21], where SMOLED is small molecule OLED, is similar to LEDs. Under the certain driving voltage, holes and electrons are injected [22] and form excitons. Light emission is observed when excitons decay from the excited state to ground state via the radiative method. The color of the emitted light is dependent on the band gap between the excited state and ground state. Therefore, the color of the OLEDs device can be designed by using materials with appropriate band gap. The basic design of OLEDs is shown as Figure 3, the overlap between metal contact and Indium-Tin-Oxide (ITO) determines the pixel size. Also, the metal contact (cathode) covers and protects the organic layers, and the light is emitted out from the opposite side (ITO). The key device steps are carrier injection, carrier transport, exciton formation, and radiative decay of excitons to emit light.

Figure 3 is a simple sketch of an OLED and the different function of each layer is represented. Figure 4 is a schematic showing carrier transport direction, and the location for the recombination zone.

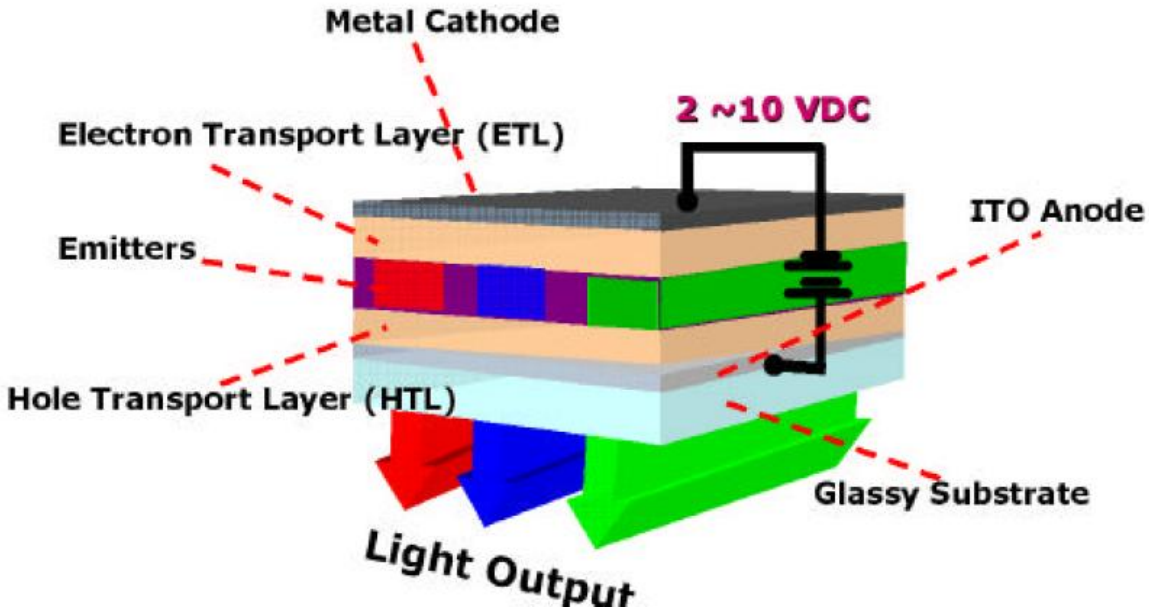

Figure 3: The basic design of OLEDs

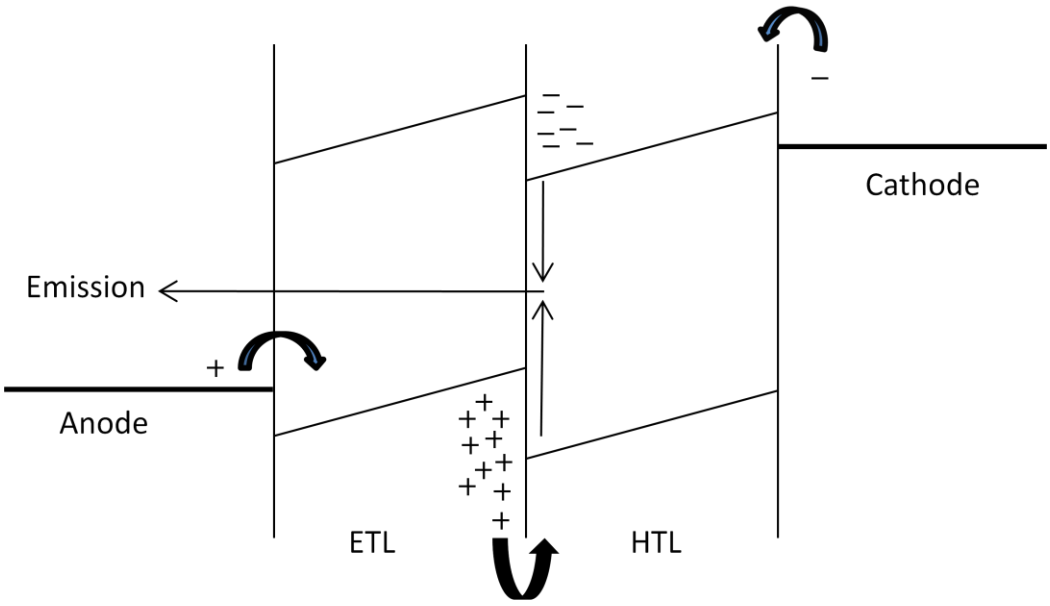

Figure 4: The simple sketch of the OLEDs system [24]

2.2.2 History of OLEDs

The first literature related to OLEDs was reported by Dr. Pope [23] in 1963. He observed the phenomenon of light emission from an organic material when he applied a very high voltage (>100 V) through an Anthracene crystal. The structure of this device is shown in Figure 5. However, this was not attractive to researchers because of the ultra high voltage and poor device performance. In 1987 Tang reported [24] the first organic light emitting diodes with a low driving voltage (<10 V) and high brightness. The fluorescent metal chelate complex Alq3 was used as the emissive layer in this device and electron-hole recombination occurred near the interface between hole transport layer (HTL) and electron transport layer (ETL). Figure 6 [24], shows the first double-layer organic light emitting diode and the structure of the Alq and Diamine organic materials. The basic science of organic light emitting diodes has progressed immensely, and researchers have improved important parameters including the life time of

operation, luminous efficiency, and color saturation. OLEDs exhibit very good luminous efficiency and power efficiency (lm/W). The performance of the OLEDs benefited from contributions by different research areas: the luminescent and transport materials from chemistry, the device processing technology and surface phenomena from engineering, and the interface phenomena from physics. Other comprehensive research areas include the architecture of OLEDs and the degradation mechanisms of OLED devices. Red, blue, and green OLEDs have been developed to produce full color.

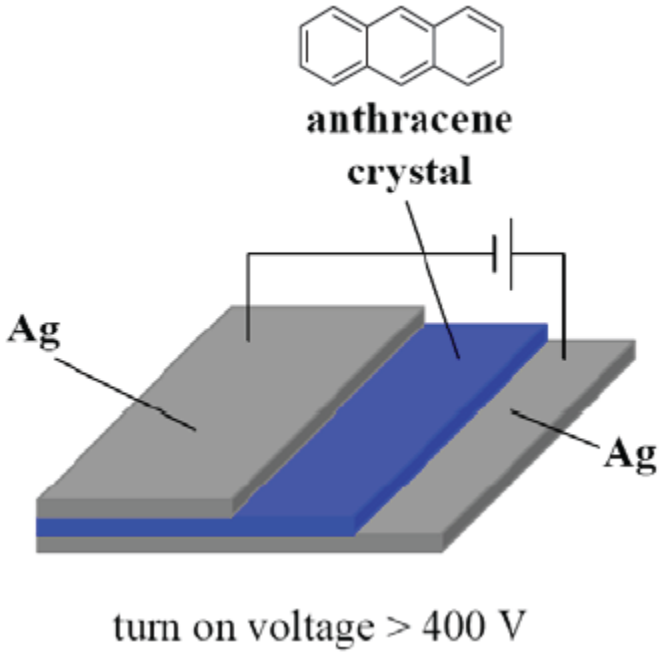

Figure 5: The structure of the first OLED. Reproduced from reference [23].

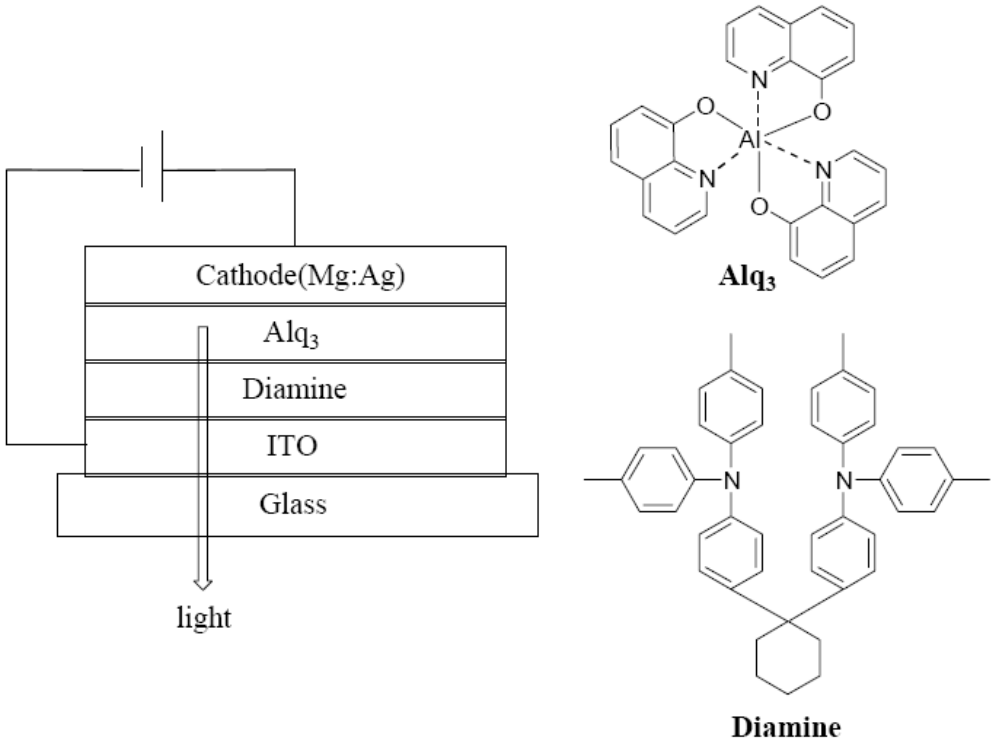

Figure 6: First double-layer OLED configuration. Reproduced from reference [24].

In 1998, Baldo and Thompson reported OLEDs which used Iridium complexes [25] as the emissive dopant. The efficiency of this device was three times larger than previous reports because there was less energy loss in the triplet excited state. Recently, researchers have been pursuing OLED full color displays as a goal. The RGB (Red, Green, and Blue) have already developed, but the performance metrics are still not good enough. Better RGB materials; especially for blue and red materials are still needed. In addition, white OLEDs are also an important research field. They can be used for general lighting, and as back-lights LCDs to reduce the space and weight. The applications of OLEDs are diverse and products have been developed as the following shows: 2~3 inch displays were used in car stereos and cell phones before year 2000, 4~8 inch multi-color displays for car navigation systems between year 2001 to

2002, 10~15 inch full color displays for laptop monitors after year 2005, 11 inch OLED TV in 2008, and larger size OLED TVs will be produced in the future. The most common approach for full color is to use white light with color filters as is shown in Figure 7.

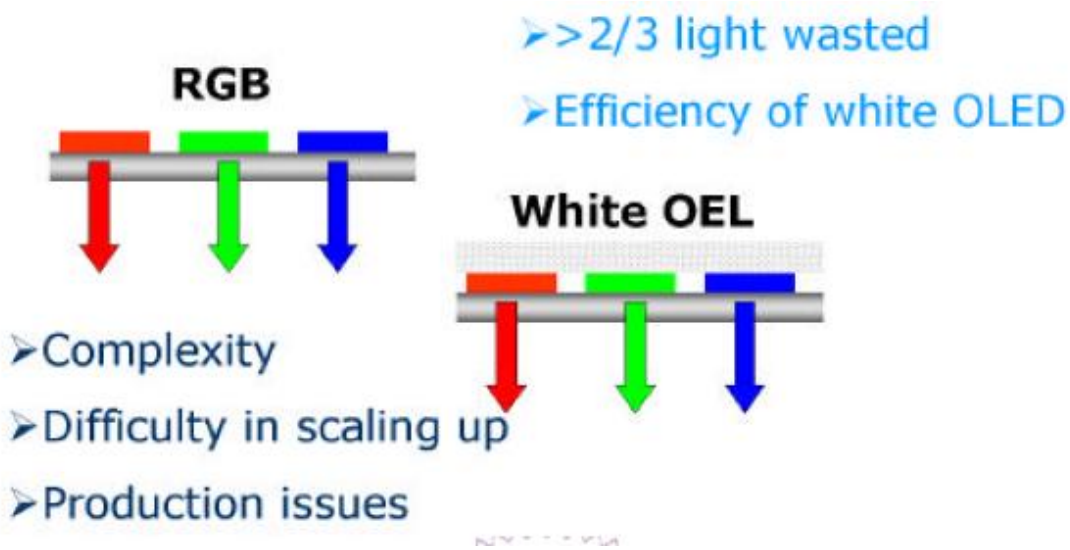

Figure 7: The white source background with the filter

2.2.3 Advantage and Disadvantage of OLEDs

In modern technologies, the flat-panel display is the main communication interface between products and the user. Therefore, high quality and various sizes are required to satisfy the various needs. Since the OLEDs will compete primarily with LCDs, it is useful to compare the two. The lists of OLED advantages include:

- Self-emissive, and large viewing angle (>170^0)

- Fast response time (ns~us)
- High brightness (200~30000 Cd/m^2)
- High efficiency (15~75 lm/W)
- Low driving voltage (2.5~10 V DC), low power loss
- Full color
- Thin display screens
- Various display sizes and flexible OLED screens

Compared to LCDs, the color in OLEDs is more vivid with higher contrast. In addition, only OLED full color panels can be achieved with screen thicknesses less than 2 cm. However several serious drawbacks need to be overcome in OLEDs including color purity and device lifetime.

Figure 8: The brightness and view angle of LCD and OLED

2.3 The Function of Each Layer in OLEDs

2.3.1 Anode and Cathode Materials

The work function of the cathode must be low in order to have a low threshold voltage and therefore efficient electron injection from the cathode. The work-function of Mg is 3.5 eV which is low enough, Mg oxidizes readily. An alloy of Mg and Ag in a 10:1 ratio is therefore used [26,27]. In addition, LiF capped with Al is also widely used as the cathode material due to its low work function [28, 29]. The anode material must have a high work function and be transparent. ITO (indium tin oxide) is the commonly used anode material [30,31, 32] because of its high work function, transparency in the visible range, good conductivity, and chemical stability. There are several methods to fabricate indium tin oxide (ITO), such as e-beam evaporation, thermal vacuum evaporation, RF sputtering deposition, and DC sputtering deposition.

2.3.2 Hole Injective Layer Materials (HIL)

The work-function of the ITO is increased to ~4.8 -5.0 eV using O_2 plasma. Suitable hole injection materials (HIL) are deposited onto the ITO to further reduce the barrier for hole injection into the device. The material CuPc [33] is commonly used as a HIL in OLEDs. In addition, PEDOT:PSS [34] is also used. PEDOT smoothens the surface of the ITO which decreases electrical shorts in devices. Recently, the HIL material m-MTDATA [35,36] has been used because of the HOMO of the m-MTDATA is 5.0 eV which is comparable to the work function of ITO The structure of CuPc and m-MTDATA is shown in Figure 9.

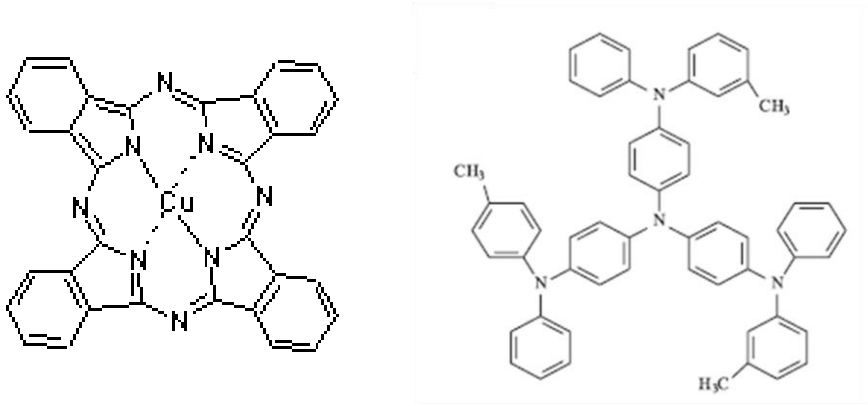

Figure 9: The structure of CuPc and m-MTDAT. Reproduced from references [33,35].

2.3.3 Hole Transport Layer Materials (HTL)

Most of the hole transport materials are triarylamine organic materials which have high hole mobility under high electric field. The mobility of these materials are around 10^{-3} cm/Vs. For use as hole transport materials in the OLEDs, not only high mobility are required, but also the capability for high vacuum deposition to form pinhole free films is necessary. Re-crystallization of thin films of the hole transport materials is observed after long periods, which results in poor device performance. For example, TPD films deposited under high vacuum have been observed to crystallize after a few hours at the room temperature. Because of the crystalline problems in the triarylamine hole transport materials, silanamine materials were developed. The crystalline problem is less in silanamine material and the HOMO is similar to that of TPD (5.5~5.7 eV). Two phenyls in TPD were replaced with two triphenylsilyl (Ph3Si-) which solved the re-crystallization problem without affecting the hole mobility. From the view point of thermodynamics and crystal structure, the crystals are not formed easily in systems with the asymmetry, large size, rigidity, and dense compounds because of the low cohesion between molecules. Ongoing efforts on the development of HTLs are:

(1) To improve the thermal stability and electrochemical stability.

(2) To increase the mobility.

(3) To increase the glass transition temperature (Tg).

(4) To reduce the energy barrier interface between the anode (ITO) and ETL.

(5) To reduce the crystallization behavior.

The new HTL material BPAPF was reported by Tao in 2002 [37] and was used as the HTL in red phosphorescent OLEDs; its high Tg was around 167^0C. In contrast, NPB is the most common HTL material in OLEDs and its high hole mobility is its biggest In addition TAPC, where TAPC=1,1-bis[(di-4-tolylamino)phenyl] cyclohexane, can be used for both hole transport layer and electron transport layer due to its high mobility and low LUMO energy level. These three structures can be seen in Figure 10.

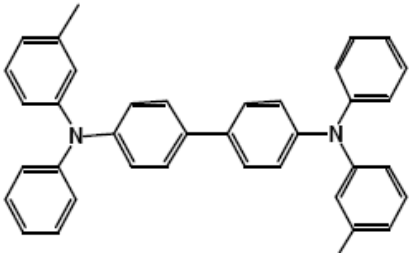

TPD

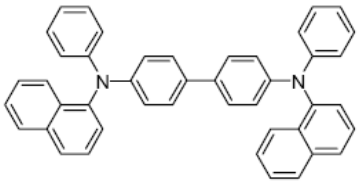

NPB

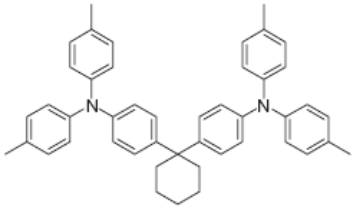

TAPC

Figure 10: The structure of TPD, NPB, and TAPC. Reproduced from reference [37].

2.3.4 Hole Blocking Layer Materials (HBL)

Ideally, the mobility of the electron transport layer (ETL) and hole transport layer (HTL) should be the same to have the recombination zone in the emissive layer, but the mobility of most ETLs is smaller than that of HTL in organic materials. Therefore, the function of the HBL [38,39] is to prevent the holes from going through the ETL in OLEDs. Some of the electron transport materials (ETL) can be also used as hole blockers because of the high HOMO energy level, where HOMO is the highest occupied molecular orbital and it is for the hole transportation. There are many materials which are used for ETL/HBL, such as BCP [40], TPBI [41] and TPYMB [42]. The HOMO of TPBI and TPYMB are 6.2 eV and 6.77eV, respectively. The ability of the HBL to block the hole depends on how large the HOMO is. The structures of these materials are show in Figure 11.

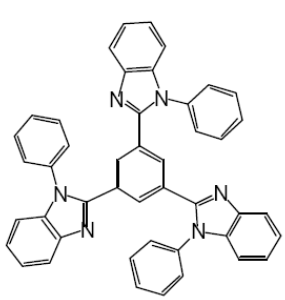

TPBI

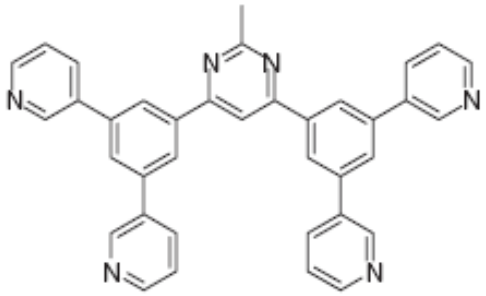

TPYMB

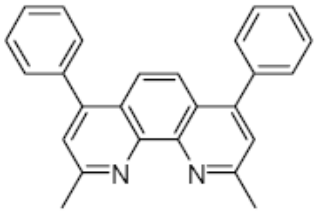

BCP

Figure 11: The structure of TPBI, TPYMB, and BCP. Reproduced from references [40,41,42].

2.3.5 Emissive layer materials (EML)

In the OLEDs the emissive layer consists of a host and a dopant. Host materials must transport charge, allow excitons to form and facilitate radiative recombination. The dopants are dispersed in the host layer by using co-evaporation. The dopant-host system was first reported by the Kodak Company [43]. They used the highly fluorescent organic dye as the dopant and obtained energy transfer from the host to dopant. However, a major problem is that the system exhibits self quenching when the dopant concentration is too high. Some organometallic light-emitting materials can be used either for dopant or host, such as Ru complexes and Pt complexes. A high triplet energy host material is very important in host-guest OLED systems because to prevent energy transferring back to the host from the dopant. CDBP and MCP, where CDBP=4,4′-bis(9-carbazolyl)-2,2′-dimethyl-biphenyl and MCP=N, N'-dicarbazolyl-3,5-benzene, are reported as good due to external quantum efficiency was increases obtained with their use [44,45]. The structures of CBP and MCP are show in Figure 12.

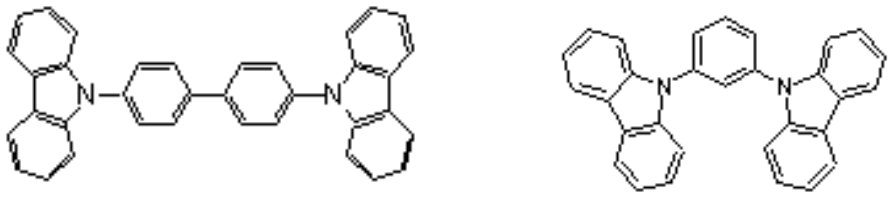

Figure 12: The structure of CBP and MCP. Reproduced from references [48,49].

2.3.6 Electron Transport Layer Materials (ETL)

Electron transport materials are used to enhance electron transport. The common ETL materials are Alq3 [46], BeBq2 [47], TAZ derivative (1,2,4-trazoles) [48], OXD (1,3,4-oxadiazole) [49,50,51], TPS (thiopyran sulfones) [52,53], and TPBI (2,2',2"-(1,3,5-benzenetriyl)-tris-[1-phenyl-1Hbenzimidazole]) [54]. The chemical structure of Alq3 is shown in Figure 13. The common feature of these compounds is a conjugated system which is used to deliver electrons. The choice of the ETL depends on the system design. For example, the low thin-film quantum yield (~10%) and the low electron mobility (10^{-5} cm^2/Vs) of Alq3 can be regarded as a bad ETL material, but it is widely used both in the academia and industry. The main reasons for this can be discussed from several points. From chemical viewpoint, Alq3 is a metal-based fluorescent material and metal-based materials are more stable than organic dyes. Therefore, the Alq3 can be regarded as a stable metal organic compound (organometallic ETL material). Alq3 is put between metal electrode and organic materials to mediate the effects of defects at the interface between organic and inorganic materials. Recently, the material TPYMB was found to be the good electron transport material because of high electron mobility and high HOMO energy level which is good for blocking holes. The structure of the TPYMB is explained in the hole block layer materials (HBL) section.

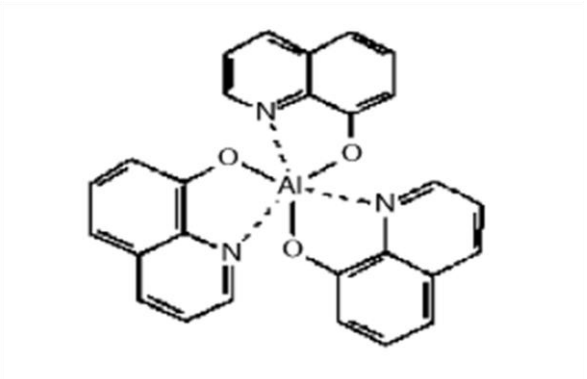

Figure 13: The structure of Alq3. Reproduced from reference [46].

2.3.7 Electron Block Layer Materials (EBL)

The EBL is used to block electrons from entering the HTL and confining electrons to the emissive layer. The LUMO of the EBL should be lower than that of EML. If the LUMO energy level difference between the EBL and EML is large, the interface barrier will be a good electron blocker. For example, TAPC and NPB are good HTL materials and also good EBL materials due to the high hole mobility and low LUMO energy level, where LUMO is lowest unoccupied molecular orbital and it is for the electron transportation.

2.4 Fluorescent and Phosphorescent Materials

2.4.1 Principle of Fluorescence and Phosphorescence

When molecules absorb visible or ultraviolet radiation, electrons are excited from the ground state to the excited state, and radiative return to ground state results in light emission. Depending on the lifetime of the excited state and the spin states of the energy levels involved, the emission is categorized as fluorescence or phosphorescence. Fluorescence is the process when electrons radiatively transition from singlet excited state to the singlet ground states, and the transition is spin allowed; therefore, the life time is very short (~ns). But the life time of phosphorescence is very long (~ms) because the spin direction in the transition from triplet excited state to the singlet ground state are the same, which is called spin symmetry and the spin forbidden causes the long life time of the phosphorescent materials. When the electrons were excited in the system, the electrons would be distributed between singlet and triplet states. From the statistical point, the ratio of the singlet excitons and triplet excitons is 1 to 3. Figure 14 schematically shows fluorescence and phosphorescence. The Jablonski diagram [55] in Figure 15

explains the photophysical processes in molecular systems, and the processes are described below.

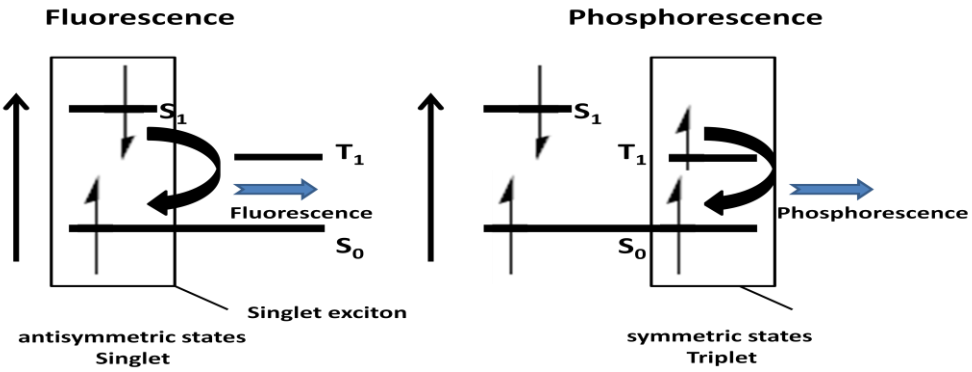

Figure 14: The schematic principle of fluorescence and phosphorescence [55]

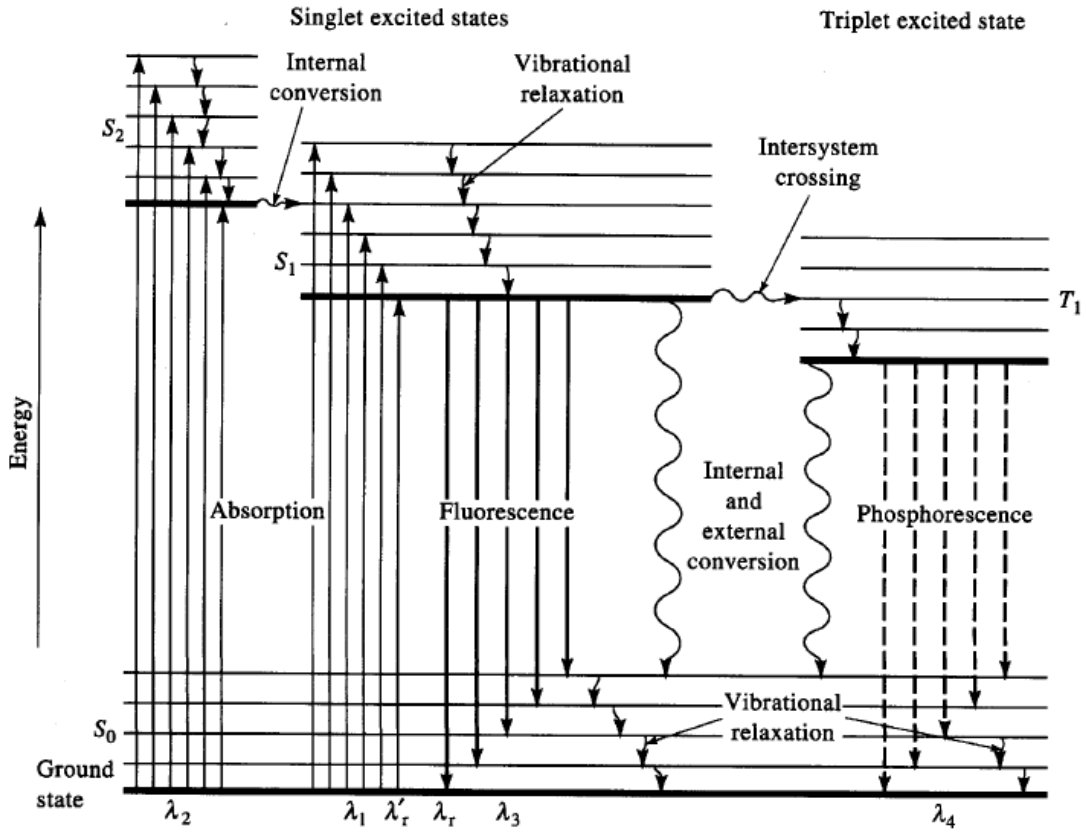

Figure 15: The different photophysical processes in molecular systems [55]

(1) Vibrational relaxation: Excited electrons relax to the lowest excited singlet state (S1) by releasing heat. The process occurs in around 10^{-14}~10^{-12} s; therefore, the excited electron relaxes to the lowest singlet state (S1) fast. Because the life time of the radiation of the fluorescent singlet excited state is around 10^{-8} s, the lowest singlet excited state (S1) would be always the initial excited state in fluorescence.

(2) Internal conversion: Internal conversion is the non-radiative process where the excited electron relaxes to a low energy excited state with the same spin direction. Because of the existence of the internal conversion, the transition from S2 (or above S2) to S0 is very difficult to observe. Fluorescence and the process of the internal conversion are in competition. The fluorescence efficiency is determined by the fluorescence decay rate constant (Kf) and the rate of internal conversion (Kic).

(3) The formation of the fluorescence and phosphorescence: fluorescent light is emitted when the transition is from the lowest singlet (S1) to the ground state via the radiation transition. If there is overlap between S1 and T1 (triplet excited state), the excited electron could transit from the S1 state to T1 state which is called intersystem crossing. Then the excited electrons radiatively decay from the lowest state of T1 to the ground state S0, the emitted light is defined as phosphorescence.

2.4.2 The Efficiencies of Fluorescent and Phosphorescent Materials

Figure 16 describes singlet excited electrons and triplet excited electrons. The probability from the theory is that 25% of excited electron are singlets and and 75% are triplets.. Based on quantum theory and the limitations of selection rule, only the 25% singlet exciton can decay radiatively and the 75% triplet excitons are wasted because they don’t obey spin and parity

selection rules. That is why the maximum efficient number of fluorescence is 25%; therefore, if we can use the triplet excitons and reduce their probability for non-radiative decay, the efficiency of the device will be improved. In the recent research, the efficiency of the phosphorescence has been increased by use of heavy atoms inside the molecule, such as Ir and Eu. Therefore, the high atomic number, 76Os, 77Ir, and 78Pt, are studied for the influence of the heavy atom effect. The effect of the heavy atom is based on the induced conservation of the angular momentum.

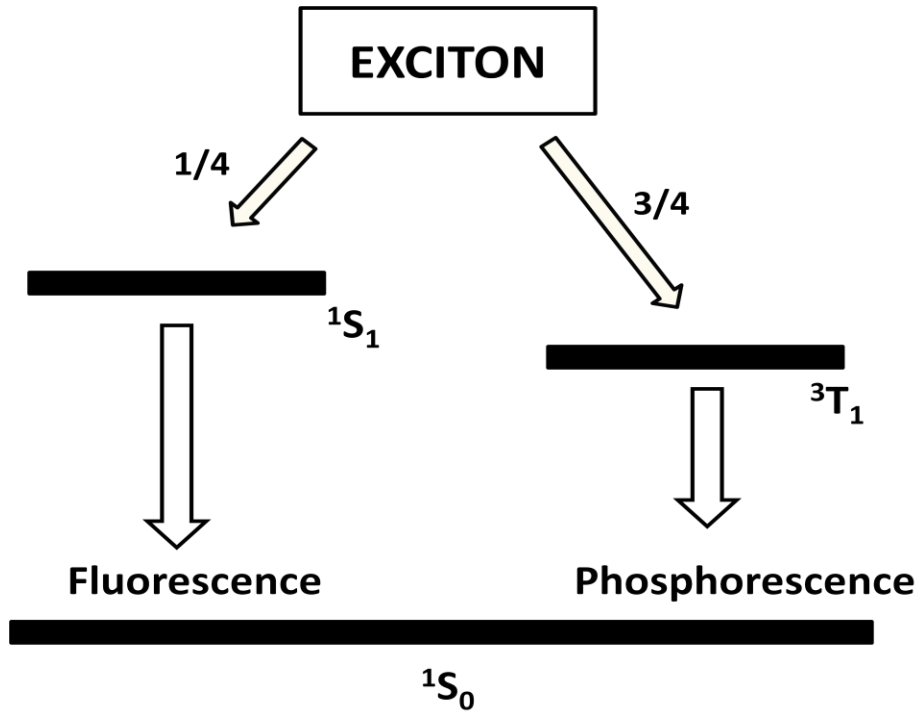

Figure 16: The ratio of the formation in fluorescence and phosphorescence

In this situation, the spin-orbit coupling is induced by the heavy atom. There are more mixed excitons of singlet and triplet in the system due to the heavy atom spin-orbit coupling and thus increase the probability of the intersystem crossing between S_1 and T_1. The internal quantum efficiency can be improved to 100% [56], and the efficiency of the whole device is

better than that without intersystem crossing. Fresnel's equation is used to relate external quantum efficiency with internal quantum efficiency. The formula is shown below, and the schematic energy transfer in the system can be seen in Figure 17.

$$_{ex} = \ _{\text{in}} \times {}^{1}/_{2\text{n}^2} \qquad \text{------1.4}$$

$$_{ex} = (\ _{\text{r}} \times \chi \times \Upsilon) \times \ _{c} \qquad \text{------1.5}$$

- $_{ex}$: External quantum efficiency
- $_{\text{in}}$: Internal quantum efficiency
- n: The index of refraction of organic emitting material (1.6~1.9)
- $_{\text{r}}$: The recombination rate of excitons
- : The excited exciton in singlet and triplet (25% for fluorescence and 100% for phosphorescence)
- Υ: Carrier injection balance (~1)
- $_{c}$: The light out from the layers (depends on the n of the material)

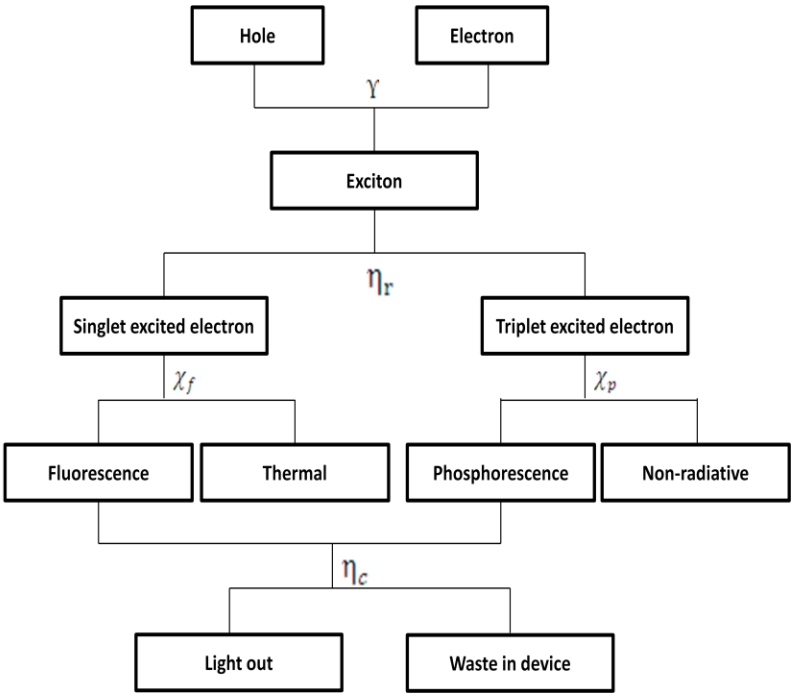

Figure 17: The schematic energy transfer in the system. Reproduced from reference [56].

From the theory, we could increase the efficiency by using phosphorescent materials. The most famous phosphorescent emitter doped into a host was PtOEP which was reported by Forrest's group in 1998, who doped PtOEP into Alq to increase the external quantum efficiency to ~4%. The strong spin-orbit coupling of the PtOEP complex occurred due to the heavy Pt which was surrounded by Porphyrine, and the efficiency of the intersystem crossing increased because of the mixed of the singlet excited states and triplet excited states. The efficiency of this phosphorescent material can reach up to 50% at room temperature, and the decay time of the triplet excited state was 91 us. The structure was ITO/CuPc(6nm)/NPB(35 nm)/PtOEP:Alq3 (x%,40 nm)/Alq3(10 nm)/Mg:Ag (15:1, 100 nm)/Ag(50 nm), where x=1, 6, and 20%. Although the triplet excited states increased the efficiency of the phosphorescence, roll-off of the

efficiencies in this structure device was observed at high current density due to the long lifetime of the PtOEP phosphorescent emitter.

2.5 The Mechanisms of the Energy Transfer in Host- Guest Systems

Energy transfer in host –dopant systems is due to energy transfer from the host to the dopant. Based on this theory, the dopant is used to adjust the color of the device. [57]. For example, when the DCM2 (dopant) was added in the Alq3 (host), the color changed from green to red with increasing dopant concentration. The dopant added not only changed the color of the device, but also enhanced the efficiency of the device because the energy was transferred to dopant which was a better fluorescent material. There are two mechanisms of the energy transfer. The first one is the radiative energy transfer and another is the non-radiative energy transfer. Radiative energy transfer is divided into the processes of emission and absorption and the rate of the radiative energy transfer is dependent on the emissive efficiency of the host material, the concentration of the guest material, and the absorption of the guest from the host. The efficiency of the fluorescent dyes would be affected by this mechanism. The second mechanism is the non-radiative energy transfer. Also, the non-radiative energy transfer is divided into two different types of energy transfer [58,59]:

(1) Forster non-radiative energy transfer:

Forster energy transfer is the non-radiative energy transfer which is caused by the dipole-dipole coupling between the donor (D) and acceptor (A) molecules and it is a long distance energy transfer (~50-100 A). The mechanism of the Forster non-radiative energy transfer is that the electron would be excited to the excited state of the acceptor species.

Moreover, the transitions should obey the electron spin direction conservation. In Figure 18, it shows the Forster energy transfer.

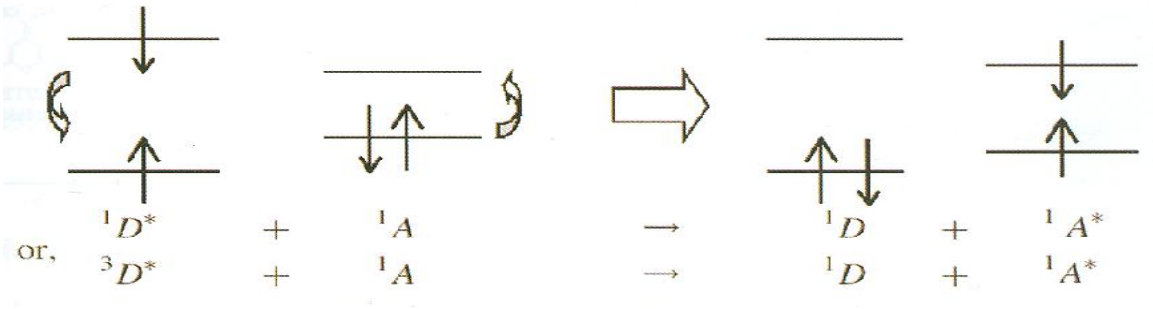

Figure 18: The schematic process of Forster energy transfer [59]

(2) Dexter non-radiation energy transfer.

Dexter energy transfer is intermolecular electron exchange. Because it occurs via the overlap in the electron cloud and molecules, the energy transfer distance should be very short (~10-15 A). The intermolecular electron exchange is conserved under the Wigner-Witmer selection rules [58]. It means that the spin conservation would be conversed before and after the intermolecular electron exchange. Therefore, Dexter energy transfer is allowed in both singlet-singlet and triplet-triplet transfers. In Figure 19, it shows the Dexter energy transfer (singlet-singlet transfer).

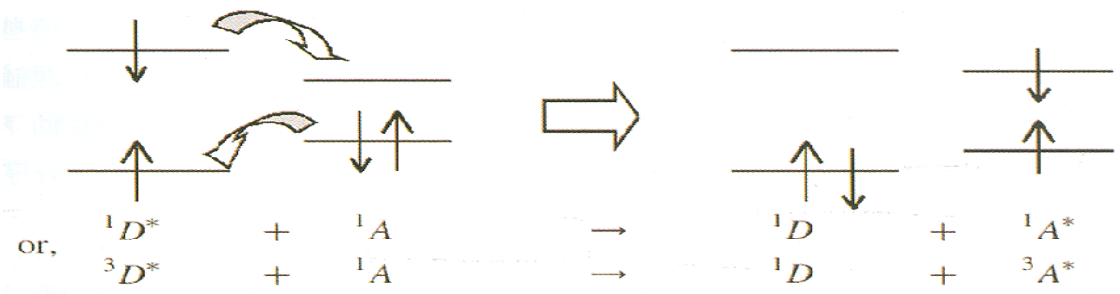

Figure 19: The schematic process of Dexter energy transfer [59]

Due to the different types of the energy transfers, we can distinguish the mechanism of the doped system. In the phosphorescent emitter doped system, the singlet exciton of the host can be transferred from singlet excited state to singlet excited state through the mechanisms of Forster and Dexter. Due to the effect of the heavy atom in the complex, the energy can be transferred from the singlet excited state to the triplet excited state through the intersystem crossing to produce phosphorescent light. In addition, the exciton of triplet excited state in the host can be transferred to the triplet excited state of the dopant to produce phosphorescent light through the Dexter energy transfer mechanism. If we use all of the energy from singlet and triplet states, the internal quantum efficiency could be increased to 100%. The ideal schematic energy transfer of the phosphorescent emitter can be seen in Figure 20.

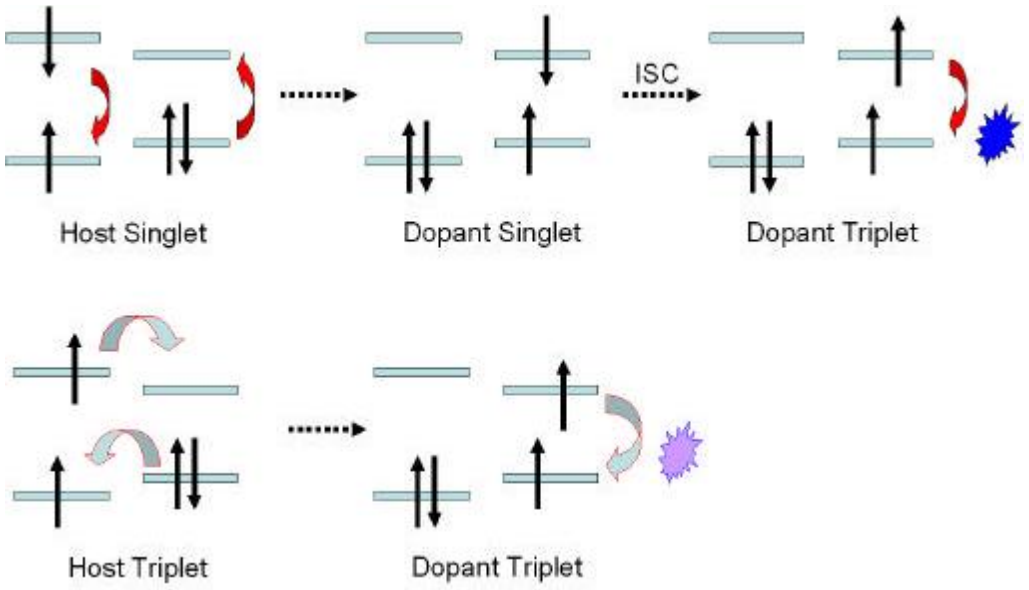

Figure 20: The schematic energy transfer of the phosphorescent emitter [59]

2.6 ITO Substrate Cleaning-Plasma Treatment

Because of its high conductivity and transparency, ITO is widely used in a emissive technologies. The surface of the ITO is very important to the efficiency of OLEDs, and the electroluminescent characteristics of the OLED devices are greatly influenced by the properties of the ITO substrate. Hence, modification of the ITO surface is required for better performance of OLEDs [60~64]. The work function of the ITO should be high enough (~4.7 eV) to match the HOMO of the hole transport layer so that holes can be injected into the emissive layer. Oxygen plasma is used to remove hydrocarbon contaminants from the surface of ITO, which lower the low work function of the ITO [65]. Cacialli [66], reported the use of oxygen plasma to increase the work function of the ITO. Some other gas plasma are also used for the surface treatment [67]. The literature [68,69], reports that the work function can also be increased by using a UV-Ozone treatment. The work function can be increased from 4.7 eV to 5.0 eV to match the work function of the HTL. There are some other plasma treatments such as wet chemical treatment [70],

mechanical polishing, coating treatments with self-assembled monolayers [71,72], and annealing processes [73~75]. The oxygen plasma treatment is the best among these treatments due to the increasing in work function.

2.7 Common OLED Devices

2.7.1 Blue Organic Light Emitting Diodes

There are several kinds of blue emitters such as triazole, styrene, oxdiazole, coumarin, perylene, and arylene. Most of them are organic materials and few of them are metal-organic materials. In 1992, Alq3 was modified to form a different molecule with a color change from green to blue [76], but the efficiency of this device was poor. Tao and Suzuki [77], reported the blue emitter LiB(qm)4 in the device structure of ITO/PVK:NPB (50nm)/LiB(qm)4 (60nm)/Mg:Ag. Blue light (~470 nm) was successfully obtained, and the power efficiency and the luminance of the device were 1.3 lm/W and 6900 cd/m^2, respectively. A few years later, the blue emitter Bepp2 was reported by Wang [78]. The Bepp2 was put in two differently structured devices: (1) ITO/NPB (60nm)/Bepp2 (50nm)/LiF (1nm)/Al (200nm) and (2) ITO/CuPc (15nm)/NPB (60nm)/Bepp2 (50nm)/LiG (1nm)/Al (200nm). The efficiencies of these two devices were good, but the spectra of the devices were too broad (~100nm). Therefore, the color was close to the green-blue instead of pure bluer. The structure of the Bepp2 is shown in Figure 21, and the performance of devices is shown in Table 1.

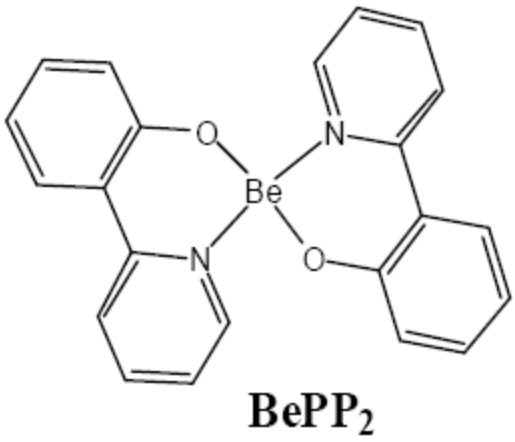

Figure 21: The structure of B_ePP_2. Reproduced from reference [78].

Table 1: The performances of the B_ePP_2 based devices

	Device A	Device B
Max Brightness (cd/m^2)	15000	11000
Power efficiency (lm/W)	3.43	3.43
EL (λ_{peak})	445 nm	445 nm

Reproduced from reference [78]

In contrast to these fluorescent emitter materials, the key point to improving the performance of OLEDs is to use phosphorescent emitters (dopants). Normally, the energy gap of the host should be larger than that of dopant, and the emission of the host must overlap the absorption of the dopant so that energy can be transferred from the host to dopant. Recently, CBP [79] has been widely used in blue OLED devices. Red, yellow, and green dopant

phosphorescent materials can be doped in this common host material with external quantum efficiencies approaching 10%. In order to increase the efficiency of blue phosphorescent devices, mcp (with high triplet excited energy) was reportedly [80] used as a host. The triplet excited energy of mcp is 2.9 eV which is 0.4 eV higher than that of CBP. More recently, the phosphorescent emitter Firpic (λ_{max}=470 nm) was doped into mcp and it was reported from the Thompson group [44]. The Firpic-based device structure was ITO/CuPc/NPB/x% Firpic: mcp/BAlq/LiF/Al, and the external quantum efficiency and power efficiency were 7.5 % and 8.9 lm/W, respectively. Because of the high triplet excited state of mcp, energy can be transferred from the mcp to the phosphorescent dopant. Another phosphorescent material used was Fir6 [77], and the structure of Fir6 based device was ITO/NPB/mcp/x% Fir6:UGH2/BCP/LiF/Al. The EQE and PE were 11.6% and 13.9 lm/W, respectively.

2.7.2 Green Organic Light Emitting Diodes

Green emitters are the most mature, developed OLEDs. Although the solid state emission rate of Alq is only 10%, Alq was still studied for the green color. For example, researchers at the Kodak Company used 1% Coumarin 6 (λ_{max}) [77] dye in the Alq. The Coumarin 6 was observed to absorb the energy from Alq and thus increase the efficiency of the device. Lately, the green emitter quinacridone (QD) [81] was published by Pioneer Company. They claimed this material (QD) was better than Coumarin 6, and the efficiency of the device was three times higher than that without the QD doping. Some other fluorescent emitters were reported, such as naphthalimide (λ_{max}=540 nm) [82], oronene (λ_{max}=500 nm) [83], and Terbium complex Tb $(acac)_3$ (λ_{max}=550 nm). At the same time, researchers are also looking at phosphorescent emitters

and some good materials are $(ppy)_2Ir(acac)r(Bu\text{-}ppy)_3$ (λ_{max}=525 nm) [84] and platinum complexes.

2.7.3 Red Organic Light Emitting Diodes

Unlike green and blue emitters, there are few high efficiency red emitters. The first red dopant dye was DCM (λ_{max}=596 nm) [85] which was reported by the Kodak Company. However, the color of the device changed with dopant concentration and the CIE coordinates (0.56, 0.44) was not located at the pure red range. When DCM2 was doped into the host Alq3, some of the emission was from Alq3, which changed the device color from red to orange-red. Materials like DCJT and DCJTB were developed for the red devices. If the DCJTB was put in the device: ITO/NPB/1.5% DCJTB: Alq/Alq/Cathode, the CIE was located at (0.63,0.37) which was a very good pure red color. The good quality of the DCJTB made it a commercial red product. Other red emitters are based on Europium (III) complex. The advantage of Eu complexes is their very sharp emission spectrum (λ_{max}=614 nm, $^5D_0 \rightarrow {}^7F_2$). The first Eu complex was $Eu(phen)(TTA)_3$, where TTA=thenoyltrifluoroacetone, phen=1,10-phenanthroline [86] and some Eu based complexes were published thereafter. Many Eu based complexes exhibit poor thermal stability and decompose during thermal evaporation. Because the results of these fluorescent emitters were not good, research on red emitters switched to phosphorescent materials. Among these phosphorescent emitters, the Iridium complex $Bep_2Ir(acac)$ is one of the best emitters. $Bep_2Ir(acac)$ was put in the structure: ITO/NPB (50 nm)/7 % Btp2Ir(acac):CBP (30 nm)/BCP (10 nm)/Alq (40nm)/Cathode, by the Thompson group [87] and the EQE was 6.6% at 1 mA/cm^2 which was better than most of the other fluorescent emitters. However, the first red phosphorescent emitter was PtOEP which was doped into the CBP (host material), and produced

an EQE of 5.6 %. Nowadays, phosphorescent Eu complexes are being used in the OLED devices due to high quantum yield, and the pure red emission [88].

2.8 References

1. M. H. Ho, Kuan-Heng Lin, Jenn-Fang Chen, and Chin H. Chen, Appl. Phys. Lett., 2009, 94. 023306.
2. M. A. Khan, Wei Xu, X. Y. Jiang, and W. Q. Zhu, Solid State Communications, 2007, 144, 343.
3. G. Horowitz, R. Hajlaoui, H. Bouchriha, and M. Hajlaoui, Adv. Mater, 1998, 10, 923.
4. G. Horowitz, R. Hajlaoui, D. Fichou, and A. El Kassmi, Appl. Phys. Lett. 1999, 85, 3202.
5. R. G. Kepler, Physical Review , 1960, 119, 1226.
6. N. Karl, and J. Marktanner, Mol. Cryst. Liq. Cryst., 1998, 315, 163.
7. N. Karl, J. Marktanner, and F. Schatz, J. Vac. Sci. Technol. A, 1999, 17, 2318.
8. M. Pope and C. E. Swenberg, Electronic Processes in Organic Crystals and Polymers, Oxford University Press, New York, 1999.
9. P. W. M. Bloom, M. J. M. deJong, and J. J. M. Vleggaar, Appl. Phys. Lett., 1996, 68, 3308.
10. G. Horowitz, Adv. Mater. 1998, 10, 365.
11. N. Karl, Synthetic Metals, 2003, 133, 649.
12. Takeshi Yasuda, and Tetsuo Tsutsui, J. J. Appl. Phys, 2002, 41, 5626.
13. Pankaj Kumar, Suresh, and R P Tandon, J. Phys. D Appl. Phys., 2007, 40, 7313.
14. V. M. Silva and L. Pereira, Journal of Non-Crystalline Solids, 2006, 352, 5429.
15. Paul A. Lane, Gary P. Kushto, and Zakya H. Kafafi, Appl. Phys. Lett., 2007, 90. 023511

16. M. A. Baldo, S. Lamansky, M. E. Thompson, and S. R. Forrest, Appl. Phys. Lett., 1999, 75. 036951
17. Hirotake Ka, Kazuya Takahashi, and Yutaka Ohmari, J. J. Appl. Phys, 2006, 45, 3721.
18. Akira Kawakami, Eiji Otsuki, and Hiroshi Kita, J. J. Appl. Phys, 2008, 47, 1279.
19. 19Victor A. Montes, Gang Li, Radek Pohl, and Pavel Anzenbacher, Adv. Mater, 2004, 16, No. 22, p2001.
20. 20Stefan Kappaun, Christian Slugovc, and Emil J. W. List, Int. J. Mol. Sci., 2008, 9, 1527.
21. 21Junsheng Yu, Jun Wang, Tao Wang, and Yadong Jiang, Display, 2008, 29, 493.
22. 22Neal R Armstrong, R Mark Wightman, and Erin M Gross, Annu. Rev. Phys. Chem, 2001, 52, 391.
23. P. Pope, H. P. Kallmann, and P. Magnante, J. Chem. Phys. 1963, 38. 2042.
24. C. W. Tang, and S. A. VanSlyke, Appl. Phys. Lett. 1987, 51, 913.
25. M. A. Baldo, S. Lamansky, P. E. Burrows, M. E. Thompson, and S. R. Forrest, Appl. Phys. Lett. 1999, 75, 4.
26. C. Shen, I. G. Hill, and A. Kahn, Adv. Mater., 1999, 73, 1523.
27. D. C. Choo, H. C. Im, D. U. Lee, T. W. Kim, J. W. Han, and E. H. Choi, Solid State Communications, 2005, 136, 365.
28. L S Hung, R Q Zhang, P He, and G Mason, J. Phys. D: Appl. Phys., 2002, 35, 103.
29. ZY Zhong and YD Jiang, Proc. Of SPIE, 2009, 6030, 60300.
30. T. Ishida, H. Kobayashi, and Y. Nakato, J. Appl. Phys. Lett. 1993, 73, 4344.
31. T. Osada, T. Kugler, P. Broms, and W. Salaneck, Synth. Met. 1998, 96, 77.
32. J. Kim, M. Granstrom, R. Friend, N. Johansson, W. Salaneck, J. Appl. Phys. 1998, 84, 6859.
33. S. A. VanSlyke, C. H. Chen, and C. W. Tang, Appl. Phys. Lett., 1996, 69, 2160.

34. A. Elschner, F. Bruder, F. Jonas, and S. Thurm, Synth. Met., 2000, 111, 139.

35. Wei Hu, Yi Zhao, Chunsheng Ma, and Shiyong Liu, Microelectronics Journal, 2007, 38, 509.

36. Jeongmoon Kim, Minchul Song, Hyunmin Hwang, and Chinho Park, Korean J. Chem. Eng., 2005, 22, 643.

37. Tao Y, and C. W. Ko, Synth. Met., 2002, 126, 37.

38. D. F. O'Brien, M. E. Thompson, and S. R. Forrest, Appl. Phys. Lett., 1999, 74, 442.

39. M. A. Baldo, S. Lamansky, P. E. Burrows, M. E. Thompson, and S. R. Forrest, Appl. Phys. Lett., 1999, 75, 4.

40. Wang Hong, Yu Jun-sheng, Tang Xiao-qing, and Jiang Ya-dong, Optoelectronics Letters, 2008, 4, 0317.

41. J. Shi, C. W. Tang, C. H. Chen, US 5, 1997, 646, 948.

42. Daisaku Tanaka, Hisahiro Sasabe, Yan-Jian Su, and Junji Kido, J. J. Appl. Phys, 2007, 46, pp. L10-L12.

43. C. W. Tang, S. A. Vanslyke, Appl. Phys. Lett. 1987, 913.

44. C. Adachi, R. C. Kwong, P. Djurovich, M. E. Thompson, and S. R. Forrest, Appl. Phys. Lett., 2001, 79, 2082.

45. S. Tokito, Y. Suzuri, H. Kita, and F. Sato, Appl. Phys. Lett., 2003,83, 569.

46. S. A. VanSlyke, C. W. Tang, US 4, 1995, 539, 507.

47. 47Y. Hamada, T. Sano, M. Fujita, and Y. Nishio, Chem. Lett., 1993, 905.

48. J. Kido, J. Appl. Phys., 1993, part 2, 32(7A), L917.

49. C. Adachi, T. Tsutsui, and S. Saito, Appl. Phys. Lett., 1989, 55, 1489.

50. M. Ohta, Y. Sakon, T. Takahashi, and K. Nagai, US 5, 1995, 420, 288.

51. S. Saito, T. Tsutsui, C. Adachi, and Y. Hamada, US 5, 1995, 382, 744.

52. M. Scozzafava, C. H. Chen, G. A. Reynolds, and J. H. Perlstein, US 4, 1985, 514, 481.

53. T. M. Kung, and C. H. Chen, US 5, 1993, 236, 797.

54. J. Shi, C. W. Tang, and C. H. Chen, US 5, 1997, 646, 948.

55. S. Shionoya and W. M. Yen, "Phosphor handbook", CRC press, Boca Raton, 1999, p. 64

56. M. A. Baldo, D. F. O'Brien, and S. R. Forrest, Phys. Rev. B, 1999, 60, 14422.

57. C. W. Tang, S. A. VanSlyke, and C. H. Chen, J. Appl. Phys., 1989, 65, 3610.

58. M. Klessinger and J. Michl, Excited States and Photochemistry of Organic Molecules (VCH Publishers, New York, 1995)

59. M. A. Baldo, D. F. O'Brien, and S. R. Forrest, Nature, 1998, 395, 151

60. C. C. Wu, C. I. Wu, J. C. Sturm, and A. Kahn, Appl. Phys. Lett., 1997, 70, 1348.

61. S. Fujita, T. Sakamoto, K. Ueda, and K. Ohta, J. J. Appl. Phys., 1997, 35, part I-350.

62. J. S. Kim, R. H. Friend, and F. Cacialli, Appl . Phys. Lett., 1999, 74, 3084.

63. J. S. Kim, F. Cacialli, A. Cola, G. Gigli, and R. Cingolani, Appl. Phys. Lett., 1999, 75, 19.

64. F. Steuber, J. Staudigel, M. Stossel, J. Simmerer, and A. Winnacker, Appl. Phys. Lett., 1999, 74, 3558.

65. M. Ishii, T. Mori, H. Fujikawa, and Y. Taga, Journal of Luminescence, 2000, 87, 1165.

66. J. S. Kim, M. Granstrom, R. H. Friend, N. Johansson, and F. Cacialli, J. Appl. Phys., 1998, 84, 6859.

67. You ZZ, Dong JY, Phys. Status Solidi A, 2004, 201, 3221.

68. S. K. Sol, W. K. Choi, C. H. Cheng, and C. F. Kwong, Appl. Phys. Lett., 1999, 68, 447.

69. Van Slyke, Chen C.H., and Tang C.W., Appl. Phys. Lett., 1996, 69, 2160.

70. Nuesch F, Rothberg L. J., and Gao Y., Appl. Phys. Lett., 1999, 74, 880.

71. Appleyard SFJ, Willis MR. Opt. Mater, 1998, 9, 120.

72. Hatton RA, Day SR, Chesters MA, Willis MR, 2001, 394.

73. Ishida T, Kobayashi H, Nakato Y., J. Appl. Phys, 1993, 73, 4344.

74. Nguyen TP, Le Rendu P, Dinh NN, and Fourmigue M, Synth. Met., 2003, 138, 229.

75. Jung S, Park NG, Kwak MY, Kim BO, Choi, and Cho YJ, Opt. Mater, 2003, 21, 235.

76. T. Shibata, JP 6, 1994, 122, 874.

77. X. T. Tao, H. Suzuki, T. Wada, S. Miyata, and H. Sasabe, J. Am. Chem. Soc., 1999, 121, 9447.

78. Y. Liu, J. Guo, J. Feng, and Y. Wang, Appl. Phys. Lett., 2001, 78, 2300.

79. D. M. Pai, J. F. Yanus, and M. Stolka, J. Phys. Chem., 1984, 88, 4714.

80. R. J. Holmes, S. R. Forrest, and M. E. Thompson, 2003, 82, 2422.

81. R. Murayama, US 5, 1993, 227, 252.

82. K. Utsuigi, and S. Takano, J. Electrochem. Soc., 1992, 139, 3610.

83. C. Adachi, S. Tokito, T. Tsutsui, and S. Saito, J. J. Appl. Phys., 1988, 27, 269.

84. W. G. Zhu, Y. Q. Mo, M. Yuan, and Y. Cao, Appl. Phys. Lett., 2002, 80, 2045.

85. C. W. Tang, S. A. VanSlyke, and C. H. Chen, J. Appl. Phys., 1989, 65, 3610

86. J. Kido, K. Nagai, Y. Ohashi, T. Skotheim, Cnem. Lett., 1991, 1267.

87. C. Adachi, M. A. Baldo, and S. R. Forrest, Appl. Phys. Lett., 2001, 78, 1622.

88. Chi Yang, and Lin-Lin Gui,Angew. Chem. Int. Ed. 2004, 43, 5009

CHAPTER 3

EXPERIMENTAL PROCEDURES

3.1 Introduction

For the transient electroluminescence phenomena studies, a broad band emitting phosphorescent platinum(II)-pyridyltriazolate complex $Pt(ptp)_2$ and two narrow band emitting europium complexes were chosen as dopants for the organic light-emitting diodes (OLEDs) devices. The detailed synthesis and characteristics of the $Pt(ptp)_2$ complex can be found in Wei-Hsuan Chen's dissertation, University of North Texas, Department of Chemistry [15]. The Eu based emitters are attractive because of their pure red color. Development of phosphorescent emitters instead of fluorescent analogues can potentially increase internal quantum efficiency by 75% [1] due to radiative relaxation from excited triplet states. When added to the 25% efficiency of emission from singlet states, the total efficiency of phosphorescent compounds is 100%. In contrast, fluorescent emitters are characterized by singlet state emission only; therefore, exhibit a maximum internal quantum efficiency of 25% [1]. Emissions from lanthanide/rare earth ions are largely due to interband and intraband transitions localized at the luminescent center. In theory, the *f*-electrons of rare earth ions are well shielded from the chemical environment, and hence are not influenced by external crystal/ligand fields. As a result, *f-f* emission spectra in general consist of sharp, distinct lines. In addition, *f-f* transitions are parity forbidden, and many are also spin forbidden. Thus, the optical transition times are generally slow, typically milliseconds [2]. The line emissions of lanthanides make them ideal candidates for obtaining true color saturation in device applications. Since the first report of OLEDs [3] with a lanthanide emissive layer 20 years ago, many more have been fabricated. However, most are characterized by poor efficiencies,

thermal stabilities, and photo-stabilities [4]. An increase of efficiency is obtained when emitting materials are doped into a suitable host material, and energy transfer from the host to the emissive molecule is achieved. Doping of emissive materials into host materials eliminates both concentration quenching and prevents crystallization of the emissive molecule after thermal deposition [5,6]. Both phenomena are leading causes of decreased luminescence efficiency in OLEDs. Recently Zhou et al. studied the mechanisms of electron and hole transport and energy transfer of $Eu(TTA)_3phen$ (TTA= thenoyltrifluoroacetone, phen= 1,10-phenanthroline) doped into CBP (4,4-*N*,*N*-dicarbazole-biphenyl), and determined that unequal carrier distribution causes electrons and holes to be separated and localized on the $Eu(TTA)_3phen$ and CBP, respectively, causing efficient exciton formation to occur in the combined or doped system. For this study, $Eu(TTA)_3phen$ (TTA= thenoyltrifluoroacetone, phen= 1,10-phenanthroline) was prepared by Dr. Chi Yang of the UNT Chemistry department. Another phosphorescent Eu based complex ($Eu(hfa)_3$ with 4'-(*p*-tolyl)-2,2":6',2" terpyridine (ttrpy)) was synthesized for comparison with the $Eu(TTA)_3$, where hfa→ hexafluoroacetylacetonato. For more information about $Eu(hfa)_3ttrpy$ (hfa→ hexafluoroacetylacetonato), the reader is referred to the dissertation of Ravi from the Omary group at the UNT Chemistry department [16]. Preparation and fabrication of the OLED devices include organic materials preparation, substrate cleaning, substrate oxygen cleaning-plasma treatment and thin film deposition. Characterizations of the OLEDs include optical, electrical, and chemical characterization.

3.2 Source Materials Preparation

3.2.1 Preparation of the Organic Materials

$Eu(tta)_3$, $Eu(hfa)_3$, and $Pt(ptp)_2$ are all phosphorescent emitters and were synthesized by collaborator at Chemistry department of UNT. The remainder of organic materials that were required for OLED fabrication were obtained from Luminescence Technology Corporation. For the synthesis of the $Eu(hfa)_3$ complex, 0.5 g (6.46 $X10^{-4}$ moles) of $Eu(hfa)_3$ was dissolved in a minimum amount of distilled tetrahydrofuran (THF). To the solution of $Eu(hfa)_3$, 0.2094 g (6.46 $X10^{-4}$ moles) of 4'-(p-tolyl)-2,2':6',2" terpyridine previously dissolved in a minimum amount of THF was added slowly. The mixture was then refluxed for 30 minutes, and the vapor was diffused with ether to obtain pure crystals. Crystals were obtained in 3 days. The structure of the $Eu(hfa)_3$ complex is shown in Figure 22. The detailed information for the $Eu(TTA)_3$ complex, can be found in the literature [7].

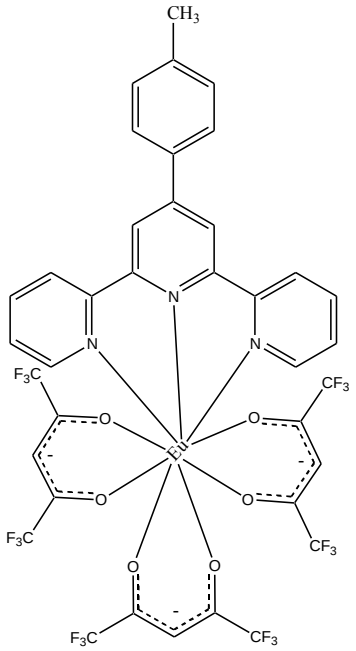

Figure 22: Chemical structure of $Eu(hfa)_3$ttrpy

3.3 Substrate Preparation

The substrate pattern of the ITO was designed by Shepherd's group at UNT, and the indium tin oxide (~20 Ω/square) films were deposited by Luminescence Technology Corporation of Taiwan. The dimension of the substrates is 5cm×5cm in order to fit in the sample holder of our thermal evaporator. The area of the OLEDs was 10 mm^2 pixel which was defined by the overlap of ITO pattern and the cathode. The ITO substrate pattern and the OLED pixel area are shown in Figure 23. (a) and (b), respectively.

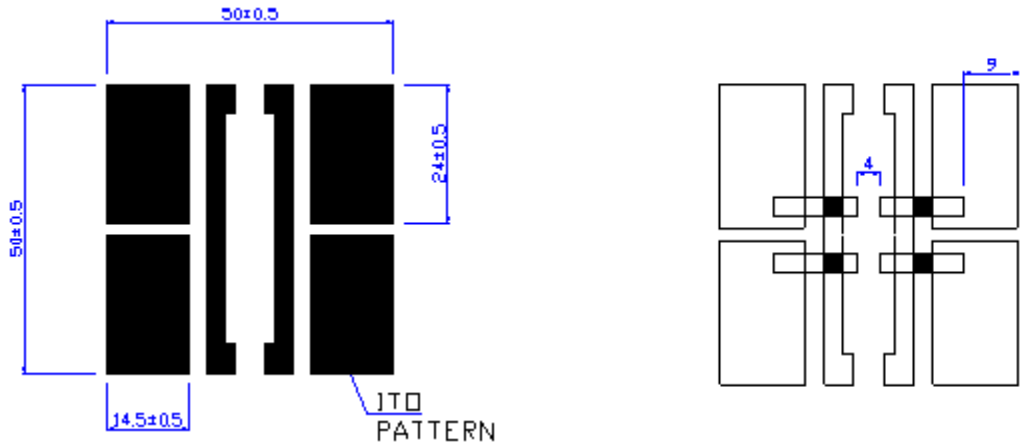

Figure 23: (a) The ITO pattern, (b) Pixel area.

3.3.1 The Procedure of the Cleaning ITO Substrate

As received ITO substrates were ultrasonically cleaned with the deionized water for 10 minutes, then in acetone and methanol for 10 minutes. The ITO substrates were then oven dried for 30 minutes to remove residual water vapor and volatile contaminants. Cleaned ITO substrates were stored under vacuum in a desiccator or moved to vacuum evaporation system for the deposition.

3.3.2 ITO Substrate Oxygen Cleaning-Plasma Treatment

The work function of the ITO substrate is very significant for OLED fabrication because it determines the energy barrier between the anode and HTL. The energy barrier between ITO and HTL should be small to allow hole injection which means that the ITO work function must be as large as possible. Plasma treatment is a good method for controlling the work function of ITO. Plasma treatment also removes the hydrocarbons that lower the ITO work function. In our lab, an oxygen plasma is used for the ITO substrate treatment. Microwave power at a frequency 2.45 GHz is used to generate the plasma. The oxygen plasma cleans organic and some inorganic contaminants from the ITO film and induces surface dipoles that increases the work function. Digitally controlled microwave power (410W) generates the O_2 plasma at a working pressure of 300 mTorr. The work function of ITO substrate can be increased from 4.7 eV to 5.0 eV that reduces the energy barrier for hole injection at the interface between ITO and HTL and improves the device driving voltage, efficiency, and lifetime.

3.4 Thin Film Growth

Several parameters including accurate thickness, suitable working pressure, and low deposited rate are important for this research. The organic layers and metal materials were grown on the pre-cleaned glass by thermal evaporation at a working pressure of 10^{-6} to 10^{-7} Torr for thickness calibration, photoluminescence measurements, composition studies, etc.

3.4.1 Vacuum System

The thermal evaporation system was mechanically pumped to 5×10^{-2} Torr, then cryo pumped to 10^{-7} Torr. A combination of thermocouple gauges and ion gauges were used to measure pressure over the whole range.

3.4.2 Thermal Deposition of Organic Layers

All of the organic materials are deposited by thermal evaporation system which is the most common method of organic thin film deposition. The tantalum boats are available from the R. D. Mathis Company and are reusable. The type of boats and covers used in this study are shown below in Figure 24 (a) and (b), respectively.

Figure 24: (a) Tantalum boat (b) The cover of tantalum boat.

The boats are connected to copper electrodes, and the computer controlled power is applied using 250A Sorensen DC power supplies to achieve resistive heating. Thickness monitors are integrated with power supplies through a PID loop for precise power delivery and deposition rate control. At suitable vacuum levels, the organic materials in the boats sublime and deposit onto the substrate surface. Lowering the pressure in the chamber, increases the mean free path for vapor particles. Most films are deposited at rates of ~ 1A/s with substrate rotation to

improve the film uniformity. A schematic deposition for the organic materials is shown in Figure 25.

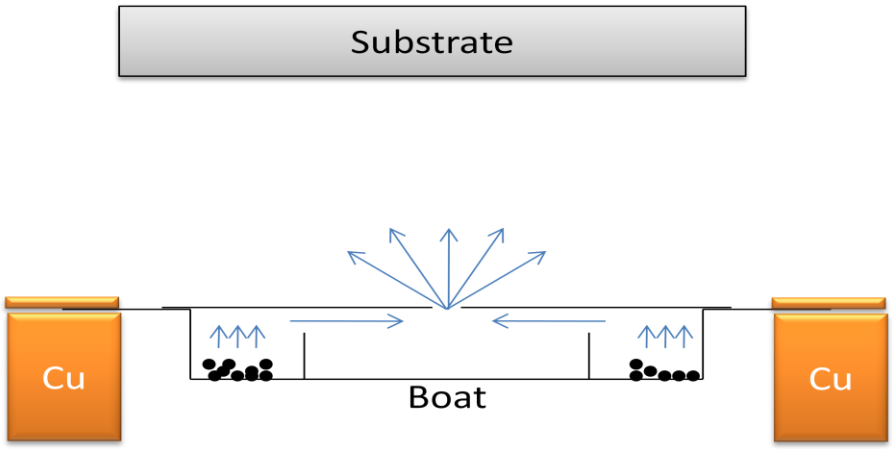

Figure 25: The schematic deposition of the vacuum system

3.4.3 Thermal Deposition of Metals (Cathodes)

Mg:Ag co-deposited layers and LiF/Al bi-layers were used as cathodes in this research. The boat for Mg deposition was the same as that of the organic materials, but the boat for the Ag was different as. Figure 26 (a) shows. Controlling the deposition rate of the magnesium and silver was essential for obtaining the Mg:Ag alloy in a 10:1 ratio. EDX was used to determine the alloy composition. Table 2 shows the best deposition parameters for the Mg:Ag alloy with the targeted composition. LiF/Al is also a common cathode for organic devices because LiF is a low work function material that reduces the Schottky barrier height between the metal cathode and adjacent organic layer. Figure 26 (b) depicts the basket boat that was used for the deposition of Al.

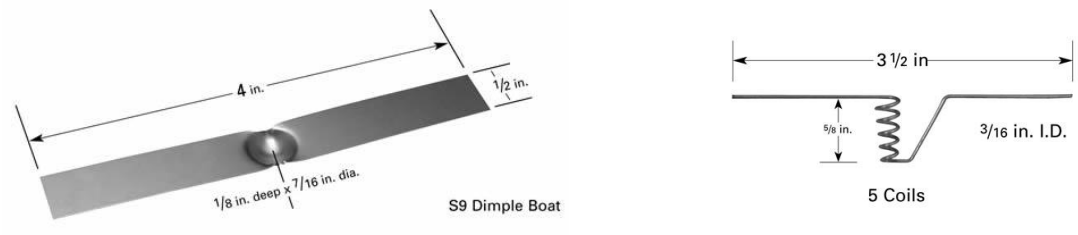

Figure 26: (a) The boat of the Ag material (b) The boat for the Al material.

Table 2: The ratio of Mg:Ag obtained at different deposition rates

Cathode	Rate	Ratio (at%)	Rate	Ratio (at%)
Mg	12.5A/S	9	14A/S	11-14
Ag	0.3A/S	1	0.3A/S	1

3.5 Characterization

Photoluminescence (PL), Photoluminescence excitation (PLE), composition of the cathode, and thickness were measured by using a stylus profilometer. Methods for optical and electrical characterizations are introduced in the following sections.

3.5.1 Surface Profilometer

Topography and roughness of the films were measured by a Dektak 150 surface profilometer. In this research, glass slides and cover slips were used to create edges in the deposited films. Figure 27 shows the architecture of a surface with steps, and the schematic diagram of the profilometer can be seen in Figure 28.

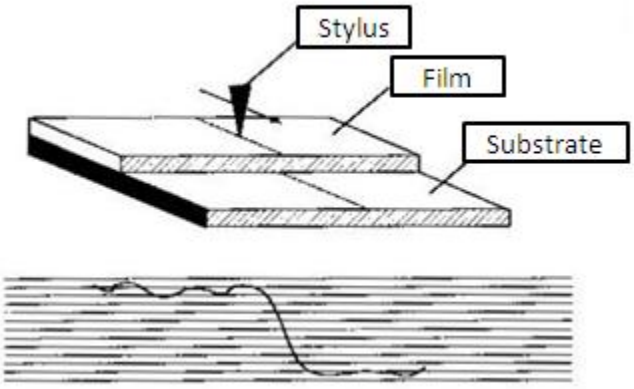

Figure 27: The architecture of the surface

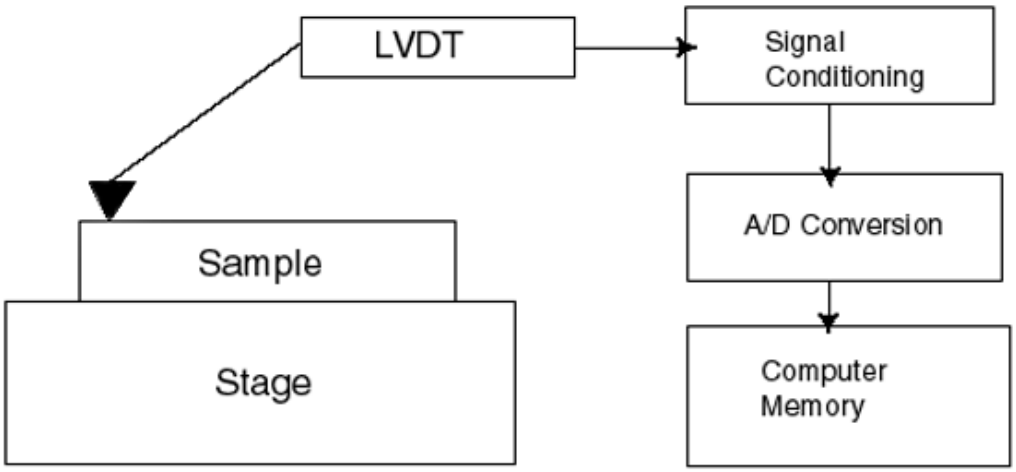

Figure 28: Block diagram of the Dektak 150 Architecture

3.5.2 Chromaticity

For the quantitative chromaticity and colorimetry, the first standard method was created by the International Commission on Illumination (CIE) and is used to define the exact position of

a light source in color space. A two-dimensional graph is plotted according to three unit-less values that are defined by CIE coordinates (x, y, and z). The CIE diagram provides a quantitative color comparison of different emitting sources. Monochromatic sources in the CIE system are regarded as the primary colors of red, green, and blue (RGB). As shown in Figure 29 [8], the tristimulus values are denoted as X, Y, and Z in the CIE 1931 diagram.

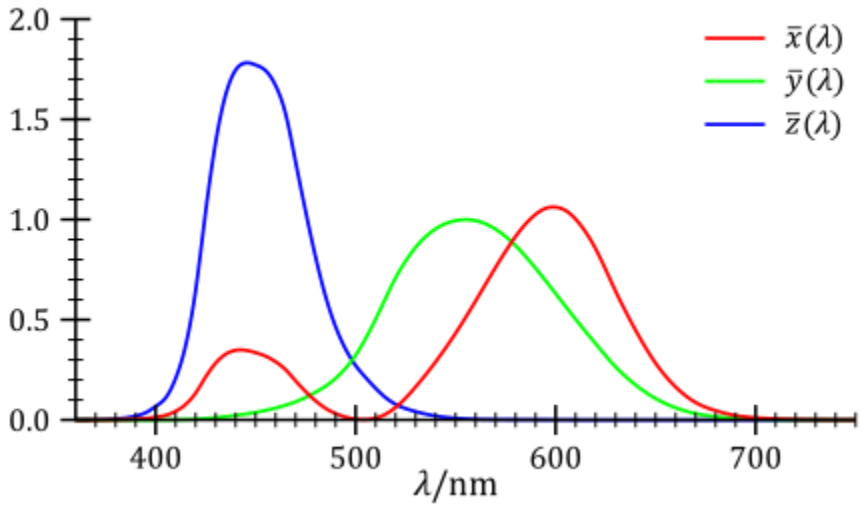

Figure 29: The tristimulus values are denoted as X, Y, and Z [8]

Tristimulus values ($\bar{x}, \bar{y}$, and $\bar{z}$) are described as the three primary colors: (Red, Green, and Blue), and the chromatic coordinate numbers are calculated according to [8].

$$x = \frac{X}{X + Y + Z}$$

$$y = \frac{Y}{X + Y + Z}$$

$$z = \frac{Z}{X + Y + Z}$$

For the 1931 CIE diagram, two chromaticity numbers are usually expressed as x and y, and are plotted in the CIE diagram shown in Figure 30 [9,10]. In this study, device electroluminescence (EL) was measured with Photo Research PR-650 camera, that provides the color rendering index (CRI), correlated color temperature (CCT), brightness, optical power, and CIE. The Photo Research PR-650 camera was integrated with a Keithley 2420 via LabView to obtain quantitative electro-optical characterization of the devices. Performance parameters of OLEDs such as luminous and power efficiency, current efficiency, brightness, external quantum efficiency and color temperature were all measured.

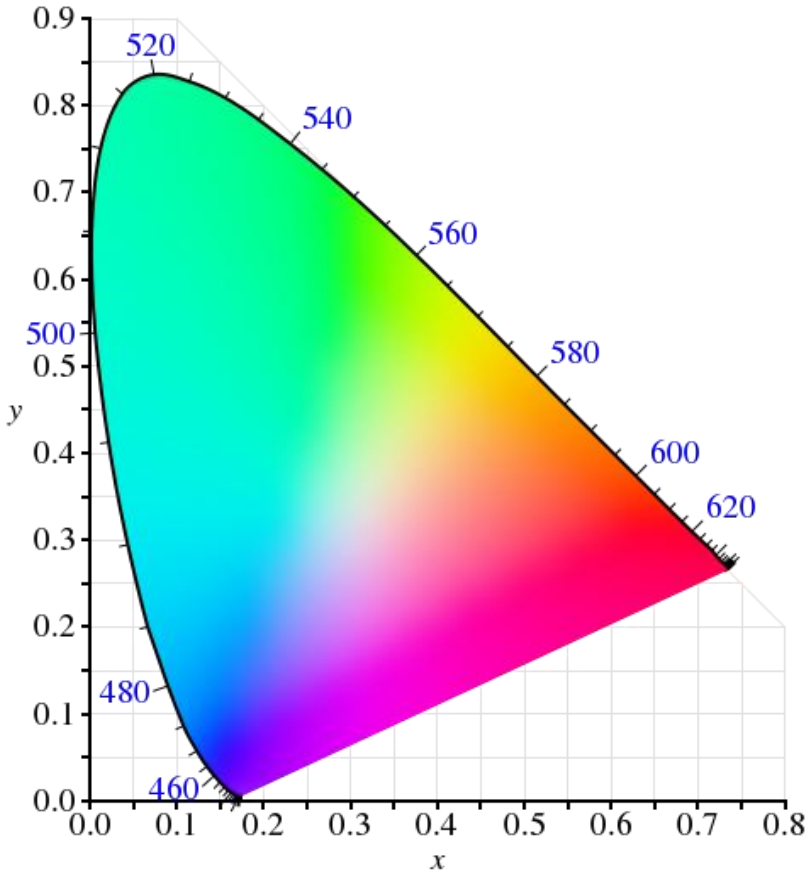

Figure 30: 1931 Commission de L'Eclariage chromaticity diagram. Reproduced from references [9,10].

3.5.3 Photoluminescence (PL) and Photoluminescence Excitation (PLE)

Photoluminescence (PL) is radiative recombination due to optical excitation. The formula between emission wavelength and energy is shown in 3.1

$$E(eV) = \frac{1240}{\lambda(nm)} \quad \text{----------3.1}$$

For photoluminescence measurements, monochromator 1 is kept at a specific excitation wavelength, and monochromator 2 measure the spectrum of light emitted by the sample. For photoluminescence excitation (PLE) monochromator 2 is kept at a specific detecting wavelength, and the excitation wavelength is changed by monochromator 1 to determine the optimal excitation wavelength for the emission being monitored as shown in Figure 31. In order to increase the signal/noise ratio, chopping and lock-in detection were used. The PL and PLE of the common hole transport materials and electron transport organic materials such as TPBI, NPB, Alq3, CBP, and mtdata were measured for this study as shown in Figures 32~35. The PL excitation wavelengths as well as the PLE monitoring wavelengths are shown in these figures. The PL and PLE of the phosphorescent Eu dopant material are shown in Figure 36. The emission main peak was at 620 nm, and 316 nm was the optimal excitation wavelength.

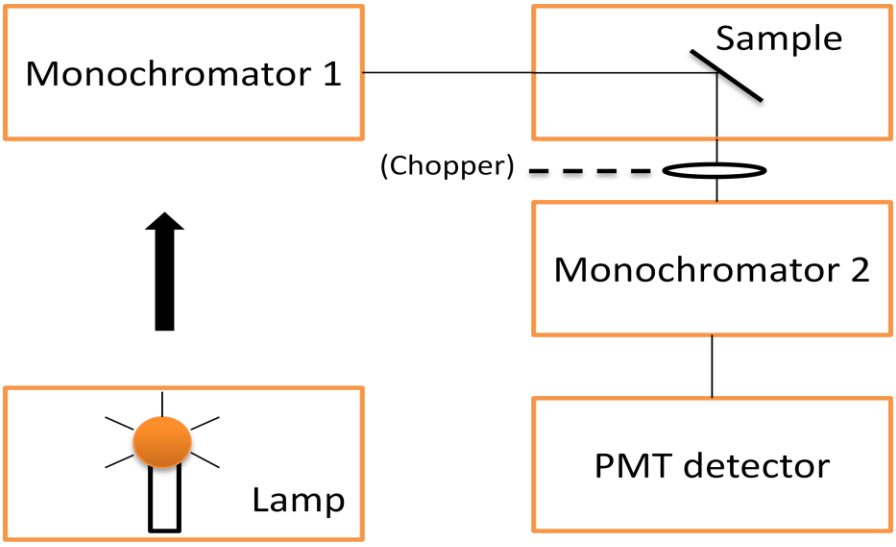

Figure 31: The schematic set-up of the PL and PLE

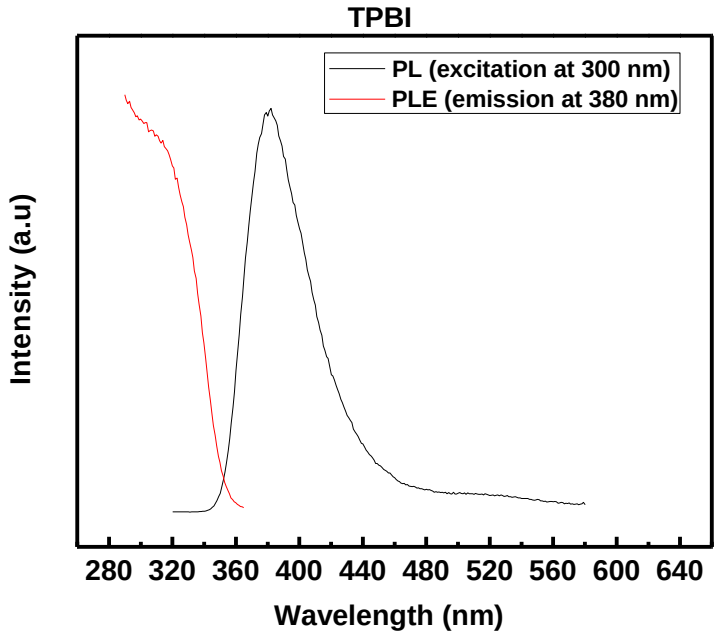

Figure 32: The PL and PLE of TPBI

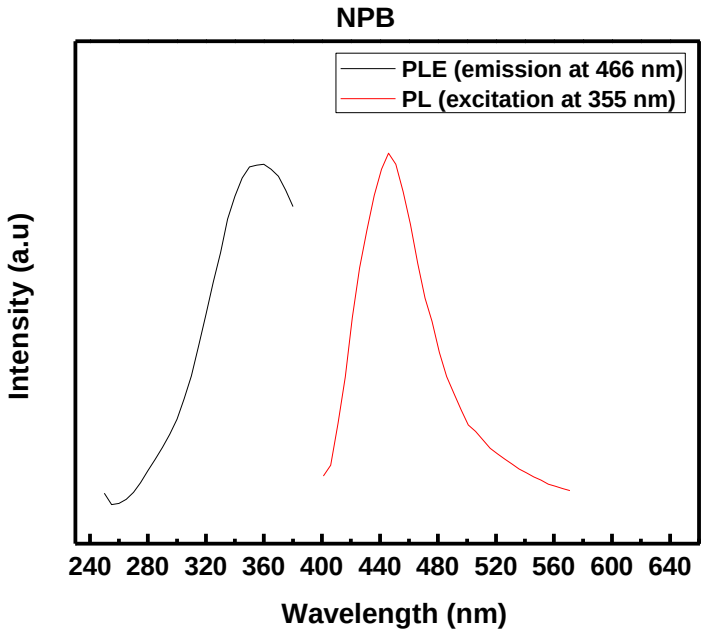

Figure 33: The PL and PLE of NPB

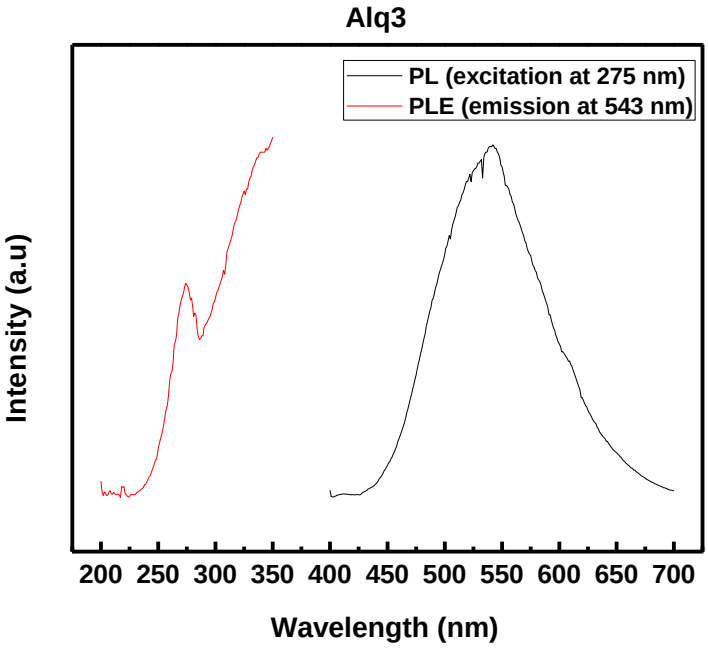

Figure 34: The PL and PLE of Alq3

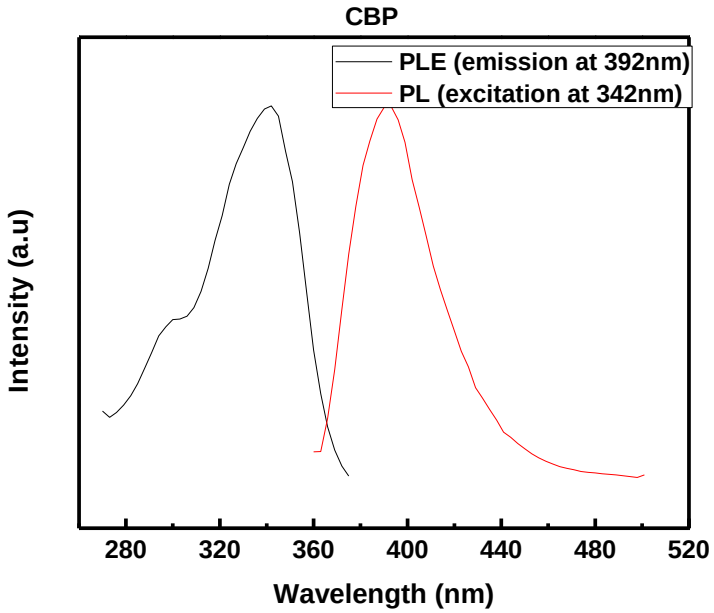

Figure 35: The PL and PLE of CBP

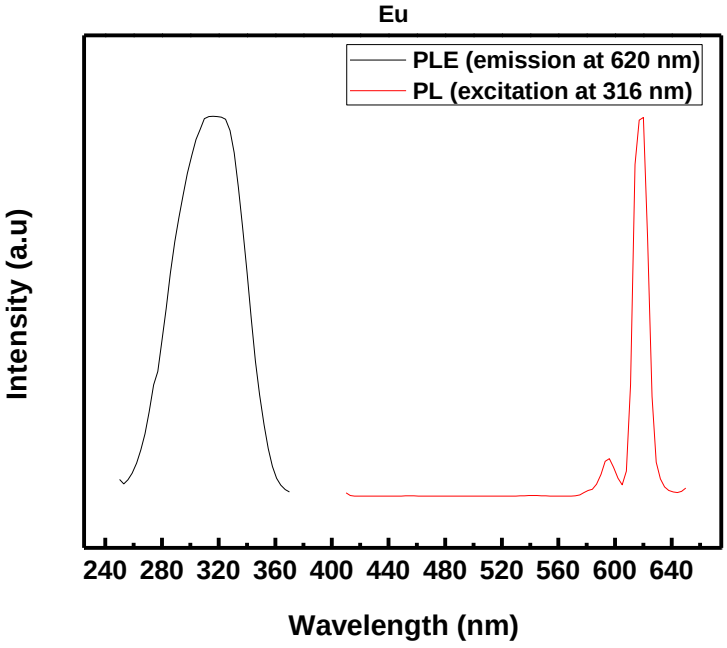

Figure 36: The PL and PLE of $Eu(hfa)_3$

3.5.4 Electroluminescence (EL) Spectrum

Electroluminescence (EL) from the OLEDs was recorded by the Photo Research PR-650 spectrometer. The organic light-emitting diodes were electrically driven by the Keithley 2420 power supply and the output light was measured by Photo Research PR-650 spectrometer. Figure 37 is the electroluminescence (EL) of OLEDs with an emissive layer consisting of 4.5% $Eu(hfa)_3$ doped into the common host CBP.

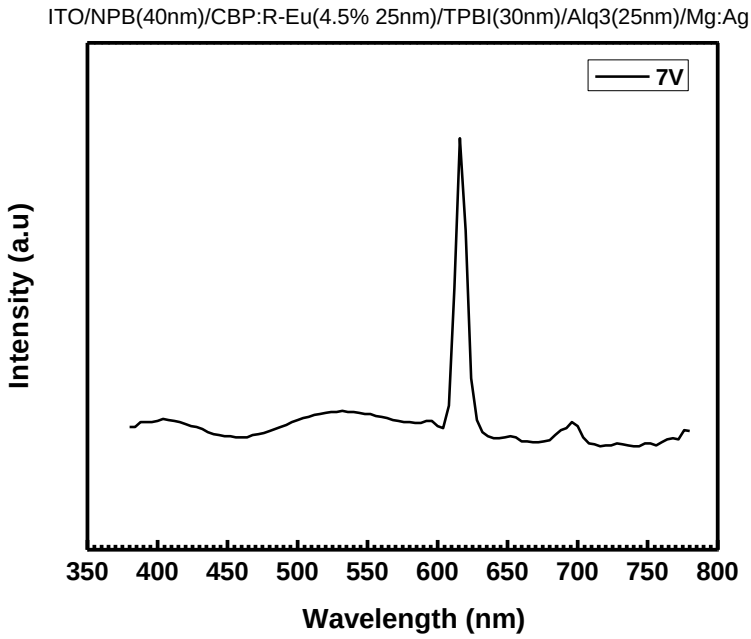

Figure 37: The electroluminescence of 4.5% $Eu(hfa)_3$:CBP

3.5.5 The Set-up for the Thin Film Lifetime

For the PL lifetime, the sample is excited by a light source, whereas for EL lifetime the sample electrically excited. A laser, a sample compartment, monochromator, and a PMT detector are used in the set-up for PL lifetime measurement. The fluorescence lifetime spectrofluorometer was manufactured by PTI, and featured an excitation range of 185nm to 920 nm. The

monochromator acts as the wavelength selector, and two different detectors can be used depending on if the decay is fast or slow. For fast decays (<1μs), a fluorescence detector is used, and a phosphorescence detector is used for slow decay (>1μs). Once the film is excited by the light source, electrons are promoted to the excited state and return back to ground state after a finite period of time. The lifetime of the sample is defined as the average time for electrons to return back to ground state from the excited state. The equipmental set-up is shown in Figure 38.

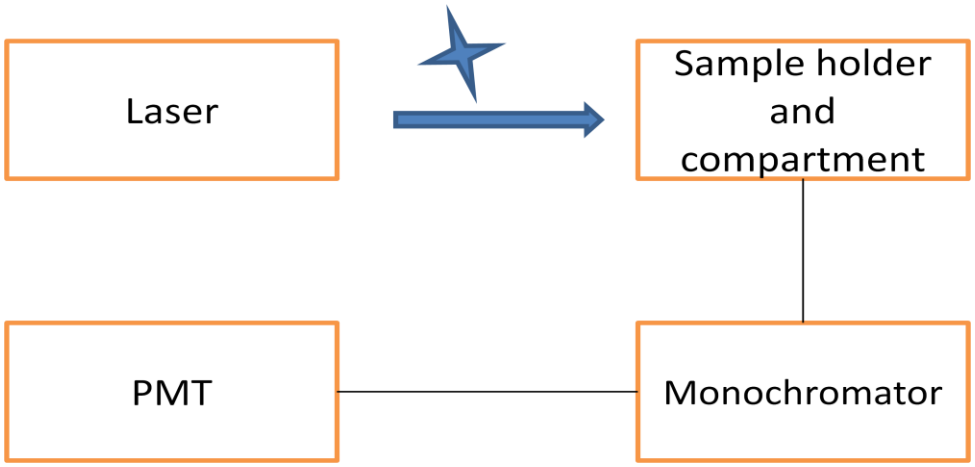

Figure 38: The equipment set-up of the lifetime measurement

3.5.6 Transient Electroluminescence

The determination of the charge carrier mobility and lifetime can be measured by various methods which were discussed in chapter 2. In this study, transient electroluminescence (EL) was used to measure the lifetime of the OLED devices. In addition to charge carrier mobility and lifetime, the phenomenon of trapping and de-trapping in OLED devices were measured by the transient electroluminescence (EL) technique [12,13]. A most interesting behavior in the study of transient electroluminescence (EL) was the delayed recombination feature which was reported by K. Leo and S. Reineke's group [14]. In some of the designed OLED structures of this study,

the delayed recombination was investigated with the transient electroluminescence (EL) method. For the transient EL measurements, small active pixel area OLEDs were used in order to keep the capacitance low. The devices were driven by a pulsed voltage of various duration and short rise time (~ns).from Tektronix AFG 3102 pulse generator. The output transient EL signal was detected by a PMT attached to a monochromator that selected the detection wavelength, and recorded by a Tektronix DPO 4000 digital oscilloscope for further analysis. The RC time constant of the OLEDs were measured with a Solartron SI 1260 impedance analyzer, respectively. The schematic of the transient EL set-up is shown in Figure 39.

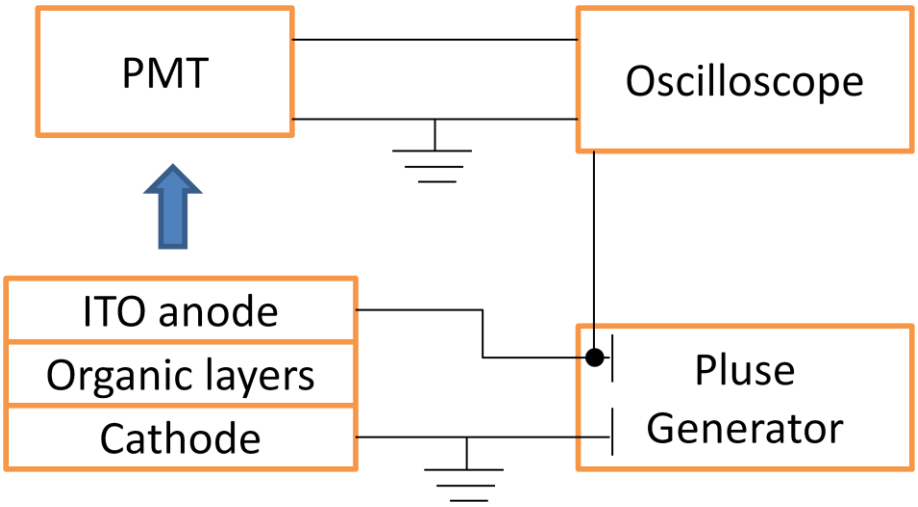

Figure 39: Schematic setup of transient EL

3.6 References

1. Review: Yersin, H., Top. Curr. Chem. 2004, 241, 1.
2. For full review, see: Evans, R. C.; Douglas, P.; Winscom, C. J. Coord. Chem. Rev. 2006, 250, 2093-2126.

3. a) Kido, J.; Nagai, K.; Ohashi, Y., Chem. Lett. 1990, 220, 657-660. b) Kido, J.; Nagai, K.; Okamoto, Y.; Skotheim, T., Chem. Lett. 1991, 235, 1267-1270.
4. a) Li, W. L.; Yu, J. Q.; Sun, G.; Hong, Z. R.; Yu, Y.; Zhao, Y.; Peng, J. B.; Tsutsui, T., Synth. Met., 1997, 91, 263-265. b) Gao, X. C.; Cao, H.; Huang, C. H.; Li, B. G.; Ibrahim, K.; Liu, F. Q.; Umitani, S., Chem. Phys. Lett., 1998, 297, 530-536
5. Wakimoto, T; Yoshinobu, Y.; Funaki, J.; Tsuchida, M.; Murayama, R.; Nakada, H.; Matsumoto, H.; Yamamura, S.; Nomura, M., Synth. Met., 1997, 91, 15-19.
6. Chen, C. H.; Tang, C. W.; Shi, J.; Klubek, K. P., Macromol. Symp., 1997, 125, 49-58.
7. Chi Yang, Li-Min Fu, Yuan Wang, Jian-Ping Zhang, Xi-Cheng Ai, Yi-Fang Qiao, and Lin-Lin Gui, Angew. Chem. Int. Ed. 2004, 43, 5009.
8. F. W. Billmeyer, Jr., M. Saltzman. *Principles of Color Technology*, 2nd edition, John Wiley & Sons, Inc., New York, 1981.
9. CIE 1971, International Commission on Illumination. Colorimetry: Official Recommendations of the International Commission on Illumination. Publication CIE No. 15 (E-1.3.1) 1971, Bureau Central de la CIE, Paris, 1971.
10. A. Zukauskas, M. S. Shur, and R. Gaska, Introduction to Solid State Lighting, Wiley (2002).
11. Dieter K.Schroder:Semiconductor material and device characterization
12. T. C. Wong, J. Kovac, L. S. Hung, and S. T. Lee, Chem. Phys. Lett. 2001, 334, 61.
13. Pankaj Kumar, and R P Tandon, J. Phys. D. 2007, 40, 7313.
14. S. Reineke and K. Leo, Phys. Stat. Sol. 2008, 245, 804.\
15. Wei-Hsuan Chen, Department of Chemistry at UNT, 2010
16. Ravi Arvapally, Department of Chemistry at UNT, 2010

CHAPTER 4

STUDY OF THE LIFETIME AND DELAY TIME OF ORGANIC LIGHT-EMITTING BY TRANSIENT ELETROLUMINESCENCE METHOD

4.1 Introduction

As mentioned earlier, low carrier mobility is a limiting factor in organic semiconductors. In some research groups [1-3], an electron blocker layer/hole blocker layer was placed between the hole transport layer/electron transport layer and emissive layer in order to confine the holes and electrons to the emissive layer, and thus improve the performance of the OLEDs. The basic structure device without an electron blocker layer used by our group has been published [4]. The peak power efficiency improved by more than 100% after adding an electron blocker layer to the structure. The effect of the electron blocker layer has also been reported by Thompson, Forrest and co-workers [5]. The peak power efficiency was 7.3 lm/W without the electron blocker layer (Irppz) which improved to 12.2 lm/W with the Irppz electron blocker. Other notable research for improving the performance of the OLEDs used [6,7] higher mobility materials to improve the performance of OLEDs. Zheng and Xue [8] reported that the performance of a device with TAPC as the hole transport material was better than that with NPB because the TAPC had a higher charge mobility, and provided a bigger barrier for blocking electrons from entering the hole transport layer. The LUMO and mobility of TAPC are 2.0eV and 1.0×10^{-2} cm^2/Vs compared to 2.4eV and 5.0×10^{-4} cm^2/Vs for NPB [9,10]. Gnade's group reported the improvement of OLEDs by controlling the carrier recombination zone. In order to get good charge balance, excitons must form and recombine at the center of the emissive layer [11]. More recently, Tandon's group has reported the method of transient electroluminescence to investigate

the performance of the OLEDs [12]. The charge carrier and trapping in the device can be measured by the transient electroluminescence (EL).

In this chapter, different OLED structures were studied for the lifetime and delay time by the transient electroluminescence method. The lifetime of the devices depends on the emissive layer of the OLEDs. Based on the concepts above, the carrier mobility in the emissive layer was estimated by using the transient EL. For the lifetime comparison Eu based complexes were compared with the Pt based complex. For the Pt based devices, only the best structures were chosen for the transient electroluminescence (EL) measurement. For the emissive layer, the phosphorescent dopant, $Pt(ptp)_2$=bis[3,5-bis(2-pyridyl)-1,2,4-triazolato] platinum(II) was doped in the common OLED host 4,4'-bis(carbazol-9-yl)triphenylamine (CBP). NPB and TAPC were chosen as the different hole transport layers, and the MCP and TPBI were chosen as the electron blocker layer and electron transport layer, respectively. The overall results of this work show that the TAPC is the best hole transport material due to its fast hole mobility and good electron blocking. Delayed recombination occurred in the transient electroluminescence (EL) of the heavily doped $Pt(ptp)_2$ devices with MCP as an electron blocker. The delayed recombination of the transient electroluminescence (EL) was dependent on the various frequencies and pulse lengths, and can be explained by disorder-induced localization [13] in which the charge carrier hops from a localized state to another localized state. The data suggests that the interfacial traps are localized between the emissive layer and electron blocker. The relation between the PL and transient EL is also discussed in this chapter.

4.2 The Study of the Thin Film Lifetime

In order to investigate the lifetime of the OLEDs, the emissive layer thin films were studied prior to device investigation. The 4.5% $Eu(hfa)_3$: CBP thin films and neat $Eu(hfa)_3$ films were deposited and their life time was measured using a PTI fluorescence lifetime spectrofluorometer. Figure 40 shows the PL and PLE of the 4.5 % Eu(hfa)3: CBP films. The excitation was at 330 nm for the 615 nm emission peak ($^5D_0 \rightarrow {}^7F_2$). The peak of CBP is also detected in the PL spectrum and indicates incomplete energy transfer from the host to the guest. Figure 41 is the lifetime of a 4.5% $Eu(hfa)_3$:CBP film that was measured using a nitrogen laser with 500-ps pulses. An exponential decay was obtained with a lifetime of around 0.85 millisecond of 615 nm. For the neat $Eu(hfa)_3$ films, the PL and PLE can be seen in Figure 42. The emission at 616 nm is due to the $^5D_0 \rightarrow {}^7F_2$ transition. The lifetime of the neat $Eu(hfa)_3$ film was measured to be around 1 millisecond at 616 nm as shown in Figure 43. In contrast to the $Eu(hfa)_3$ film, 65% $Pt(ptp)_2$ doped in CBP was used to study the lifetime of Pt phosphorescent emitter. As seen in Figure 44, the PL and PLE of the 65% $Pt(ptp)_2$ in CBP films is characterized 582 nm PL emission by exciting at 350 nm. This emission is attributed to excimers. The lifetime of the 65% $Pt(ptp)_2$: CBP film at the peak wavelength of 582 nm was around 638 ns which can be seen in Figure 45.

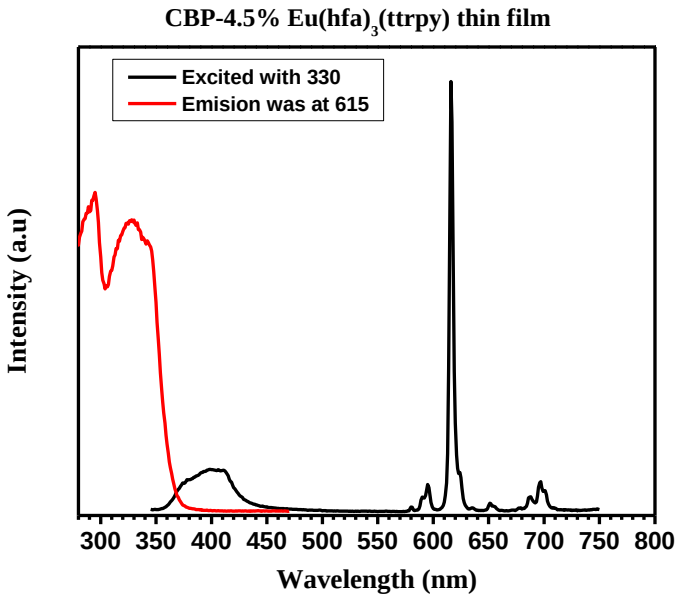

Figure 40: The PL and PLE of the 4.5% Eu(hfa)3: CBP films

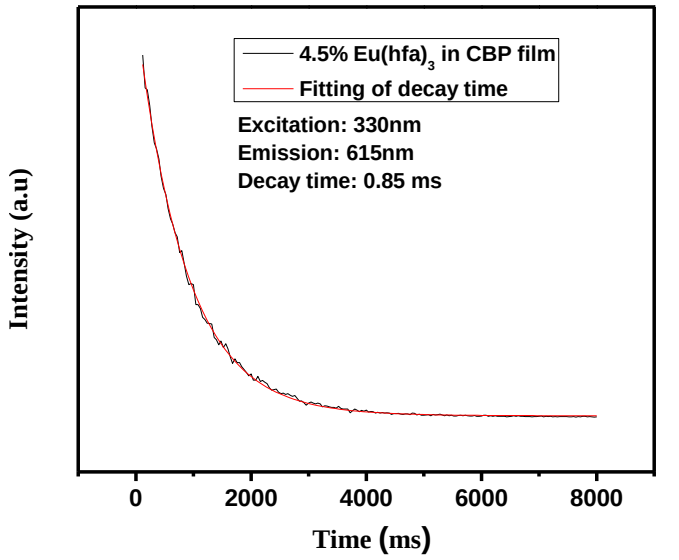

Figure 41: The lifetime of 4.5% $Eu(hfa)_3$:CBP film

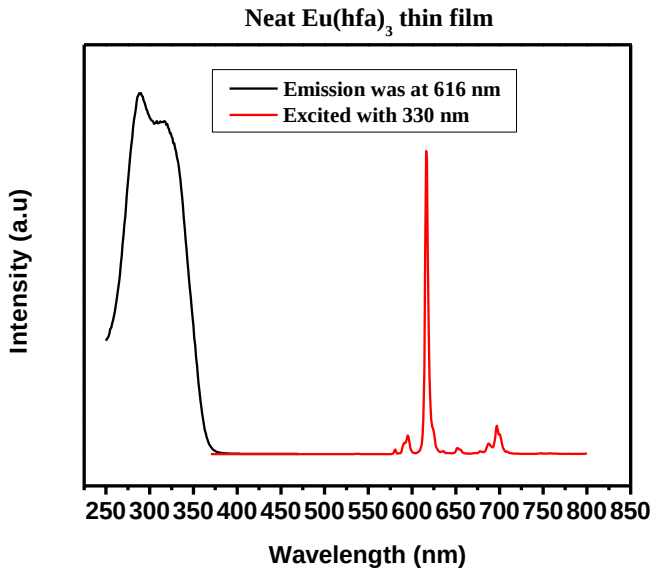

Figure 42: The PL and PLE of neat $Eu(hfa)_3$:CBP films

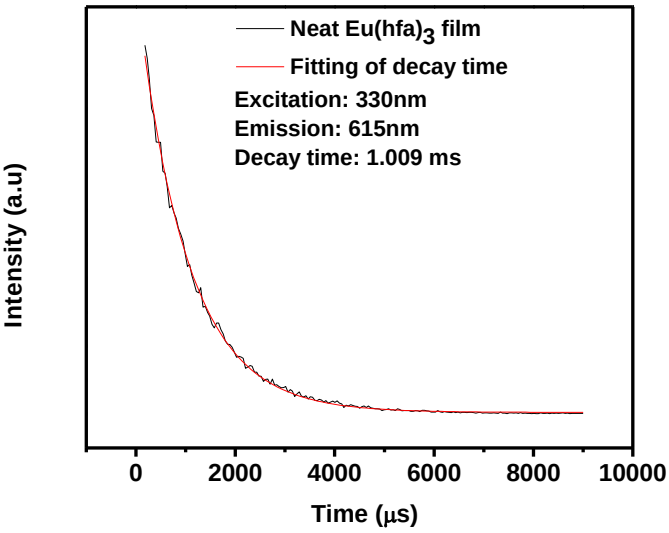

Figure 43: The lifetime of neat $Eu(hfa)_3$ film

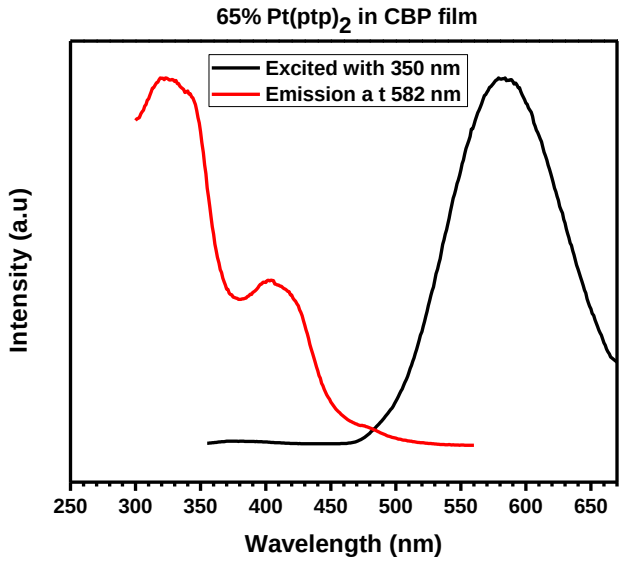

Figure 44: The PL and PLE of 65% Pr(ptp)2 in CBP films

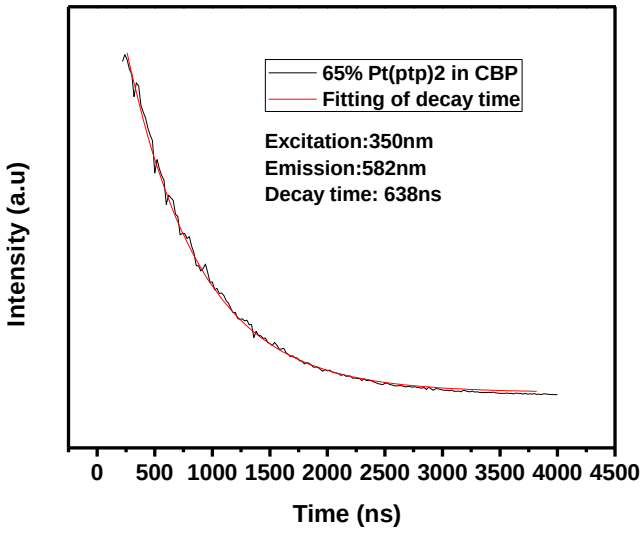

Figure 45: The lifetime of 65% Pr(ptp)2 in CBP films

4.3 Setup and Method for Delay Time from Transient Electroluminescence

4.3.1 The Structure of $Pt(ptp)_2$ Based Devices

The organic light emitting diodes with the structure ITO/NPB (40nm)/CBP:$Pt(ptp)_2$ (x%, 25nm)/TPBI (30nm)/Cathode were studied and reported in 2009 [4]. The Eu based devices are discussed in chapter 5. In both phosphorescent dopants (Pt and Eu), the characterization of devices were hugely different due to the difference in emission peak, molecular structure, and lifetime. In contrast to the simple structure $Pt(ptp)_2$ based device, the electron blocking material MCP was added to the structure and due to exciton confinement, the $Pt(ptp)_2$ based devices with the blocking layer showed improved performance. The structure of the device with the blocking layer was ITO/NPB (40 nm)/MCP(10 nm)/CBP:$Pt(ptp)_2$ (25 nm)/TPBI (30 nm)/Cathode. The 65% $Pt(ptp)_2$ based device with MCP was the best among devices with different $Pt(ptp)_2$ concentrations and therefore the 65 % $Pt(ptp)_2$ based devices with and without MCP were chosen for the study using transient EL The structure of the $Pt(ptp)_2$ based devices were shown in Figure 46 .

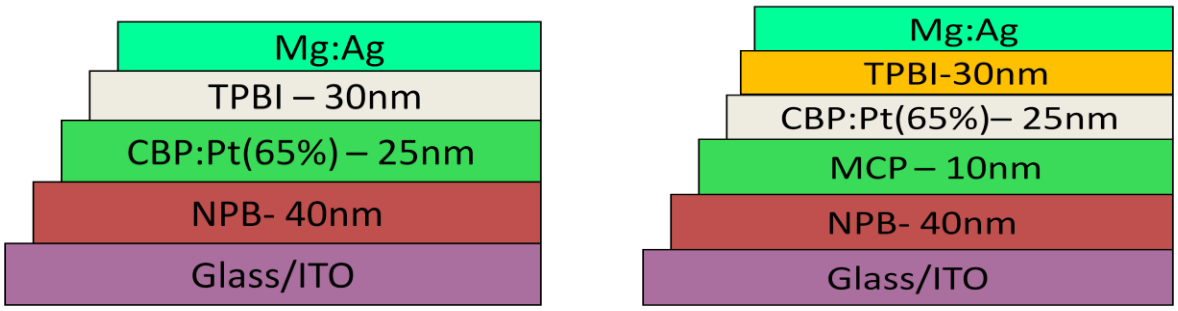

Figure 46: The $Pt(ptp)_2$ based device with and without MCP

4.3.2 The Delay Time of the $Pt(ptp)_2$ Based Devices by Using Transient Electroluminescence

Due to the requirement of the low capacitance, fresh, small active area of OLEDs were prepared for the EL transient measurement. The RC time constant of the devices were obtained using a Solartron SI 1260 impedance analyzer. Devices with and without MCP were compared. A pulse generator integrated with a fast storage oscilloscope, and fast photo multiplier tube (PMT) were used to measure the transient electroluminescence (EL) response as previously described. The transient electroluminescence (EL) at certain voltage was measured at various frequencies and duty cycles. Before the transient electroluminescence (EL) study, the EL spectra of the OLEDs were measured. As seen in Figure 47, the EL spectrum of the ITO/NPB (40nm)/CBP:$Pt(ptp)_2$ (25nm)/TPBI (30nm)/Cathode device clearly shows the 572 nm $Pt(ptp)_2$ emission peak and a shoulder NPB at 450 nm indicating electron were not confined to the emissive layer. This problem was solved by adding the electron blocking material MCP to the OLED structure as Figure 48 shows. Both of the band diagrams are shown in Figure 49 and 50. The power efficiency was 2.28 lm/W in the 65% $Pt(ptp)_2$ based device without a MCP layer, and it increased to 24 lm/W after adding the electron block layer MCP. It was more than 100 percent improvement of power efficiency and shows the function of electron blocker layer. Table 3 summarizes the difference.

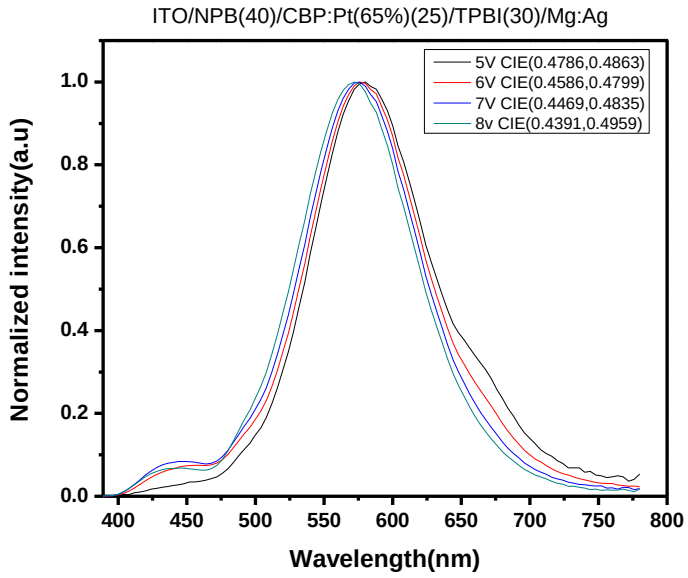

Figure 47: EL of 65% Pt:CBP device without MCP

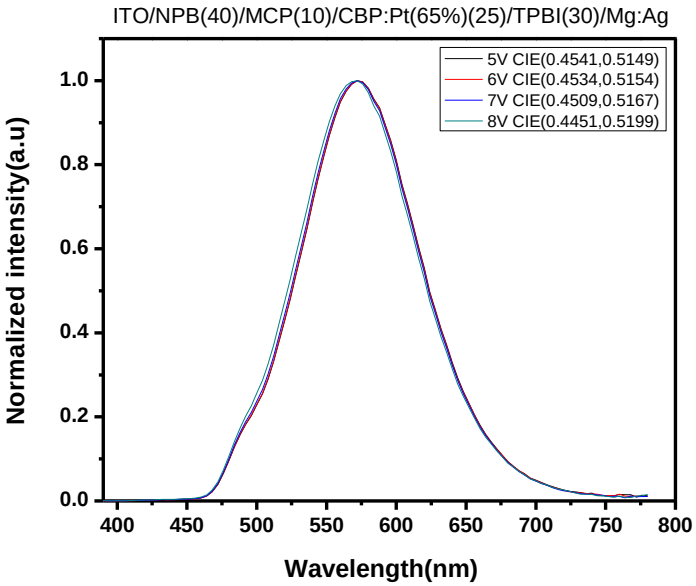

Figure 48: EL of 65% Pt:CBP device with MCP

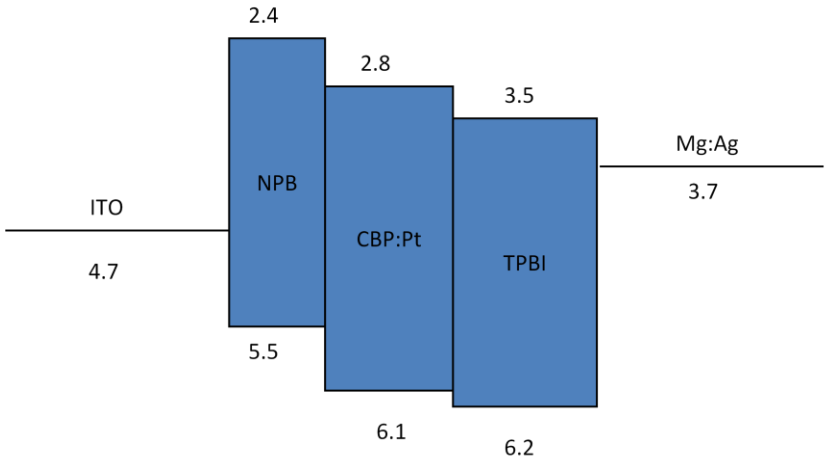

Figure 49: Band diagram of 65% Pt:CBP device without MCP

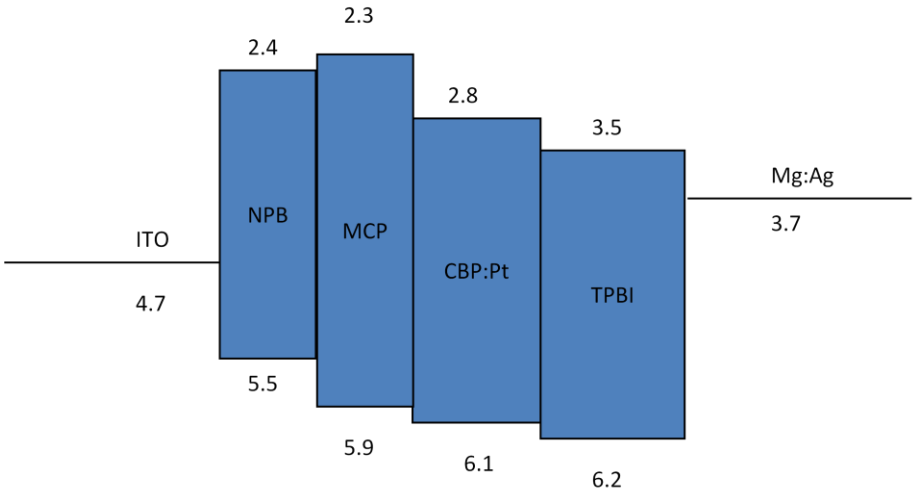

Figure 50: Band diagram of 65% Pt:CBP device with MCP

Table 3: Comparison of 65% $Pt(ptp)_2$:CBP devices with and without MCP

Device ID	PE_{peak} (lm/W)	PE_{1000} (lm/W)	EQE_{peak} (%)	EQE_{1000} (%)	V_T (V)
65% Pt(ptp)2 without MCP	2.28	1.17	1.69	1.09	4.2
65% Pt(ptp)2 with MCP	24	16.4	10.64	9.79	3.8

Figure 51 is the EL response to a pulsed DC signal operating at a frequency of 100kHz frequency with a 50% duty cycle. As Figure 51 shows, there is a delay in the rise of the EL signal after the pulse has been applied. In addition, the rise time was faster with increasing pulse voltage [14,15], and the delay time was shorter at 9 V than that at 7 V. This indicates that EL threshold and carrier mobility are field dependent. The delay time is related to recombination of holes and electrons after applying the voltage [12]. The model of the delay time is $t_d=t_{inj}+t_{trans}$, where the charge injection delay time is t_{inj} and the charge transport time is t_{trans} The charge injection time (t_{inj}) is related to the RC time constant of the device and is defined by equation 5.1 where V_{max} is the maximum of the applied rectangular voltage, RC is the time constant of the device and V_{th} is the threshold voltage of device [16]. The charge transport time (t_{trans}) is defined by equation 5.2 and 5.3 which assume the electron mobility is significantly larger than the mobility of holes. Here d_e is the travel distance for electrons to recombine with the holes in emission layer, d is the total thickness of organic layers, u_e is the electron mobility, V is the

applied voltage, and V_{bi} is the built-in voltage. From the literature [12], the value of V_{bi} is taken to be the difference between the work functions of the cathode and anode. Therefore, the value of the V_{bi} is 1.0 eV given the work functions of ITO and Mg:Ag are 4.7 eV and 3.7 eV, respectively.

$$t_{inj} = RC \ln\left(\frac{V_{\max}}{V_{\max} - V_{th}}\right) \quad \text{---------- 5.1}$$

$$t_{trans} = \frac{d_e}{(u_e + u_h)E} \quad \text{---------- 5.2}$$

$$t_{trans} = \frac{d_e d}{u_e (V - V_{bi})} \quad \text{---------- 5.3}$$

Transient EL measurements were also performed on device with the MCP electron blocker. As shown in Figure 52 delayed recombination was observed in these devices. The schematic energy diagram of device structure was shown in Figure 50 which can be used to explain the delay recombination behavior in the $Pt(ptp)_2$ device with MCP. It is assumed that the hole-electron recombination in this structure occurs near the interface between EBL and EML. When the excitation pulse is off, excitons are trapped at the interface resulting in the delayed recombination that is seen in the transient EL response. When the MCP was not included in the device, the delay recombination was not seen in the transient EL as can be seen in Figure 51. The explanation is the small barrier between NPB and EML does not allow electrons and excitons to accumulate in the interface between NPB and EML, and, apparently, there is no disorder induced trapping. As Figure 52 shows, the rise time of 65% $Pt(ptp)_2$ based device with MCP was also dependent. The fact that delayed recombination only occurred in the structure with the MCP suggests that the recombination zone is near the interface between MCP and emission layer.

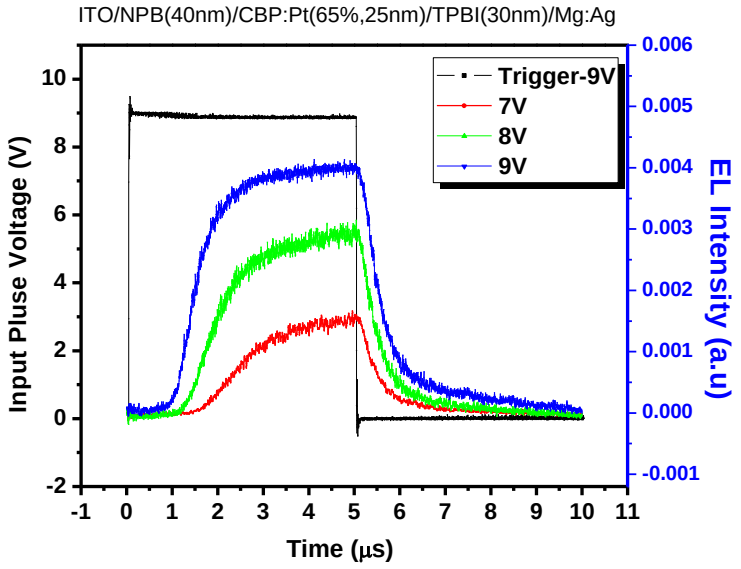

Figure 51: The transient EL of 65% Pt:CBP device without MCP

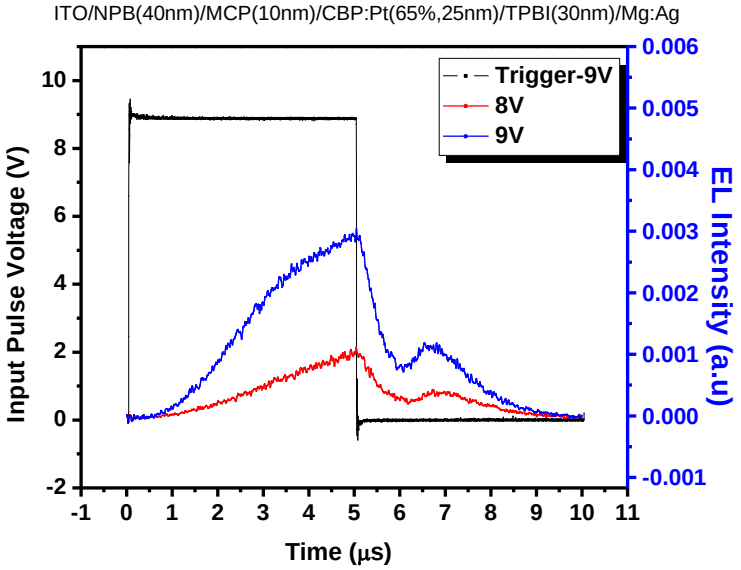

Figure 52: The transient EL of 65% Pt:CBP device with MCP at different driving voltages

Figure 53 shows the typical device electroluminescence response to an applied voltage pulse. Before the pulse application (t<0), the electric field in the device is essentially determined by the built-in voltages associated with interface barriers. Under the assumption that the device equivalent circuit is a resistor in series with a capacitor, upon application of the voltage pulse at t=0, the organic–electrode interfaces become charged within the *RC* time of the experimental setup, and significant carrier injection into the bulk of the device occurs only after flatband conditions have been established within the device, i.e., when $V_{applied}+V_{built\text{-}in}=0$. The time delay between the rise of the applied voltage pulse and the onset of electroluminescence therefore provides a measure of carrier transport, accumulation and trapping of carriers at interfaces, and exciton formation and recombination. The transient EL response of the device shown in Figure 53 was excited by a 9 V pulse operating at 100 kHz with a 50% duty cycle. The model of the delay time is $t_d=t_{inj}+t_{trans}$, where the charge injection time (t_{inj}) is the time required to charge the device and is related to the RC time constant of the device by Formula 5.1. Here V_{max} is the maximum of the applied rectangular voltage, RC is the device time constant, and V_{th} is the device threshold voltage of. The second component of t_d is the charge transport time (t_{trans}) which is defined by Formula 5.2, where d_e is the distance traveled by injected electrons before recombination with holes, u_e is the electron mobility, u_h is the hole mobility, and E is the electric field applied to the device. The RC time constant of the device was determined to be 0.43 μs from measurements with the Solartron 1260. The threshold voltage was 3.8 V. Using these values, t_{inj} was determined to be 0.24 μs using Equation 5.1. The charge transport time (t_{trans}) is therefore the difference between the measured t_d and the charge injection time, or 0.22 μs since t_d was measured to be 0.46 μs (see Figure 53). Based on the delayed emission (discussed below) which was observed only in devices with the mCP electron blocker, and, that NPB emission is

observed at high voltages in devices without the mCP electron blocker as Figure 47 shows, it is assumed that $u_e >> u_h$, and the hole mobility can be equated to zero in Equation 5.2. Following the methodology outlined in, we simplify the multiple interface problem by taking the TPBI to be part of the cathode and the NPB to be part of the anode, which is justified due to the relatively high carrier mobility of these electron and hole transporters. With these assumptions the bulk of the applied voltage drops across the emissive layer, and at 9V the field strength across the device shown in Figure 50 is 3.6×10^6 V/cm. Taking t_{trans}= 0.22 μs and d_e=25 nm, from Equation 5.2 the electron mobility of the 65% $Pt(ptp)_2$ doped CBP film was determined to be 3.2×10^{-6} cm^2/V.s. This compares to an electron mobility of 10^{-7}~ 10^{-5} cm^2/V.s for CBP films doped with Irppy (17]. The result shows the recombination occurs at the electron blocker/emissive layer interface (18,19).

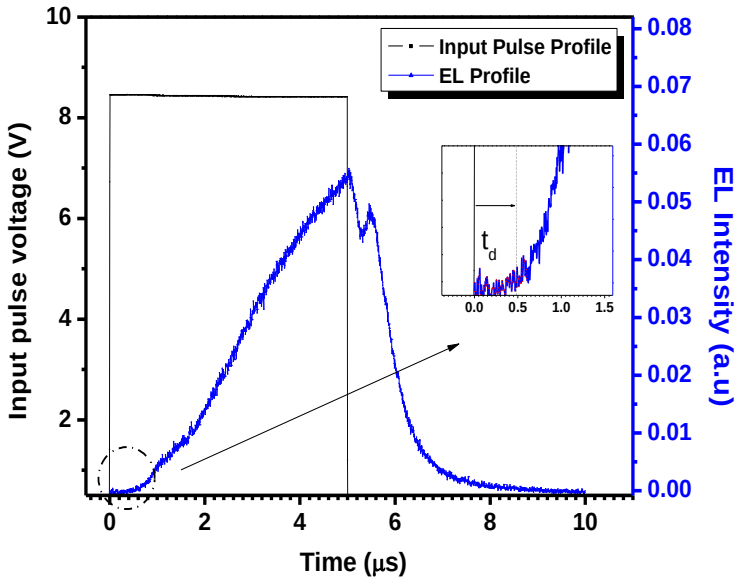

Figure 53: The transient EL of 65% Pt:CBP device with MCP

The delay recombination behavior was found to be dependent on the applied frequency and pulse duty cycles. Figure 54 shows how the delay recombination behavior was related to the duty cycle indicating more time for the electrons and excitons to pile up and be trapped near the interface. Furthermore, as Figure 56 shows, a decrease in the delay recombination at a given duty cycle (50%) was generally accompanied by an increase in frequency which is consistent with insufficient de-trapping times.

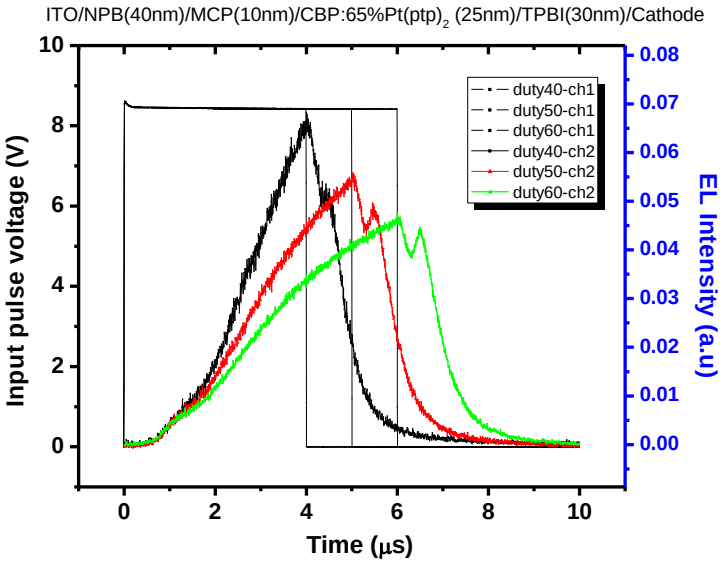

Figure 54: The transient EL at different duty cycles

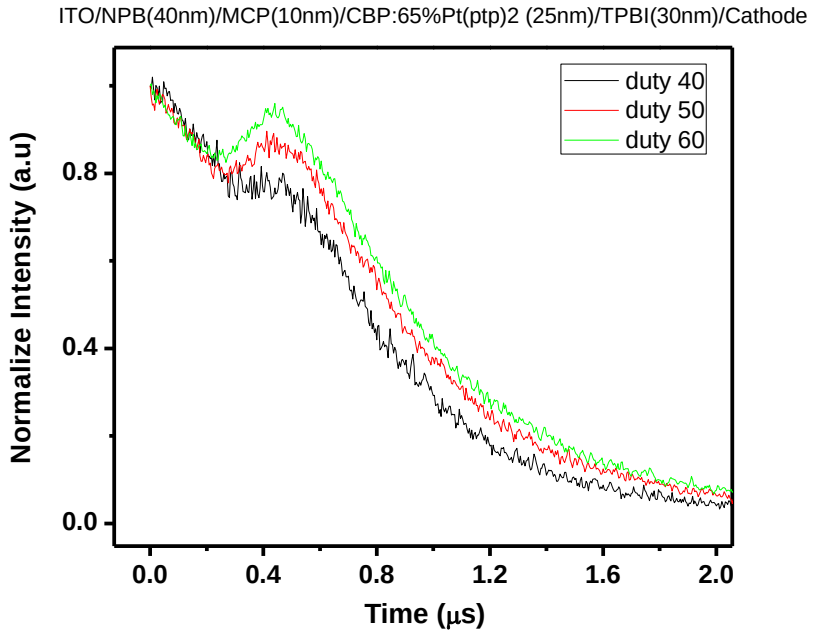

Figure 55: The delayed recombination at different duty cycles

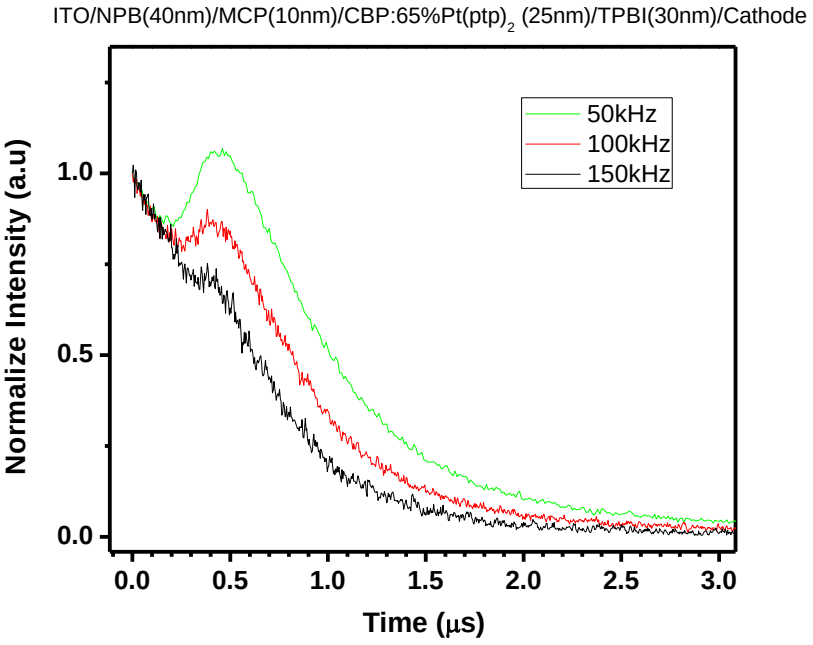

Figure 56: The delayed recombination at different frequencies.

In addition, the luminance of the OLEDs was dependent on the frequency. Figure 57 shows the luminance as the frequency was increased from 10 kHz to 150 kHz. The lowest luminance was at 150 kHz possibly due to insufficient time for injecting carriers. In addition, the trapping and de-trapping behavior at very short times (150kHz) appears to be ineffective, and the trapped charge and polarization effects reduces the effective field that the device experiences resulting in lost luminance. The effect of frequency on luminance is shown in Figure 57. Figure 58 shows the effect of frequency on power efficiency.

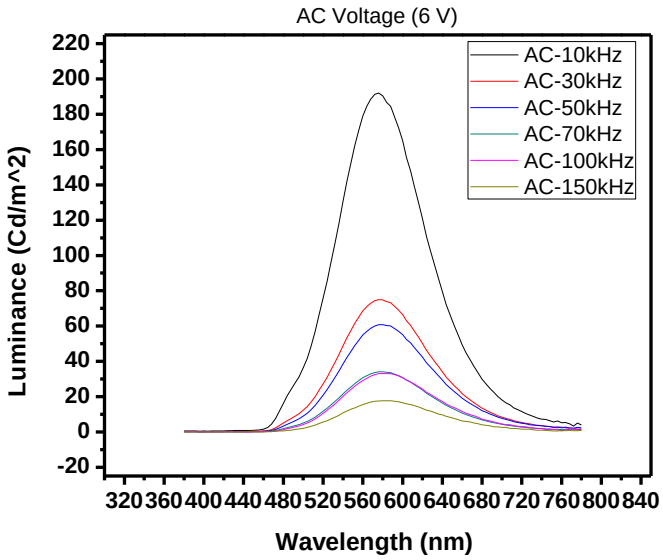

Figure 57: The EL and luminance of OLEDs at different operation frequencies

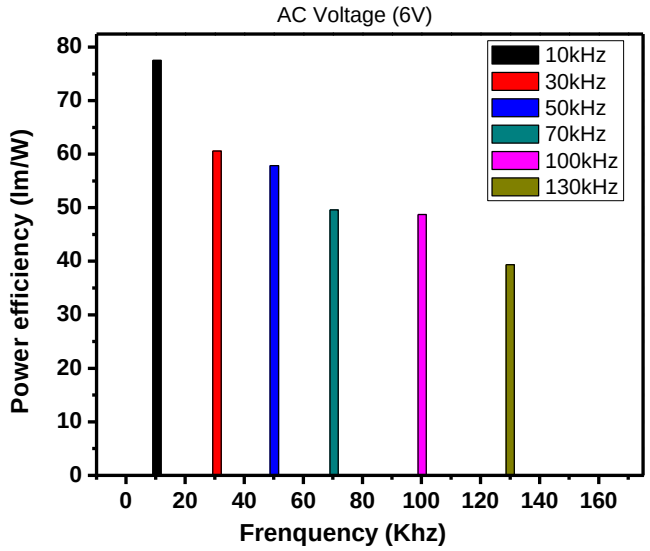

Figure 58: The power efficiency of device at different operation frequencies

4.4 Setup and Method for Decay Time from Transient Electroluminescence

4.4.1 The Decay Time of the $Pt(ptp)_2$ Devices by Using Transient Electroluminescence

The roll-off behavior in efficiency has been observed in the electro-phosphorescence OLEDs device at high current density [20,21]. Here, the decay time was measured with the transient EL method. The decay time of the device can be seen in Figure 59. The exponential decay can be divided into two parts. The first fast decay is related to the intrinsic process, and the slow decay is caused by the carrier trapping in the organic layers. The lifetime of this 65% $Pt(ptp)_2$ based device without MCP is 555 ns which corresponds to the lifetime of the phosphorescent emitters from their triplet excited state. Figure 60 and 61 show the decay time of the 65% $Pt(ptp)_2$ based device with TAPC as an electron blocker at the thickness of emissive layer at 25 nm and 36 nm. The decay time of the device with 25nm emissive layer was 845 ns,

and the decay time was 541 ns for the device with a 36 nm emissive layer. The reason for the shorter lifetime of 36 nm emissive layer is that the thicker the emissive layer, the packing between molecules is more like the behavior of neat $Pt(ptp)_2$ emitter. Accordingly, the lifetime of the $Pt(ptpt)_2$ is decreased with the increasing concentrations of $Pt(ptp)_2$ doped films.

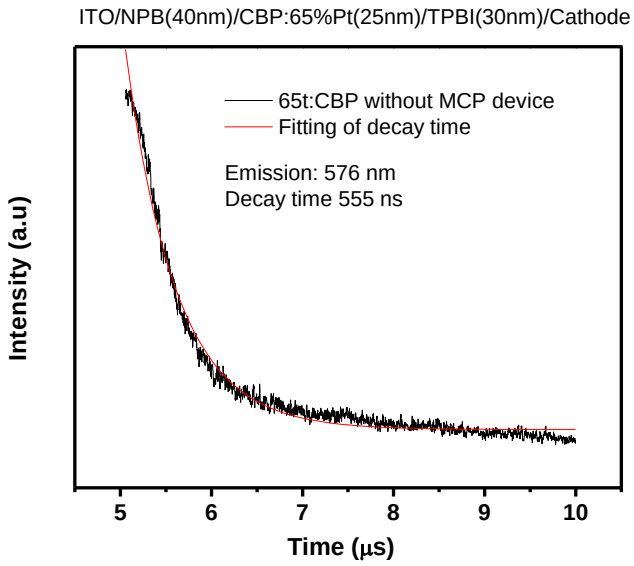

Figure 59: Decay time of 65% $Pt(ptp)_2$:CBP device

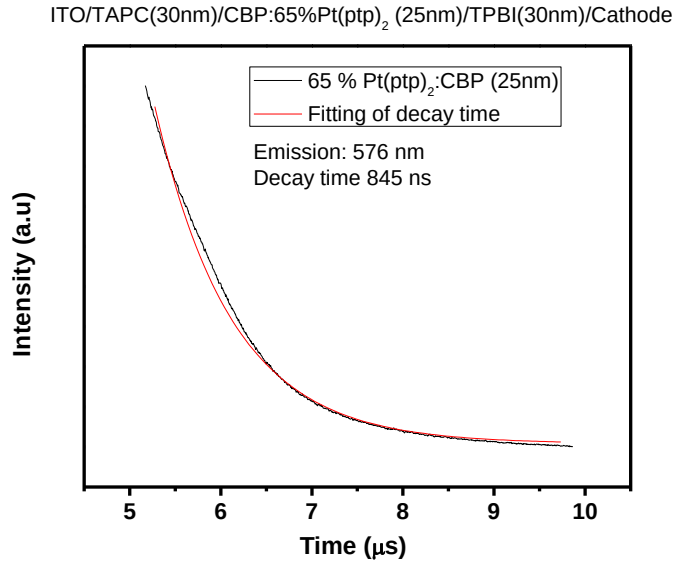

Figure 60: Decay time of 65% $Pt(ptp)_2$:CBP (25nm) device with TAPC

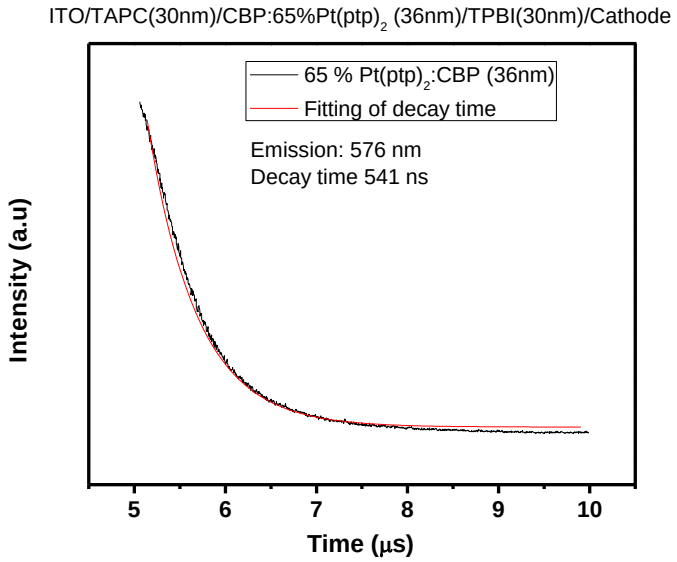

Figure 61: Decay time of 65% $Pt(ptp)_2$:CBP (36nm) device with TAPC

4.4.2 The Delay Time of the $Eu(hfa)_3$ Based Devices by Using Transient Electroluminescence

Lifetime of the emitter is very important because it can determine the efficiency at high current density. When the samples are given at a certain electrical input, the charge trapping, formation and relaxation of the excitons in the triplet state can be observed from the phosphorescent emitter. Efficiency roll-off is one of the main problems with phosphorescent OLEDs. The lifetime of phosphorescent emitters are hugely different and can range from the microsecond range (Ir, Pt) to the millisecond range of Eu. The structure of the device was ITO/NPB(40nm)/CBP:4.5%$Eu(hfa)_3$(25nm)/TPBI(30nm)/Cathode for this study. The 616 nm emission was the most intensity peak that is due to the $^5D_0 \rightarrow {}^7F_2$ transition. In addition to the $^5D_0 \rightarrow {}^7F_2$ transition, an emission at 408 nm was clearly observed, and the intensity increased with increasing applied voltage. A possible explanation is incomplete energy transfer in the host to guest at the high current density. Moreover, the energy decay of the CBP or ligand in this system is from S_1 to S_0 which is singlet-singlet transition resulting in the short lifetime. However, the emissions from the Eu^{+3} ions can be observed at several wavelengths owing to the interband and intraband Eu^{+3} transitions. From the literature, the Eu^{+3} electrons in the f orbits are shielded and not affected by the ligands. According to the reason above, the sharp and high intensity peak at 616 nm dominated in the spectrum. Furthermore, the spin direction and f-f transitions are forbidden, resulting long decay times. As the EL spectra in Figure 62 show, 616 nm and 408 nm emission peaks were observed clearly, thus indicating the $^5D_0 \rightarrow {}^7F_2$ transition and the emission of CBP. The intensity of peaks increased with the increasing voltage, and the Eu 616 nm emission dominated at low voltage because of the good energy transfer in the system. However, the 408 nm contribution increased at high voltage due to the incomplete energy transfer in the system that is caused by saturation of Eu^{+3} emitting sites and the long excited state lifetime. As seen in

Figure 63, the decay time of the 408nm emission is to the CBP singlet to singlet transition, and the decay time was around 92 ns. The decay of the 616 nm emission was 238 μs as Figure 64 shows. The explanation of the long lifetime of Eu based complex is that the f-f transitions are parity forbidden, and sometimes are also spin forbidden resulting in the very long lifetime, typically microseconds to milliseconds [22]

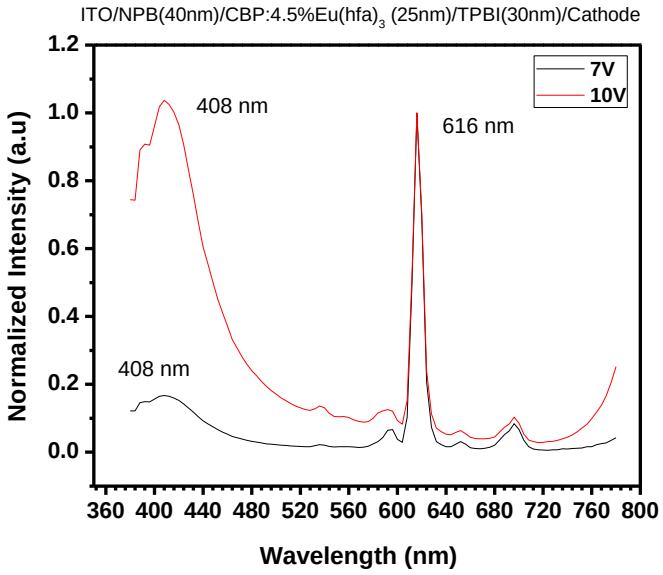

Figure 62: The EL spectra of 4.5% $Eu(hfa)_3$:CBP device

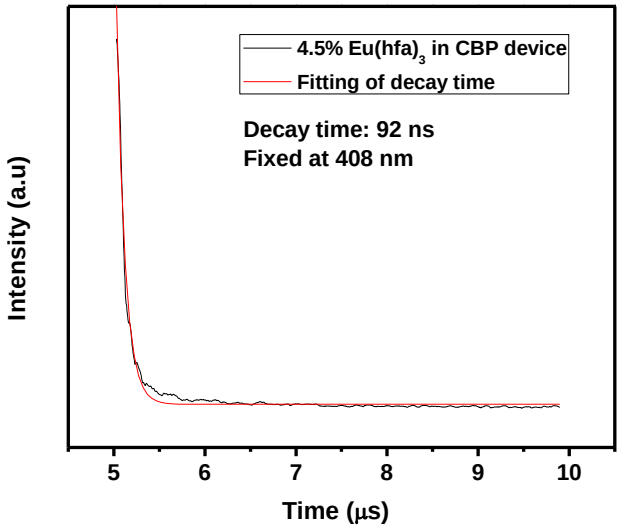

Figure 63: Decay time of 4.5% $Eu(hfa)_3$:CBP device at a fixed wavelength of 408nm

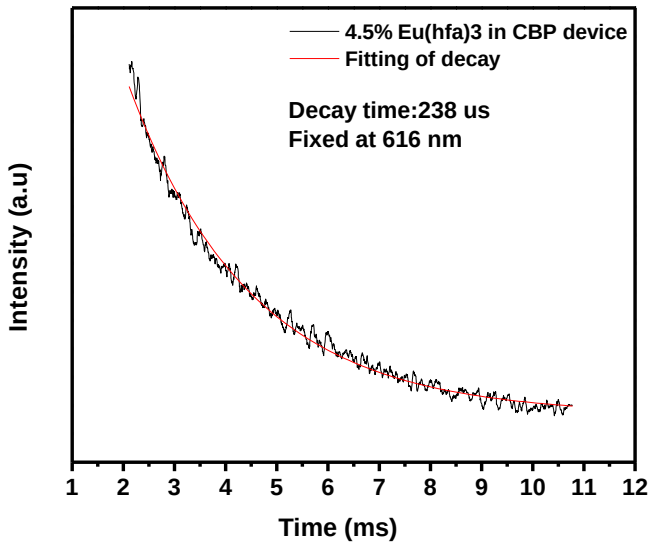

Figure 64: Decay time of 4.5% $Eu(hfa)_3$:CBP device at a fixed wavelength of 616 nm

4.5 References

1. Ta-Ya and Ok-Keun, Appl. Phys. Lett. 2007, 90, 203512.
2. Takeshi Yasuda and Tetsuo Tsutsui, J. Appl. Phys. 2002, 41, 5626.
3. T. C. Wong, J. Kovac, L. S. Hung, and S. T. Lee, Chem. Phys. Lett. 2001, 334, 61.
4. Minghang Li, Ming-Te Lin, and Nigel Shepherd, Organic Electronics 2009, 10, 863.
5. Vadim Adamovich, Jason Brooks, and Mark E. Thompson, New J. Chem. 2002, 26, 1171.
6. Takeshi Yasuda and Tetsuo Tsutsui, J. Appl. Phys. 2002, 41, 5626.
7. Ta-Ya and Ok-Keun, Appl. Phys. Lett. 2007, 90, 203512.
8. Ying Zheng, Sang-Hyun Eom, and Jiangeng Xue, Appl. Phys. Lett. 2008, 92, 223301.
9. Jaewon Lee, Neetu Chopra, Sang-Hyun Eom, Ying Zheng, and Jianmin Shi, Appl. Phys. Lett. 2008, 93, 123306.
10. Wen Wen, Yu Jun-Sheng, and Jiang Ya-Dong, Optoelectronics Lett. 2008, 4, 0201-0204.
11. Unnat S. Bhansali, Mohammad A. Omary, and Bruce E. Gnade, Appl. Phys. Lett. 2007, 94, 203501.
12. Pankaj Kumar, and R P Tandon, J. Phys. D. 2007, 40, 7313.
13. Lebedev E, Dittrich T and Brutting W, Appl. Phys. Lett. 1997, 72, 2686.
14. Zucker J, J. Appl. Phys. 1978, 49, 2543.
15. Nakamura S, Umeda J and Nakada O, IEEE Trans. Electron Devices 1972, 19, 995.
16. Maari F and Bouchriha, Synth. Met. 2000, 114, 255.
17. Changhee Lee, Heume-Il Baek, Jeonghun Kwak, Joon Youp Kim and Byung Doo Chin, Proc. Of SPIE, 2008, 7051, 70510M-1.
18. Naoki Matsumoto and Chihaya Adachi, J. Phys. Chem. C. 2010, 114, 4652.
19. S. Reineke and K. Leo, Phys. Rev. B. 2007, 75, 125328.

20. Ramchandra Pode, Seung-Joon Lee, Sung-Ho Jin, and Jang Hyuk Kwon, J. Phys. D: Applied Physics, 2010, 43, 025101.
21. Jonghee Lee, Jeong-Ik Lee, Jun Yeob Lee, and Hye Yong Chu, Appl. Phys. Lett. 2009, 94, 193305.
22. For full review, see: Evans, R. C.; Douglas, P.; Winscom, C. J. Coord. Chem. Rev. 2006, *250*, 2093-2126.

CHAPTER 5

WHITE BY RED: ENERGY TRANSFER IN EUROPIUM BASED OLEDs

5.1 Introduction

The advantages of Eu(III) emitters in organic light-emitting diodes (OLEDs) include pure-red emission and low driving voltage. Neutral complexes of Eu(III) with ttrpy and hexafluoroacetylacetonato (hfa) ligands as well as the $Eu(tta)_3$ complex were synthesized for evaluation as dopants in organic light emitting diodes. Device characteristics such as CIE, luminance, power efficiency, and current efficiency are also discussed.

5.2 Experimental

The experimental techniques used for thin film deposition and device fabrication have been described in Chapter 3.

5.2.1 PL and PLE Spectra

Figure 65, is the PL and PLE of the CBP host films. The PL peak emission wavelength is 392 nm which was optimally excited by 342 nm light. The emission peak wavelength corresponded to the transition between the LUMO and HOMO of CBP. The PL and PLE of the $Eu(hfa)_3$ films are plotted in Figure 66. The peak PL emission at 615 nm was optimally excited by 316 nm. The peak 617 nm emission is due to the $^5D_0 \rightarrow {}^7F_2$, Eu^{3+} radiative transition. The primary focus was to evaluate the feasibility of its use in OLEDs. Thus, thin films of CBP/3% $Eu(hfa)_3$ttrpy and CDBP/3% $Eu(hfa)_3$ttrpy were co-deposited onto glass substrates and their photoluminescent properties evaluated. As Figure 67 and 68 show the emission was dominated

by the 615nm ($^5D_0 \rightarrow {}^7F_2$) Eu^{3+} radiative transition in both cases. As evidenced by the weak emission from the host in the case of the CBP:3% $Eu(hfa)_3$ttrpy film, energy transfer from the CBP host to the $Eu(hfa)_3$ttrpy dopant was not as complete compared to the CDBP:3% $Eu(hfa)_3$ttrpy material system. This is due to better overlap between the CDBP emission (compared to CBP) and excitation of the europium complex, and the fact that no emission from the ttrpy ligand was observed leads to the conclusion that the antenna effect (whereby energy is transferred from the ligand to the Eu) [1] is efficient.

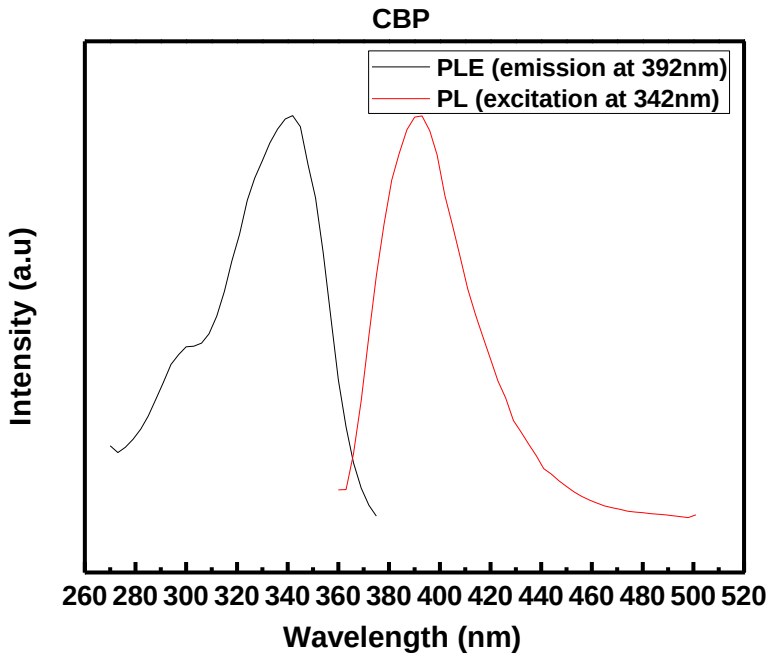

Figure 65: PL and PLE of a CBP film

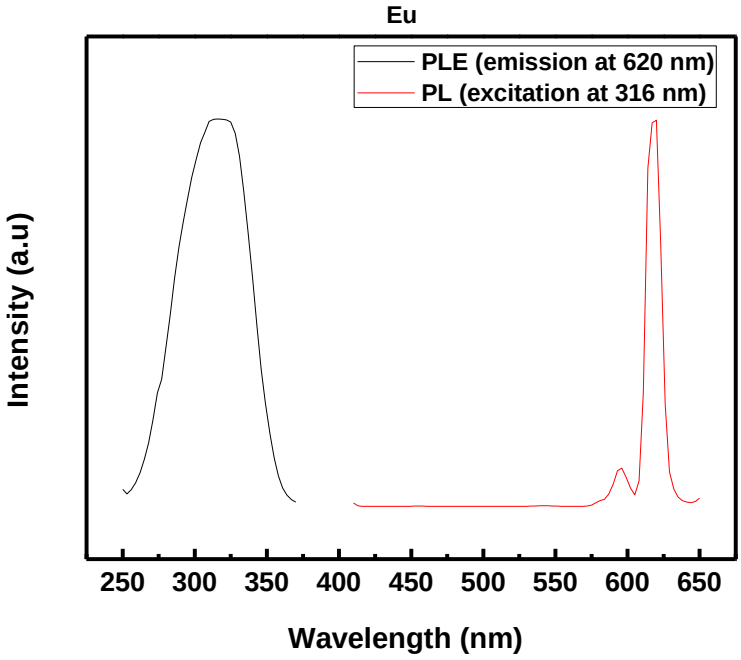

Figure 66: PL and PLE of a neat $Eu(hfa)_3$ film

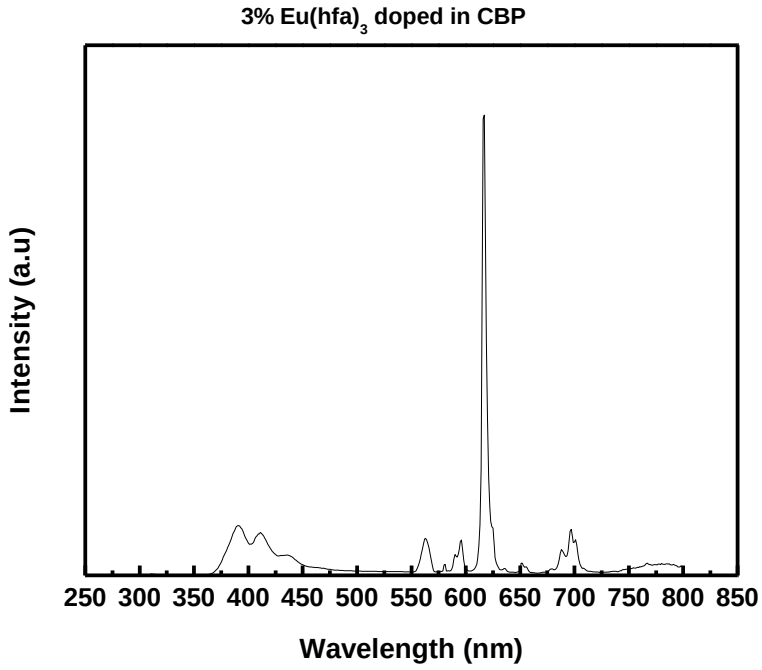

Figure 67: PL of the 3% $Eu(hfa)_3$:CBP film

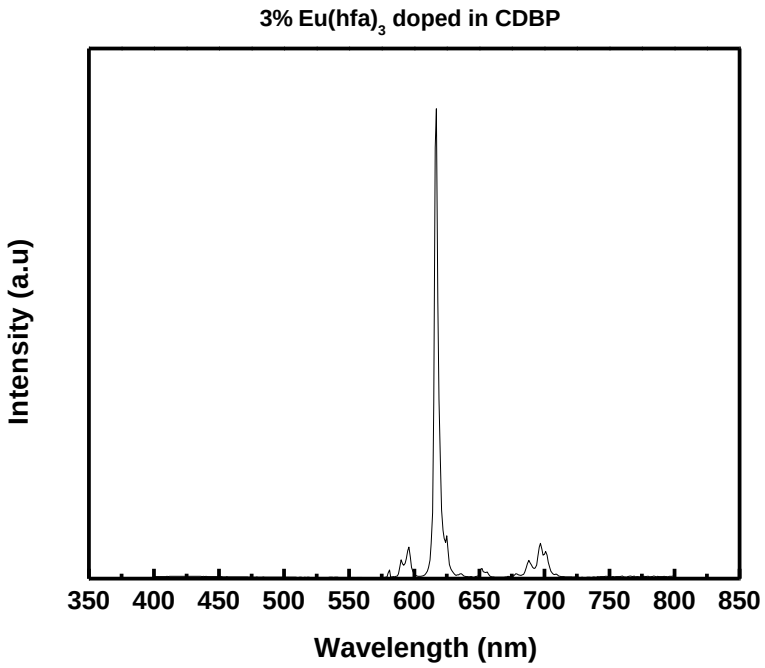

Figure 68: PL of the 3% $Eu(hfa)_3$:CDBP film

5.2.2 The Structure of OLEDs: 4.5% Eu Complexes in Both CBP and CDBP Host

5.2.2.1 4.5% $Eu(hfa)_3$ and $Eu(tta)_3$ Doped in Common Host CBP

The host-dopant system must be considered from several points including the overlap between emission of the host and excitation of dopant, and the energy band gap of dopant and host (the energy band gap of host must be bigger than that of the dopant). In this research, 4.5% $Eu(hfa)_3$ and $Eu(tta)_3$ were doped into a the common host CBP (4,4-*N*,*N*-dicarbazole-biphenyl) [2], and devices with the structure shown in Figure 69 were fabricated. The energy band diagram is shown in Figure. 80. NPB (N, N'- diphenyl-N, N'- bis(1-naphthyl)-1, 1'-biphenyl-4,4"-diamine was chosen for the hole transport layer because of its good ability for transporting holes. Another advantage of NPB is the low LUMO value which is 2.4 eV and 0.4 eV higher than the

emission layer and serves as an electron blocker. It helped to prevent electrons coming from the cathode side and let the electrons combine with holes in the emission layer. TPBI (1,3,5-tris(phenyl-2-benzimidazolyl)-benzene) was selected as both the electron transport layer and hole blocking layer. In this structure, Alq3 was also used for electron transport. The 100 nm Mg:Ag cathode was deposited by using the thermal evaporation after the organic layers.

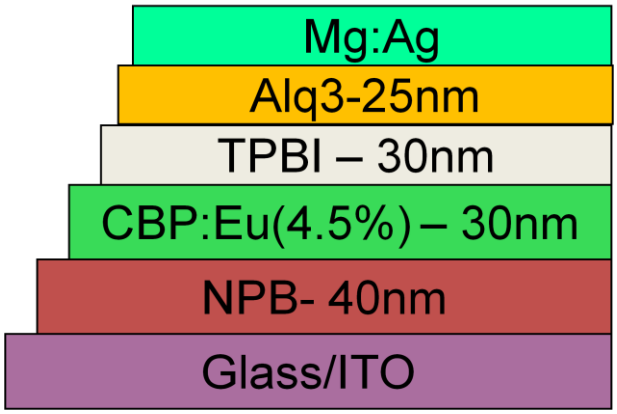

Figure 69: The structure of 4.5% Eu(III):CBP device

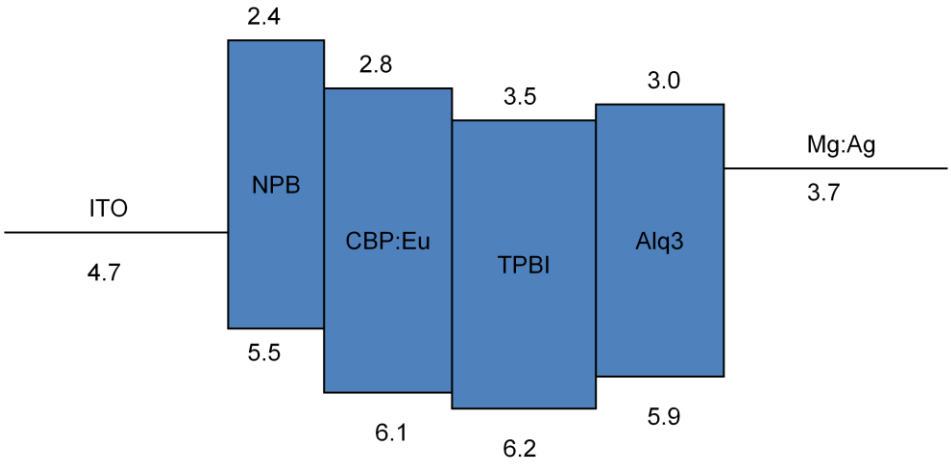

Figure 70: The band diagram of 4.5% Eu(III):CBP device

5.2.2.2 Voltage vs. Current Density and Voltage vs. Luminance Curves

Power efficiency (lm/W), color, current efficiency (Cd/A), and external quantum efficiency (%) are the main parameters used for characterizing OLEDs. OLEDs with the low turn on voltage, high brightness and low current, yield high power efficiency and luminous efficiency. Devices with CBP layers doped with 4.5% $Eu(hfa)_3$ and $Eu(tta)_3$ were fabricated for this study. Figures 71 and 72 are the voltage vs. current density and voltage vs. luminance curves. The turn on for the 4.5% $Eu(hfa)_3$ based device was 6.5 V, and 5.5 V for the $Eu(tta)_3$ based device. However, the brightness in both systems did not exceed 1000 cd/m^2 presumably due to the narrow emission profile and inefficient radiative relaxation process as indicated by the long excited state lifetime. The behaviors of the current density and brightness were almost the same below 8.5 V in both devices. Thus the power efficiency and current efficiency performance were similar in the same voltage range.

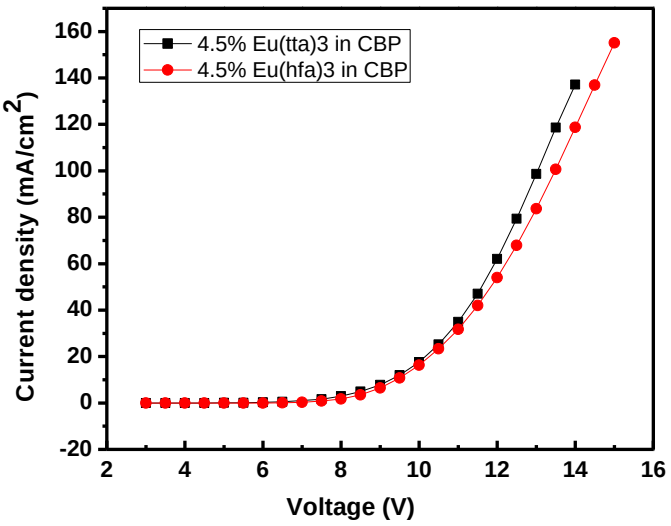

Figure 71: Current Density versus Voltage for both 4.5% Eu(III) emitters

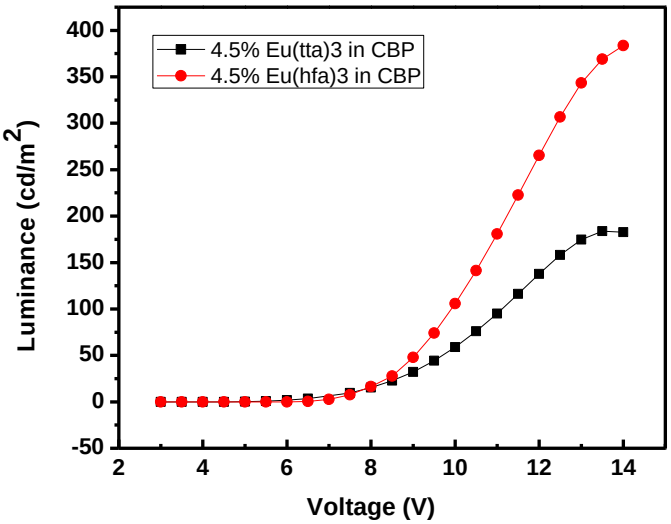

Figure 72: Luminance versus Voltage for both 4.5% Eu(III) emitters

5.2.2.3 Current Density vs. Power Efficiency and Current Efficiency

Current efficiency and luminous power efficiency are the ratio of luminous flux (lumens) to the power (watts). Here, the method to calculate the power efficiency and current efficiency is the ratio of luminous flux emitting from the pixel area to the power consumed at a driving current or voltage. Basically, they are used to describe the efficiency of the output light that is converted from the electricity. The formulas of the current efficiency and luminous power efficiency are shown below:

$$\text{Current efficiency LE (cd/A)} = \frac{L}{j}$$

$$\text{Luminous Power efficiency PE (lm/W)} = \frac{\pi * L}{jV}$$

where j is the current density and V is the applied voltage

As shown in Figure 73, both systems had relatively high power efficiency and current efficiency at low driving voltage that worsened with increasing voltage due to the current quenching at high electric fields. In the $Eu(tta)_3$ based OLEDs, the roll-off was more significant than that of $Eu(hfa)_3$ based OLEDs. This roll-off is typical in phosphorescent layers or devices at high current density and has been explained as the triplet excited transition [3]. The current and power efficiencies obtained for $Eu(tta)_3$ based devices were typically around 0.86 Cd/A and 0.54 lm/W, respectively. For $Eu(hfa)_3$ based devices, current and power efficiencies were 1.09 Cd/A and 0.53 lm/W. Table 4 summarizes the performance metrics.

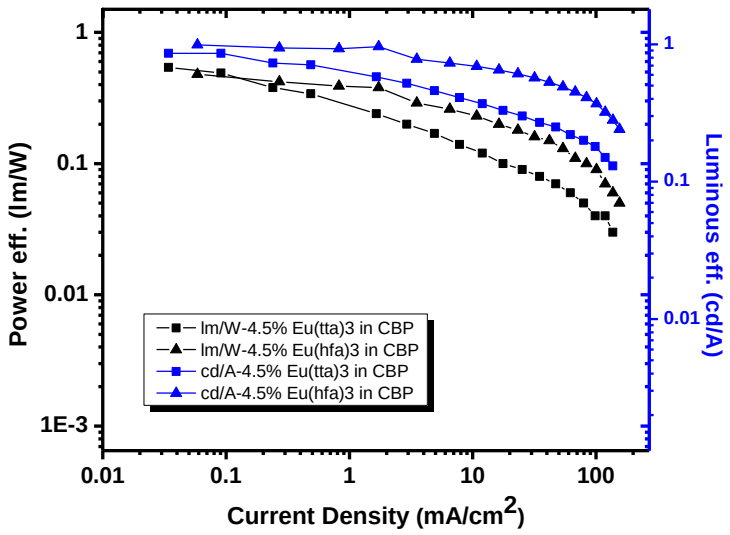

Figure 73: The power eff. and current eff. versus Current Density in both Eu emitters

Table 4: Performances in both Eu based devices

	Lu. eff. (cd/A)	Power eff.(Lm/W)	Turn-on voltage
$Eu(tta)_3$ 4.5% in CBP	0.86 ±0.033	0.54 ±0.016	5.5 V
$Eu(hfa)_3$ 4.5% in CBP	1.09 ±0.038	0.53 ±0.015	6.5 V

5.2.2.4 EL Spectrum and CIE of Devices

As shown in Figure 74, not only 615 nm ($^5D_0 \rightarrow {}^7F_2$) Eu(III) emission was observed, but also the emission peaks from CBP (392 nm), Alq3(540 nm), and NPB (450 nm). However, the 615 nm Eu(III) emission ($^5D_0 \rightarrow {}^7F_2$) dominated at low voltage. Figure 75 shows the electroluminescence spectra of $Eu(hfa)_3$ at relatively higher driving voltages. The peaks of Alq3, CBP, and NPB increased with the increasing voltages and these peaks were larger compared to the increase in Eu(III) emission. This was because the lifetime of Eu(III) is long and the carriers diffuse to other layers instead of all excitons being confined to the emissive layer. Due to the contribution of blue (CBP and NPB), green (Alq3), and red (Eu^{3+}), the white like color was observed at high voltage instead of the red emission at low voltage. The phenomenon of "white by red" was because of the bottleneck effect [4] and a function of $Eu(hfa)_3$ that acted as an intermediary for charge transfer. At low drive voltages, energy transfer from the host was effective, and emission of the dopant dominated. At some higher critical device field and charge injection level, this process became saturated due to the long excited state lifetime of the dopant, and a bottleneck was formed. Under the influence of the high electric field, "excess" injected carriers were transported to the adjacent device layers where radiative recombination occurred.

The emission colors of the device at different drive voltages were recorded and plotted into 1931 International Commission on Illumination (CIE) graphs as shown in Figure 78 (a). The red emission at low voltage changes to white with increasing voltage. For the $Eu(tta)_3$ based device, the behaviors and performances were very similar to that of $Eu(hfa)_3$ as can be seen in Figure 76, and 77. The various colors of $Eu(tta)_3$ with a different driving voltage are recorded in Figure 78 (b).

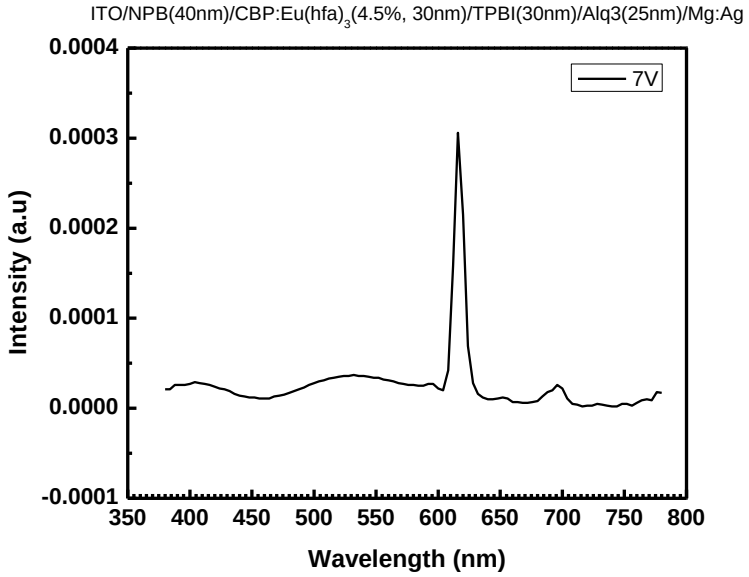

Figure 74: The EL of 4.5%$Eu(hfa)_3$:CBP device

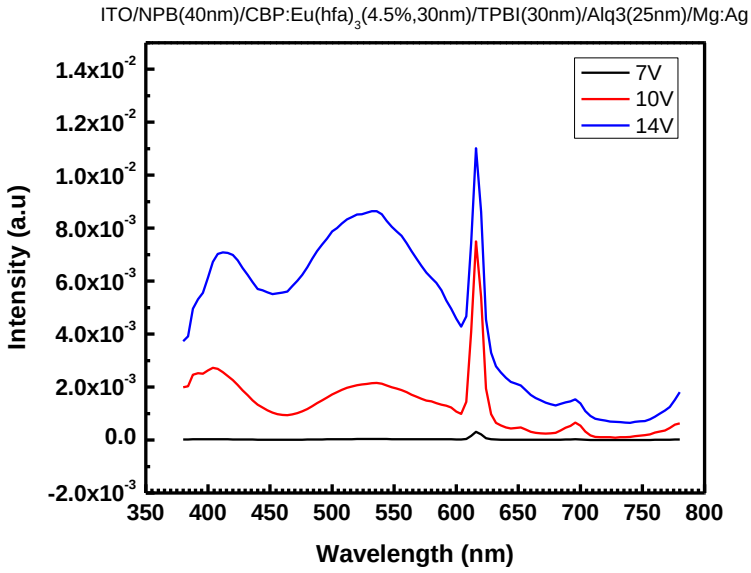

Figure 75: EL spectra of $Eu(hfa)_3$ based device at relatively higher driving voltages

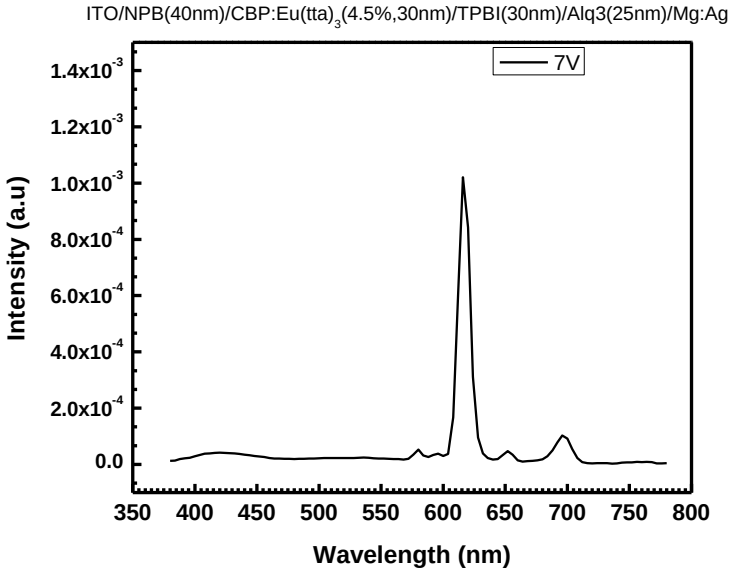

Figure 76: The EL of 4.5%$Eu(tta)_3$:CBP device

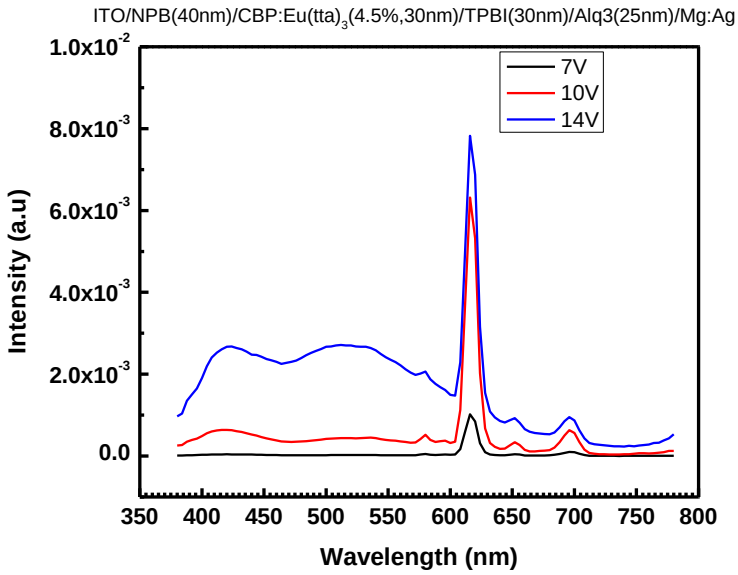

Figure 77: EL spectra of $Eu(tta)_3$ based device at relatively higher driving voltages

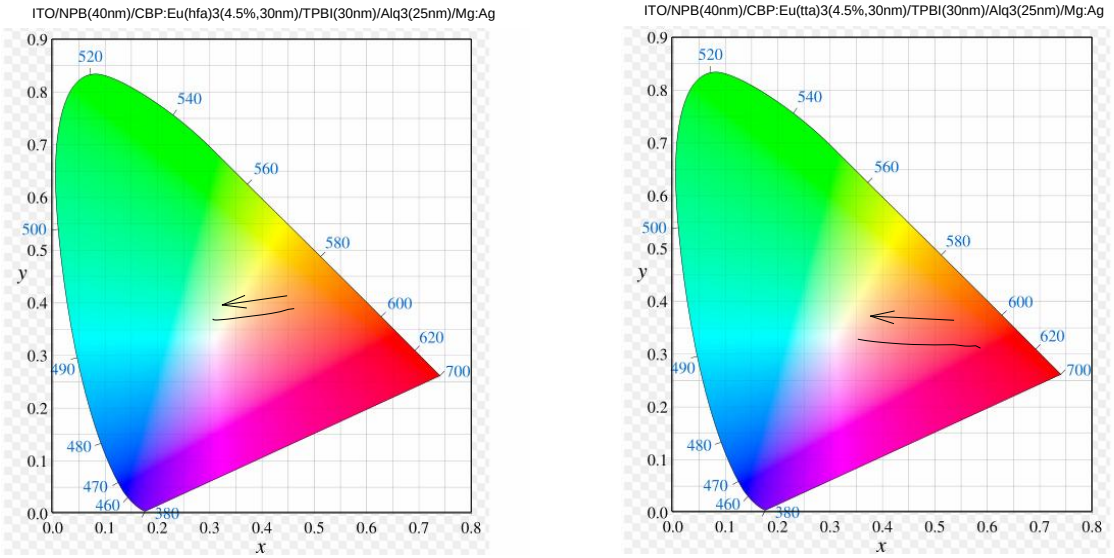

Figure 78: (a) The various colors of CBP:4.5%$Eu(hfa)_3$ based device with the different driving voltage, and (b) The various colors of CBP:4.5% $Eu(tta)_3$ based device with the different driving voltage.

5.2.2.5 4.5% $Eu(hfa)_3$ and $Eu(tta)_3$ Doped in Common Host CDBP

In this section, the CBP host was replaced by 4.4'-bis(9-carbazolyl)-2,2'-dimethyl-biphenyl (CDBP) which is a derivative of CBP. The energy transfer mechanisms between host and fluorescent dopant and between host and phosphorescent dopant were discussed in Chapter 2. The triplet energies of CBP and CDBP are 2.6 eV and 3.0 eV, respectively. In this comparison, the 0.4 eV difference is a larger barrier to prevent energy transferring from the triplet states of phosphorescent Eu complex back to the triplet states of the CDBP host. In this section 4.5% $Eu(hfa)_3$ and $Eu(tta)_3$ were to doped into CDBP (4.4'-bis(9-carbazolyl)-2,2'-dimethyl-biphenyl) [5] as the emissive layer. The architecture of the device is shown in Figure 89 which is similar to the CBP device with the exception of the emissive layer.

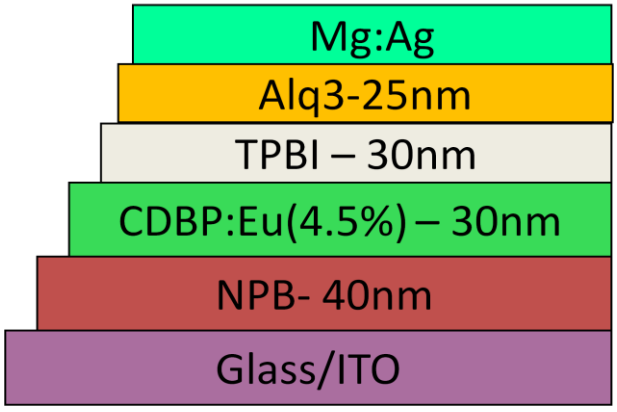

Figure 79: The structure of 4.5%$Eu(hfa)_3$:CDBP device

5.2.2.6 Voltage vs. Current Density and Voltage vs. Luminance Curves

Figures 80 and 81 show the voltage vs. current density and voltage vs. luminance curves for comparison. The turn on for the 4.5% $Eu(hfa)_3$ based device was 6.5 V, and 6 V for the

$Eu(tta)_3$ based device. The brightness in both systems did not exceed 1000 Cd/m^2 due to mechanism described for the CBP devices. Figures 80 and 81 show that the behaviors of the current density and brightness were almost the same at lower than 8 V which is similar to the behaviors already been seen in CBP:Eu devices The power efficiency and current efficiency performance were also similar.

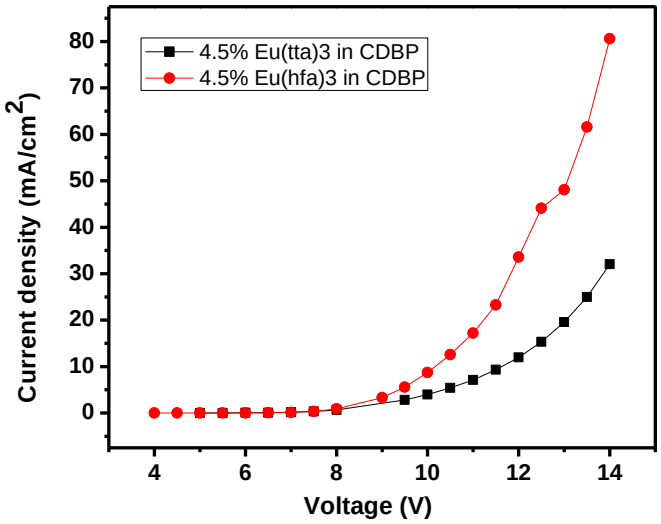

Figure 80: Current density versus voltage in different Eu emitters

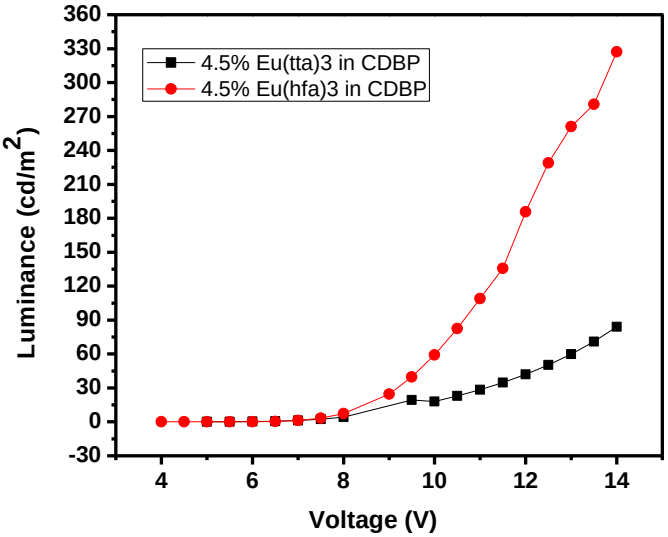

Figure 81: Luminance versus voltage in different Eu emitters

5.2.2.7 Current Density vs. Power Efficiency and Current Efficiency

As Figure 82 shows, both systems had relatively higher power efficiency, and current efficiency at low driving voltage worsened with increasing voltage due to luminance or current quenching at high electric field. In $Eu(tta)_3$ based OLEDs, the behavior of roll-off was more obvious than that of $Eu(hfa)_3$ based devices. Table 5 summarizes the performance metrics.

Table 5: The performance of CDBP devices with different Eu emitters

	Lu. eff. (cd/A)	Power eff.(Lm/W)	Turn-on voltage
$Eu(tta)_3$ 4.5% in CDBP	0.93 ±0.037	0.49±0.013	6 V
$Eu(hfa)_3$ 4.5% in CDBP	1.05±0.038	0.51±0.015	6.5 V

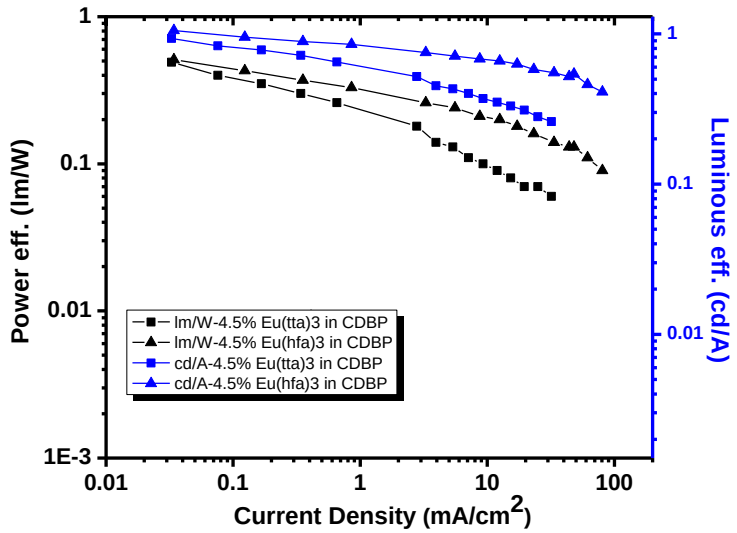

Figure 82: Current density vs. power and current efficiencies for different Eu emitters

5.2.2.8 EL Spectrum and CIE of Devices

As shown in Figure 83 the 615 nm Eu(III) emission ($^5D_0 \rightarrow ^7F_2$) dominated at low voltage indicating good energy transfer from the CDBP to Eu(III). The emission peaks from CDBP (392 nm), Alq3(540 nm), and NPB (450 nm) were also observed at relatively high driving voltage as in the previous case presumably due to the same mechanism discussed above. The phenomenon of "white by red" is presumed to be the same as with the CBP:Eu based devices. We can assume energy transfer from the host was effective, and emission of the dopant dominated at low drive voltage. At some higher critical device field and charge injection level, this process became saturated due to its long excited state lifetime of the dopant, and a bottleneck effect was formed. Under the influence of high electric field, "excess" injected carriers were transported to the adjacent device layers where radiative recombination occurs.

The colors emitted by the device at different voltages are depicted in 1931 International Commission on Illumination (CIE) plots as shown in Figure 87 (a). Red emission is observed at low voltage that changes to white with the increasing voltage. The behavior and performance of $Eu(tta)_3$ based devices can be seen in Figure 85 and 86. Only Eu(III) emission ($^5D_0 \rightarrow ^7F_2$) was observed at the low driving voltage. Eventually, as observed with the previous devices, other peaks showed up with increasing voltage and the device color changed from red to white. The various colors of $Eu(tta)_3$ with a different driving voltage were recorded in Figure 87 (b). The data suggests that the long lifetime of the f-f transition of the Eu ion is a principal limiting factor irrespective of how efficient the energy transfer from the host to the dopant and the antenna effect are.

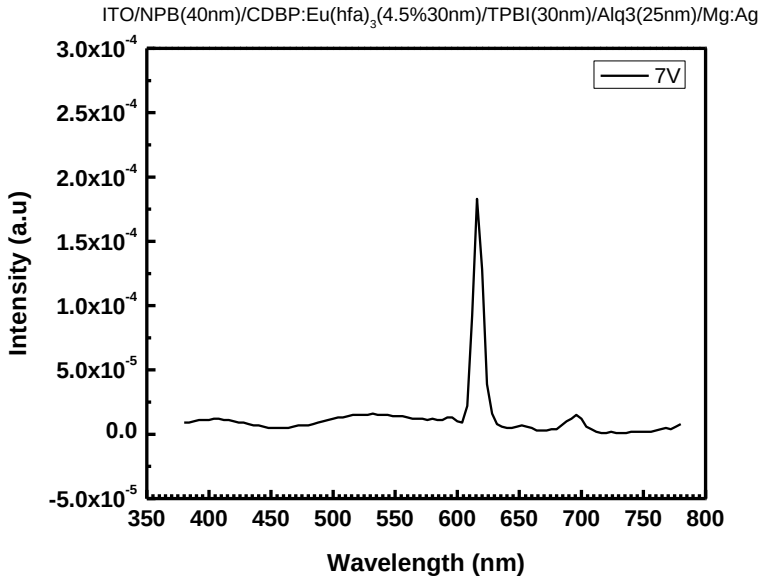

Figure 83: The EL of 4.5%Eu(hfa)$_3$:CDBP device

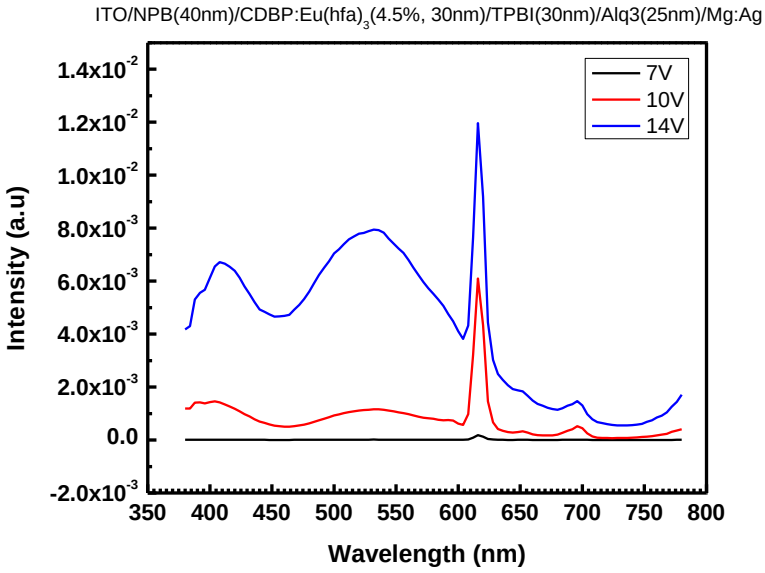

Figure 84: EL spectra of CDBP:4.5% Eu(hfa)$_3$ based device at relatively higher driving voltages

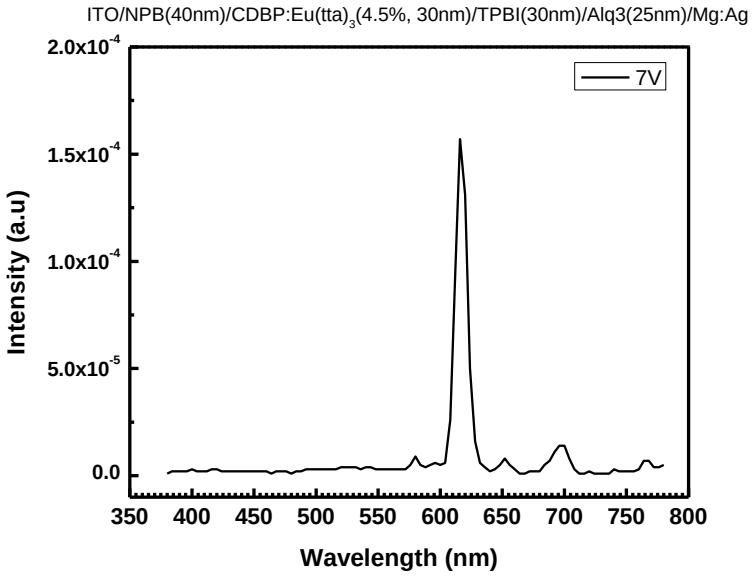

Figure 85: EL spectra of 4.5%Eu(tta)$_3$:CDBP device

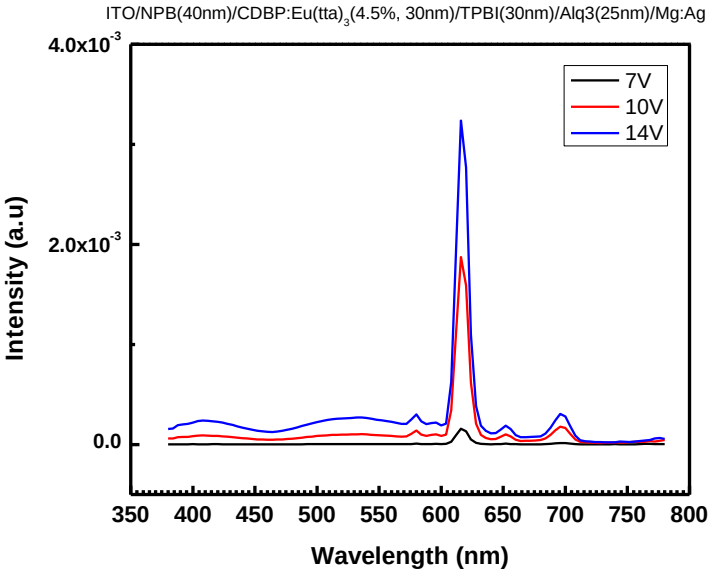

Figure 86: EL spectra of CDBP:4.5% Eu(tta)$_3$ based device at relatively higher driving voltages

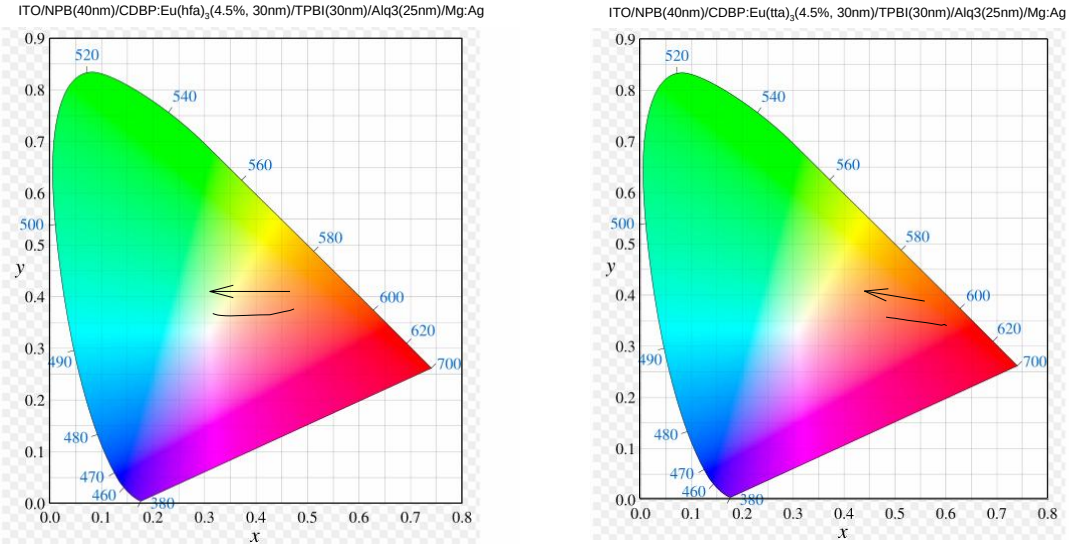

Figure 87: (a) The various colors of CDBP:4.5% $Eu(hfa)_3$ based device with the different driving voltage, and (b) The various colors of CDBP:4.5% $Eu(tta)_3$ based device with the different driving voltage.

5.2.2.9 Neat CBP as the Emission Layer for the Control Device

The interesting observation of "white by red" was seen in the Eu based devices. In order to develop insight to the phenomenon, control devices were designed to compare with other Eu devices where CBP (4,4-*N*,*N*-dicarbazole-biphenyl) was used as the emissive layer. The device structure is shown in Figure 88, and the band diagram is shown in Figure 89**.**

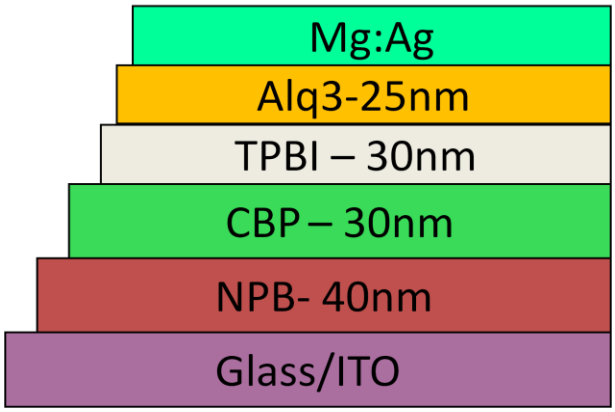

Figure 88: The structure of the CBP control device

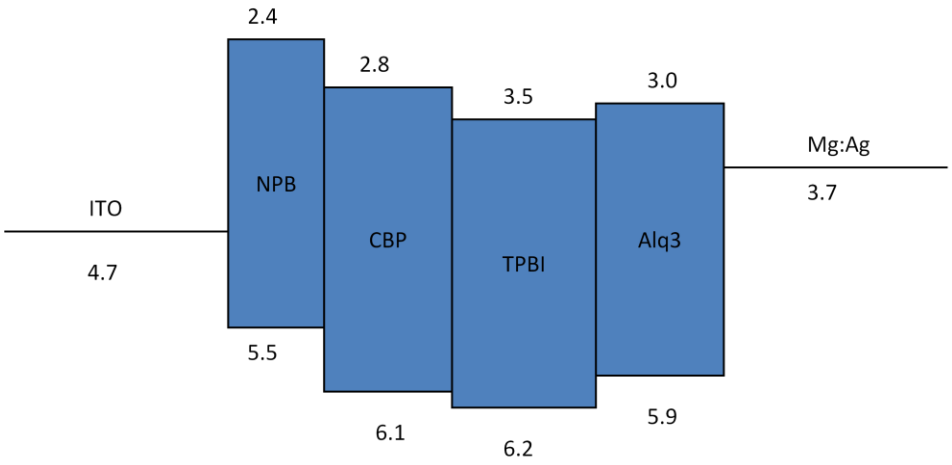

Figure 89: The band diagram of CBP control device

5.2.2.10 The Performances of the CBP Control Device

Alq3 and NPB peaks were not observed in this control device indicating that the "white by red" was related to the energy transfer mechanism and bottleneck effect in the Eu emitters. The power efficiency and current efficiency versus current density are shown in Figures 90 and 91, respectively. The maximum brightness was around 600 cd/m^2 for this control device, and the

turn-on voltage was 5V. The power efficiency and current efficiency were 0.19 lm/W and 0.30 cd/A that are tabulated in Table 6.

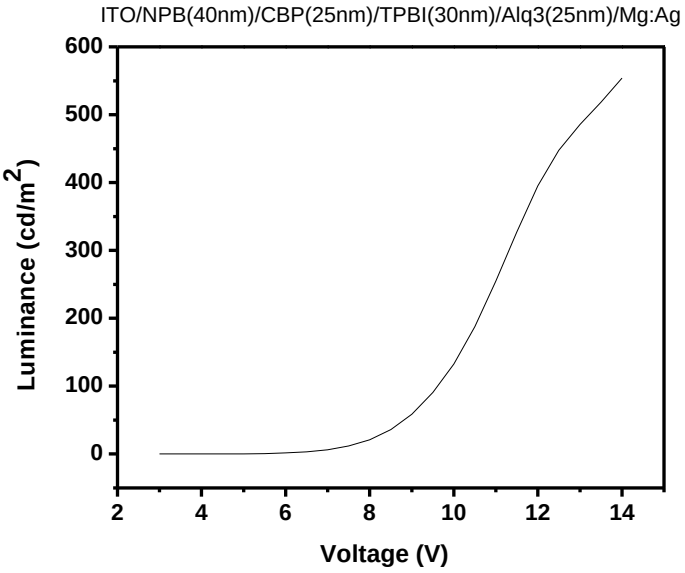

Figure 90: The luminance versus voltage in CBP control device

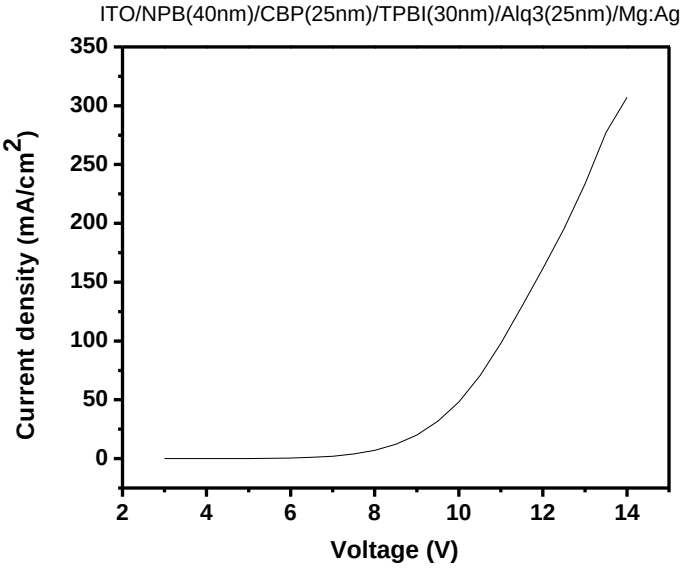

Figure 91: The current density versus voltage for the CBP control device

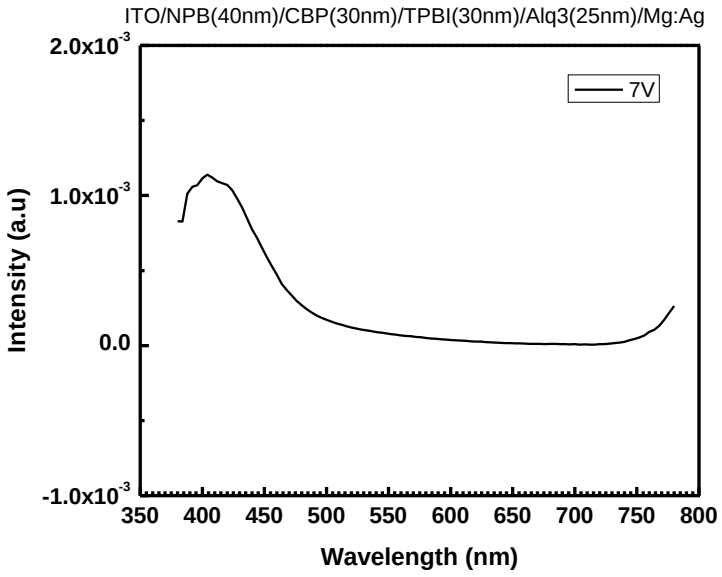

Figure 92: EL of CBP control device

Table 6: The performance of CBP control device

	Lu. eff. (cd/A)	Power eff.(Lm/W)	Turn-on voltage
CBP control device	0.30±0.011	0.19±0.008	5V

5.2.3 Various Concentrations of $Eu(hfa)_3$ in Common Host CBP Devices

5.2.3.1 The Various Structures of $Eu(hfa)_3$ Doped in Common CBP Host Devices

As discussion in previous sections, the 4.5% $Eu(hfa)_3$ was doped in both CBP and CDBP host for the comparison. In this section, four different concentrations of $Eu(hfa)_3$, (1.4%, 2%, 4.5%, and 7%), were doped into CBP to determine the optimal concentration for OLEDs. The device structure is shown in Figure 93.

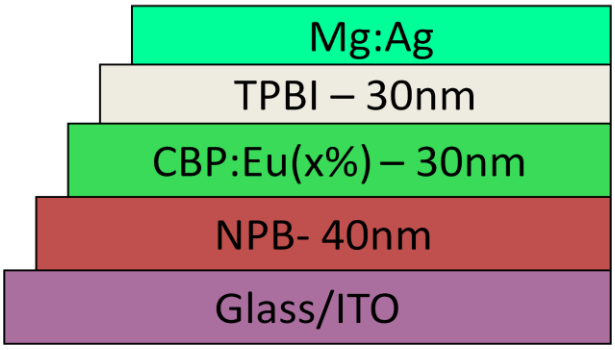

x=1.4,2,4.5, and 7

Figure 93: The various concentrations in $Eu(hfa)_3$ doped on CBP OLEDs devices

5.2.3.2 Voltage vs. Current Density and Voltage vs. Luminance Curves

Figures 94 and 95 show the voltage vs. current density curve and voltage vs. luminance curve for the comparison. It is clear that the brightness was higher in the low dopant concentration devices. The relatively larger contribution to the emission from the host, NPB and Alq3 at lower doping levels are probably responsible for this dependence.

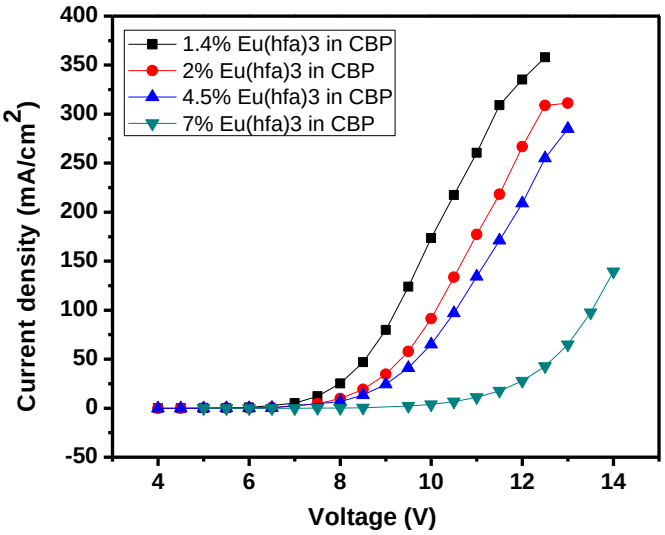

Figure 94: The current density versus voltage in different doped concentrations with CBP devices

In these figures, the turn-on voltages can be observed at around 5.5 V. For the 1.4% CBP:Eu(hfa)$_3$ device, the brightness was the highest, but the current density was also the highest. Therefore, the power efficiency and current efficiency were not the best.

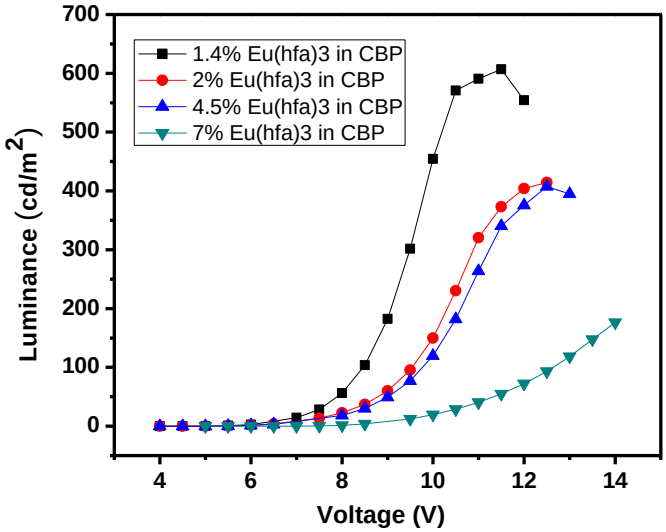

Figure 95: Luminance versus voltage in different doped concentrations with CBP devices

5.2.3.3 Current Density vs. Power Efficiency and Current Efficiency

The efficiency roll-off is dependent on doping concentration due to the self-quenching and triplet-triplet annihilation. Figure 96 is a plot of the power efficiency and current efficiency vs. current density for various doping concentrations. The highest power efficiency among these devices was 0.53 lm/W at the 4.5% Eu(hfa)$_3$ doping level that decreased with increasing drive voltage as expected for phosphorescent emitters. However, the highest brightness was obtained with 1.4% Eu(hfa)$_3$ doping. Although the 1.4% Eu:CBP device had higher luminance, it also had relatively higher current density. That was why the 1.4% Eu:CBP device did not have the highest

power efficiency. The current and power efficiencies obtained from different concentration $Eu(hfa)_3$ devices were typically around 1 Cd/A and 0.53 lm/W, respectively. All of the performance metrics are shown in Table 7.

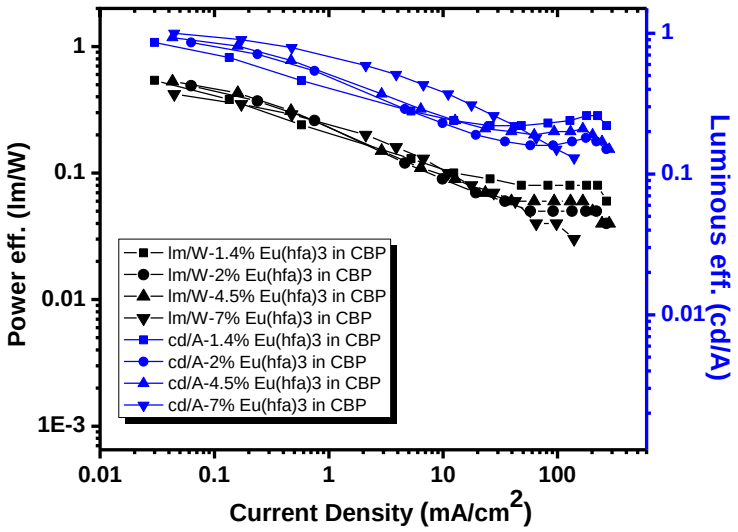

Figure 96: The power efficiency and current efficiency vs. current density at different dopant concentrations in $Eu(hfa)_3$ devices

Table 7: The performance of different dopant concentrations $Eu(hfa)_3$ devices

	Lu. eff. (cd/A)	Power eff.(Lm/W)	Turn-on voltage
$Eu(hfa)_3$ 1.2% in CBP	0.86±0.033	0.54±0.016	5.0 V
$Eu(hfa)_3$ 2% in CBP	0.86±0.032	0.49±0.013	5.5 V
$Eu(hfa)_3$ 4.5% in CBP	0.93±0.037	0.53±0.017	5.5 V
$Eu(hfa)_3$ 7% in CBP	1.00±0.037	0.42±0.012	7.0 V

5.2.3.4 EL Spectrum and CIE of Devices

Figure 97 is the EL spectra for different doping concentrations of $Eu(hfa)_3$ in CBP at a low operation voltage. The highest doping concentration in this series was 7% clearly showing complete energy transfer at a low driving voltage. Owing to the insufficient $Eu(hfa)_3$ and long lifetimes, energy transfer from CBP to Eu is ineffective resulting in the emission of CBP even at low driving voltages. As shown in Figure 98, the CBP emission peak dominated except at 7% Eu:CBP where there is sufficient $Eu(hfa)_3$. Nonetheless, the phenomenon of "white by red" was also observed in this series at appropriate voltages. The various colors of $Eu(hfa)_3$ at different concentrations and different driving voltages are shown in Figure 99 (a)~(d).

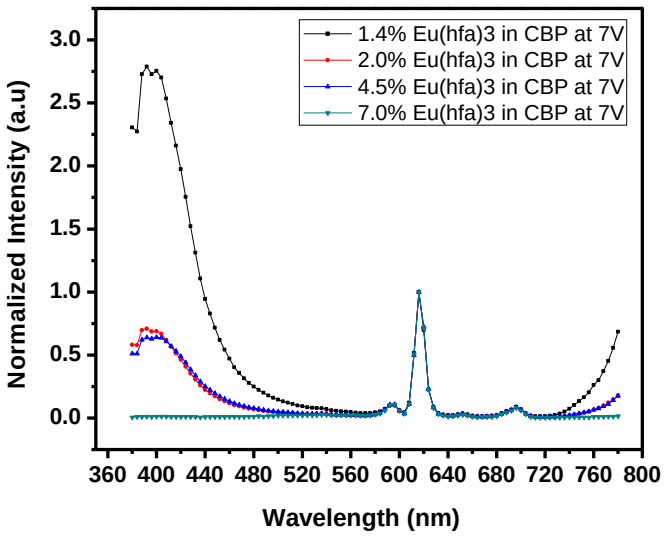

Figure 97: The EL spectra in different doping concentrations of $Eu(hfa)_3$:CBP devices at low operation voltage

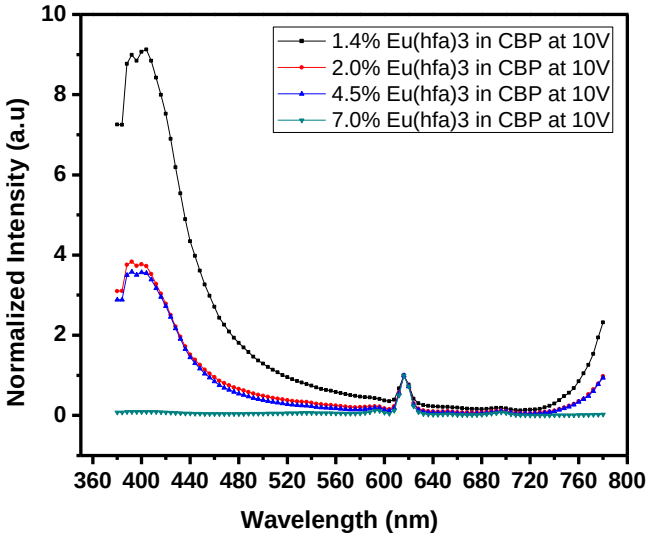

Figure 98: The EL spectra at different doping concentrations of $Eu(hfa)_3$ in CBP devices at high operation voltage

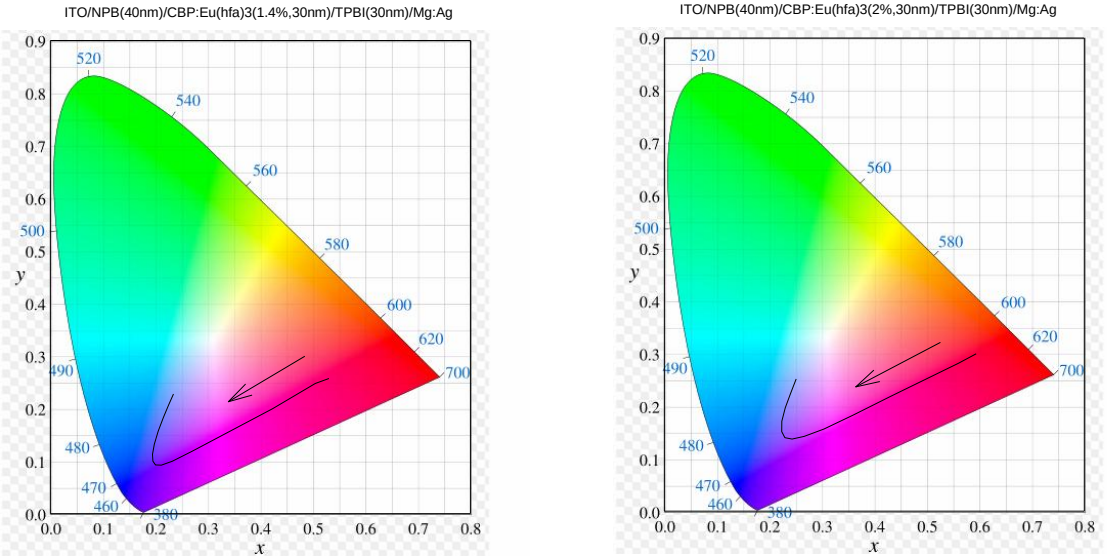

Figure 99: (a) The various colors of CBP:1.4% $Eu(hfa)_3$ based device with the different driving voltage, and (b) The various colors of CBP:2% $Eu(tta)_3$ based device with the different driving voltage.

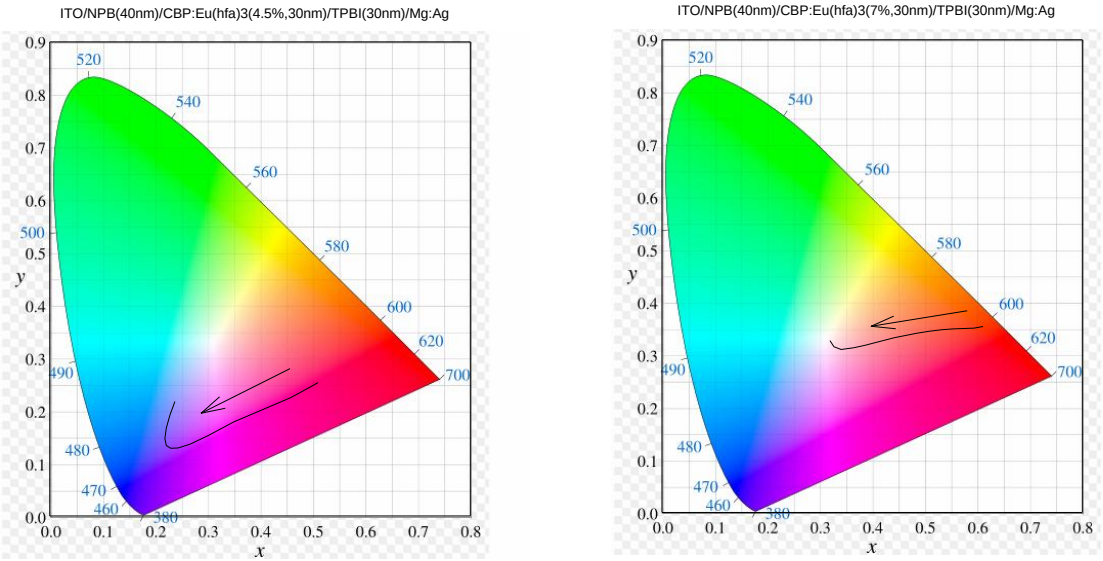

Figure 99: (c) The various colors of CBP:4.5% $Eu(hfa)_3$ based device with the different driving voltage, and (b) The various colors of CBP:7% $Eu(tta)_3$ based device with the different driving voltage.

5.2.4 Influence of Electron Blocking in $Eu(hfa)_3$:CBP Devices

5.2.4.1 The Structure of the 4.5% $Eu(hfa)_3$:CBP Device with The Electron Blocking Layer

The function of a electron blocking layer was to prevent electrons from drifting into the hole transport layer (NPB). For this purpose MCP was used. The device structure is shown in Figure 100 and the band diagram is shown in Figure.101.

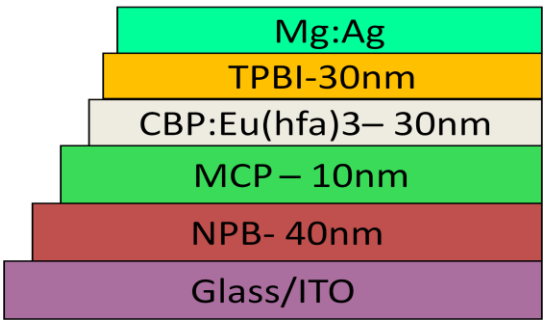

Figure 100: The structure of CBP:$Eu(hfa)_3$ device with MCP

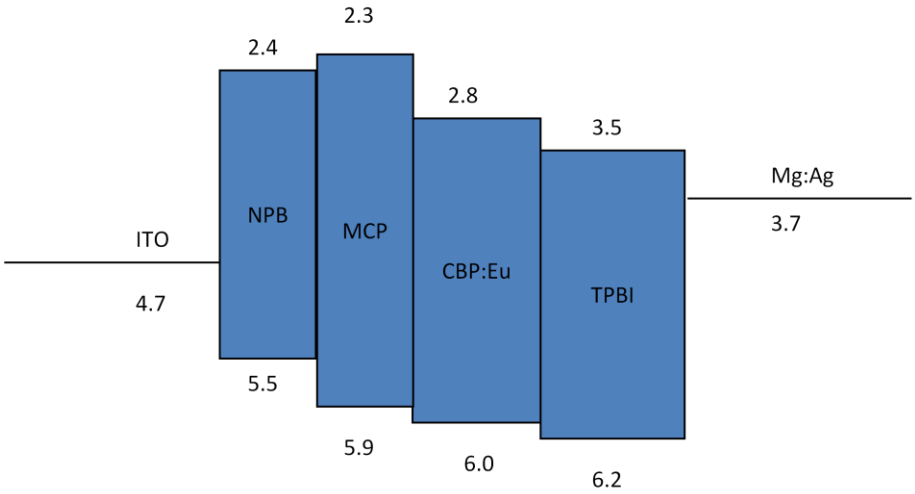

Figure 101: The band diagram of CBP:Eu(hfa)$_3$ device with MCP

5.2.4.2 Voltage vs. Current Density and Voltage vs. Luminance Curves

As shown in Chapter 4, a significant enhancement was obtained when the MCP electron blocking layer was added to the device. Here, we used the electron blocker in Eu(hfa)$_3$ devices and compared with the performance of devices without a electron blocker. The MCP did not enhance the performance of Eu(hfa)$_3$ OLEDs-the performance was very similar to devices without MCP. Figures 102 and 103 show voltage versus current density and voltage versus luminance curves. The turn-on voltage of 4.5% Eu(hfa)$_3$:CBP with MCP devices was 6.5V.

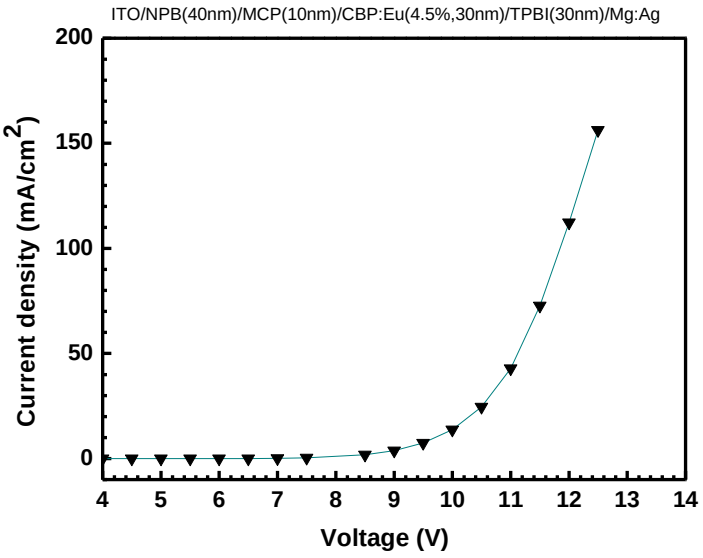

Figure 102: Current density versus voltage in $Eu(hfa)_3$ based device with MCP

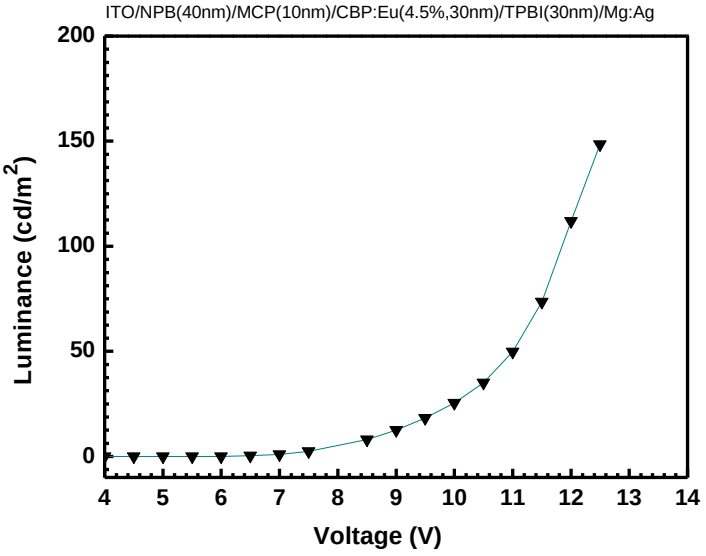

Figure 103: Luminance versus voltage in $Eu(hfa)_3$ based device with MCP

5.2.4.3 Current Density vs. Power Efficiency and Current Efficiency

As shown in Figure 104, roll-off with increasing voltage and current density was .dramatic. The peak power efficiency was 0.47 lm/W at 6.5 V. The highest current efficiency was 0.98 cd/A at 6.5 V which dropped to 0.1cd/A at 12 V due to current induced quenching. This was discussed in previous sections, and the performances are shown in Table 8.

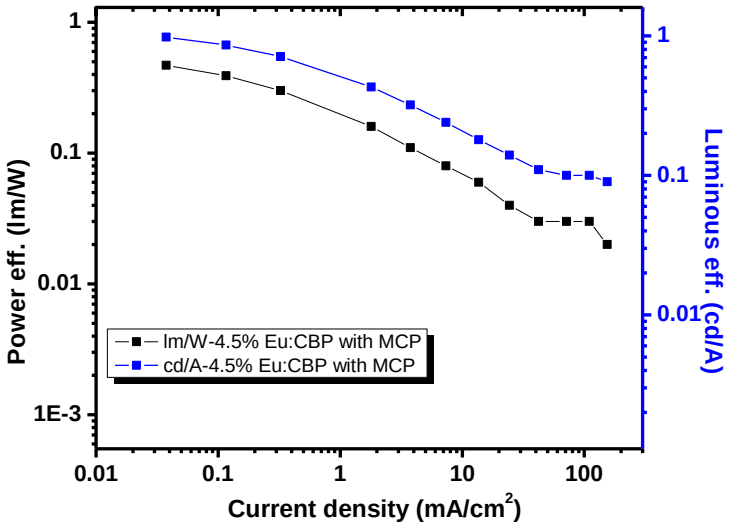

Figure 104: Power efficiency and current efficiency vs. current density in 4.5% $Eu(hfa)_3$:CBP device with MCP

Table 8: The performances of the 4.5% $Eu(hfa)_3$:CBP device with MCP

	Lu. eff. (cd/A)	Power eff.(Lm/W)	Turn-on voltage
4.5Eu:CBP with MCP	0.98	0.47	6.5V

5.2.4.4 EL Spectrum and CIE of Devices

The EL spectrum of the 4.5% Eu:CBP with MCP device is plotted in Figure 105. The peak at 614 nm dominates at low driving voltage indicating the $^5D_0 \rightarrow {}^7F_2$ transition. With the increasing driving voltage, the CBP emission is clearly observed here. As with previous devices, the color changed sequentially from pure red to pink, blue, and then white with increasing voltage due to the long lifetime of $Eu(hfa)_3$ as is shown in Figure 106.

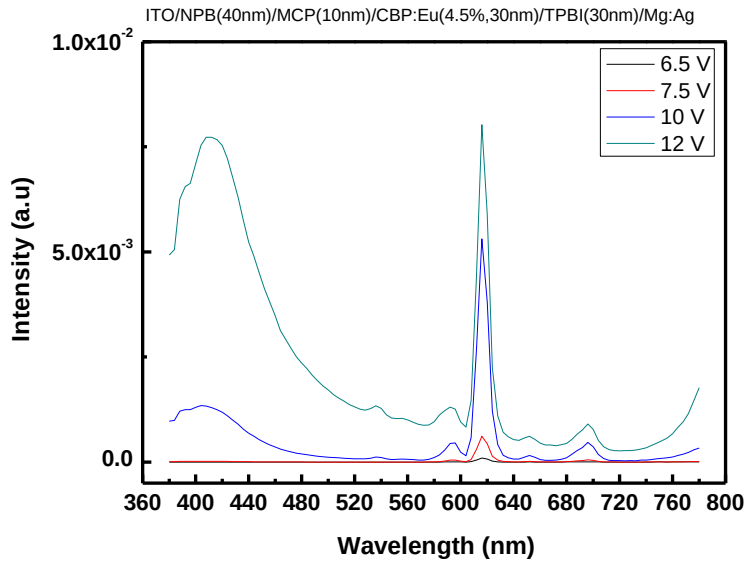

Figure 105: The EL spectrum of 4.5% Eu:CBP with MCP device

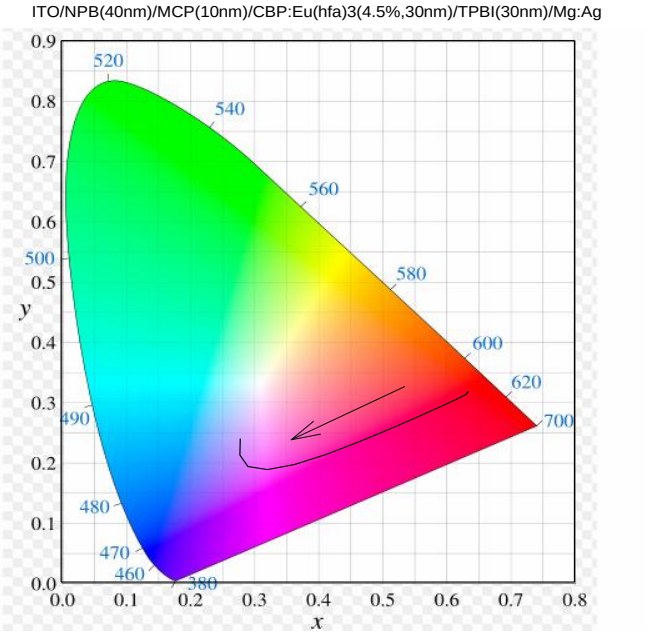

Figure 106: The various colors of $Eu(hfa)_3$ with increasing voltage and MCP

In summary, the data suggests that irrespective of the efficiency of the energy transfer from the host to the dopant and how effective the antenna effects associated with the ligands are and how effectively charge is injected and confined to the emissive layer, the long lifetime of the f-f transition of the Eu ion and the bottleneck effect appear to be the principal limiting factors for high luminance and efficiency.

5.3 References

1. Edimar DeOliveira, Claudio R. Neri, and Alexandre G. S. Prado, Chem. Mater., 2007, 19, 5437-5442.
2. So-Young Kim, Jun-Ho Kim, Yunkyoung Ha, Seung-Hee Lee, and Young-Kwan Kim, Current Applied Phys., 2007, 7, 380-383.

3. Ramchandra Pode, Seung-Joon Lee, Sung-Ho Jin, Suhkmann Kim, and Jang Hyuk Kwon, J. Phys. D: Appl. Phys. 2010, 43, 025101.
4. Dharma-wardana, M. W. C., and Zgierski, J. Opt. A. Pure. Appl. Opt. 2002, 4, 278-281.
5. Shizuo Tokito, Toshiki Iijima, Yoshiyuki Suzuri, Toshimitsu Tsuzuki, and Fumio Sato, Appl. Phys. Lett. 2003, 83, 569-571.

CHAPTER 6

CONCLUSIONS AND FUTURE WORK

6.1 CONCLUSIONS

Photoluminescence and photoluminescence excitation were used to study the energy transfer processes of Eu dopants in order to develop insights to the energy transfer processes and select the ideal host for OLEDs. The PL of $Eu(hfa)_3$ was dominated by the $^5D_0 \rightarrow {}^7F_2$ transition at 615 nm.

The lifetime of neat $Eu(hfa)_3$ film was around 1 millisecond at 615 nm. Similarly the lifetime of the 4.5%$Eu(hfa)_3$:CBP film was around 0.85 milliseconds at 615 nm which is expected for f-f forbidden transitions. The PL of 65% $Pt(ptp)_2$:CBP films was dominated by 572 nm excimer emission. The lifetime of 65% $Pt(ptp)_2$:CBP phosphorescent film was studied for comparison with $Eu(hfa)_3$ and the lifetime was around 638 nanosecond and much faster than that of $Eu(hfa)_3$ which supports the significantly higher efficiency obtained from the $Pt(ptp)_2$ devices.

The power efficiency and the current efficiency of the 4.5% $Eu(hfa)_3$ and $Eu(tta)_3$ devices were all~ 0.53 lm/W and ~ 1.09 cd/A. These were the best values obtained from among devices doped at different levels up to 7%. This was true for both CBP and CDBP hosts and was unaffected by the use of an electron blocker (MCP) to confine injected electrons to the emissive layer. The "white by red" phenomenon was also observed at high operation voltage in all devices and is probably due to the long excited state lifetime and the "bottleneck" effect. The data indicates that irrespective of how efficient the energy transfer from the host to the dopant is, how effective the antenna effects associated with the ligands are and how effectively charge is injected and confined to the emissive layer, the long lifetime of the f-f transition of the Eu ion

and the bottleneck effect appear to be the principal limiting factors for high luminance and efficiency.

In order to compare the lifetime and energy transfer effects of a lanthanide phosphorescent emitter with a transition metal phosphorescent emitter, 65% $Pt(ptp)_2$:CBP devices were fabricated with and without MCP. The power efficiency of the device without MCP was 2.28 lm/W which increased to 24 lm/W after adding the MCP electron blocker. Delayed recombination was observed in the ITO/NPB(40nm)/MCP(10nm)/65% $Pt(ptp)_2$: CBP(25nm)/TPBI(30nm)/Cathode device and is ascribed to disorder induced carrier trapping at the MCP/emissive layer interface, based on its frequency and duty cycle dependence. The data suggests that the recombination zone is close to or at the MCP/emissive layer interface. The utility of transient optical methods for measuring the mobility of organic semiconductors is demonstrated, and based on the results obtained, $Pt(ptp)_2$:CBP thin films are classified as n-type organic semiconductors.

6.2 FUTURE WORK

Temperature dependent current-voltage and transient electroluminescent measurements are required to gain deeper insights to the transport mechanisms (tunneling, Schottky emission, or field emission) involved in the observed interfacial trapping. In inorganic material field, Schottky emission is also called image-force-induced lowering of the potential barrier and the Schottky barrier height which can be calculated based on theoretical formula might be influenced by same effects. For organic material field, the Schottky emission caused from electron occurs within the electric field or thermal energy, and the emission current would be increased by the electric field of magnitude force at the emitter surface. It would be observed in the device which

is Shottoky contact or energy barrier at the interface. In addition, this work has discussed the transient EL in the OLEDs which consisted of several different functional layers. Therefore, it would be more interesting if we observe it with the different temperature and electric fields. Field emission is also called Fowler-Nordheim tunneling which is caused by a high electric field. In a metal-semiconductor, the carriers can tunnel through an energy barrier at a given electric field. With the increasing electric field, the more carriers can overcome the energy barrier or tunnel through the barrier due to the reducing barrier caused from band bending. Owing to the energy barriers, the field emission can be addressed for the study to see how the electrons tunnel through the energy barrier inside the OLEDs when we apply a high electric field. Furthermore, the carrier mobility should be understood clearly due to its change under the various electric fields and temperature. Based on the ideas above, this is necessary to quantify its effect on device efficiency with the various temperatures.

There are few ways to enhance the efficiency of organic light emitting diode, such as the modification of the device substrate, the organic materials, and light out-coupling. The 100% IQE of OLEDs has already achieved; therefore, the higher EQE is a goal for OLEDs field. In order to catch the most light from OLEDs, to enhance the light out-coupling by using microlens arrays or engineering scattering mechanisms for the same effect are expected to lead to higher device luminance and efficiencies. As we know, microlens array is used to increase the luminous current efficiency and power efficiency. However, the improper design would reduce the efficiencies. For example, if the pixel size of the device is too close the microlens dimension, the efficiencies of the devices might decrease. For the use of microlens array, the different pixel sizes and the various microlens array need to be investigated further to enhance the efficiencies of OLEDs. By using the light scattering, the light can be extracted out from OLEDs to enhance

the efficiencies. Adding the scattering films on the light-out side to enhance the outcoupling efficiency is also an important future work.

In this work, to design and fabricate a novel structure to optimize the efficiencies of OLEDs in a joint development project for Department of Energy (DOE) with research team from Department of Chemistry. The performances of our devices were comparable to those commercial products; however, the results gave two times higher power efficiency at PNNL (Pacific Northwest National Laboratory) even we used the same structure. At this point, there should be some effects in our fabricated facilities or measuring equipments. In order to fabricate the high quality device, we have to improve the processes of the device fabrication by preventing the contamination from the environment. For example, the oxygen and water vapor contaminations. Therefore, to design a chamber for the device fabrication without breaking the vacuum chamber is a key point when the metal contact materials are deposited on the organic layer. Furthermore, it is also important to investigate the various pixel sizes and the distance between the light target and the photo camera. For the selection of the camera, the photodiode detector might be a good choice due to its faster measuring time. Once we have the optimum setup of fabricated chamber and the measuring equipments, the result would be more close to its essential characterization.